LUND UNIVERSITY

Experimental measurements of water mist systems and implications for modelling in CFD

Husted, Bjarne

2007

Experimental measurements of water mist systems and implications for modelling in CFD

Doctoral Thesis

Bjarne Paulsen Husted

Department of Fire Safety Engineering
Lund University
Sweden

Lund 2007

Department of Fire Safety Engineering
Lund Institute of Technology
Lund University
Box 118
S-211 000
Sweden

ISSN 1402-3504
ISBN 978-91-628-7240-3
ISRN LUTVDG-1036-SE

August 2007

To Mette

Abstract

The use of water mist for fire extinguishment has increased rapidly in recent years. The main reason is the abandonment of halon-based extinguishing systems in favour of environmentally friendlier systems. Furthermore the use of water mist systems has spread from mainly marine applications to also include the protection of buildings.

The main problem in this regard is to verify the effectiveness of the system. At present time this can only by done by full-scale tests. This is however expensive and in some cases also unrealistic and expensive when it comes to water mist systems for buildings.

The aim of this thesis is to provide experimental data that can serve as a basis for simulations of the interaction of water mist and a fire and to demonstrate that CFD can predict the performance of a water mist system.

The physics of water mist systems has been studied by theoretical considerations as well as experimental work.

Measurements of droplet velocities, diameters and volumetric water distribution were carried out on the spray from a high-pressure system of 100 bars. Experiments have been conducted on a hollow cone nozzle without fire and with fire, as well as a full cone nozzle without fire.

Relevant measurement results were obtained with Phase Doppler Anemometry and Particle Image velocimetry as well as Laser Tomography and High Speed camera. Suggestions were made for improvement of the water density apparatus.

The measurements have been the basis for simulations of water mist with CFD. Initial simulations involving the complex zone around the nozzle resulted in droplets with radial velocities and insufficient transfer of momentum to the air.

A new approach has been used for the simulations with the LES model in FDS 4.07. In this approach the simulations of the water mist spray is not done in the zone close to the nozzle. Instead the boundary conditions are set further downstream, based on the conducted measurements.

This approach resulted in droplets and air moving downwards at relatively high velocities as expected. However, the momentum transfer is limited, and the simulations did not give sufficient mixing.

Suggestion are made of how sufficient mixing can be obtained with the new approach, with regards to implementation of spray boundary conditions and treatment of the turbulence model interacting with the movement of the droplets.

Key words:
water mist, PIV, PDA, FDS, fire safety engineering, CFD, fire suppression

Acknowledgement

This work was carried out as an industrial Ph.D. project, financed by the Danish Institute of Fire and Security Technology (DBI) and The Danish Academy of Technical Sciences (ATV).

I greatly appreciate that the management of DBI has supported this project. In particular I want to thank my supervisors at DBI, Jesper Ditlev and Henrik Bygbjerg for their patience and encouragement.

I would also like to thank my supervisor Göran Holmstedt for his inspiring ideas and advice on this thesis and my good colleague at Lund University Ulf Göransson for the many fruitful discussions and suggestions.

I value the input from my colleagues at DIFT. Special thanks to David Westerman for his many comments during the reading of the manuscript and to Brian V. Jensen and Kim Sommerlund for their input with regard to the simulations. Also special thanks to our librarian Dorrit Hansen, - who has been very helpful.

Lastly I thank my family for their patience. To my wife Mette for her support and valuable input to this thesis. and to my children Kirstine and Michael for their help at home and entertaining baby sister Anna.

Also thanks to the extended family and friends for their help.

Table of contents

List of publications and the candidate's contributions

This thesis is based on the following papers:

Paper 1
B.P. Husted and G. Holmstedt, Influence of draft curtains on sprinkler activation – comparison of three different models. Journal of Fire Protection Engineering, Reviewed, not published.

The candidate was the main contributor to this paper and did all the simulations.

Paper 2
B.P. Husted and G. Holmstedt and T. Hertzberg, The physics behind water mist systems, in IWMA Conference. 2004: Rome.

The candidate was the main author of this paper.

Paper 3
J. Carlsson, B.P. Husted, U. Göransson, and A.S. Dederichs, Anwendung von CFD-Programmen für brandtechnische Berechnungen. vfdb-Zeitschrift, 2006. 3: p. 127-131.

The candidate contributed to this paper.

Paper 4
Husted, B.P., P. Petersson, I. Lund and G. Holmstedt, Comparison of PIV and PDA droplet velocity measurement techniques on two high-pressure water mist nozzles. Fire Safety Journal, Submitted.

The candidate was involved in all the experimental work and did most of the treatment of the measurement results. Further the candidate wrote the main part of the paper.

Paper 5
B.P. Husted, M.D. Holst, J. Rusås and T. Condra, Lagrangian prediction of particulate two-phase flows at high particle loadings. Fourteenth International Conference on Numerical methods in Fluid Dynamics. 1994. Bangalore, India: Springer-Verlag, 1995.

The candidate was together with M.D. Holst the main contributor to this paper.

In addition to these papers the author has also contributed to the following publications with are outside the review of the thesis

Paper 6
B.P. Husted, J. Carlsson and U. Göransson. Visibility through inhomogeneous smoke using CFD. in Interflam 2004. 2004. Edinburgh.

Paper 7
U. Göransson and B.P. Husted. Can water mist be used to extinguish deep-seated cellulose fibre smouldering fires? - Experiments and Calculations. Interflam 2007. University of London, Egham, UK.

Chapter 1 Introduction

Man has used water for fire extinguishing for millennia. So why write a thesis about using water to put out a fire? Everyone knows it works! However, dividing the water into fine droplets, a so-called water mist, gives old water new properties and possibilities, which should be explored. According to Särdqvist, the fire brigade often uses more water and larger nozzles than necessary in order to control a fire with water [1]. Further the use of water is not very efficient - in another study, Särdqvist showed from a number of controlled experiments that the amount of water required to control a fire was between 0.15 kg/m^2 and 0.35 kg/m^2, whereas actual fire tests showed that in real fires the amounts used were between 10 kg/m^2 and 4,000 kg/m^2 [2]. This gives an extra useage of water for extinguishment thirty to twenty five thousand times larger than necessary, which can only lead to water damage to property and the environment. One possible solution to this problem is the use of water mist.

1.1 Water mist for fire extinguishing

Water mists are fine droplets, where 99% of the droplets are less than 1 mm in diameter [3]. Typically, the droplets are much smaller, in the range of 20 μm to 500 μm, depending on the water pressure and method used to create the droplets.

1.2 Historical background

Water mist has been used to extinguish fires for more than fifty years. It was initially used for manual fire fighting, but it has become increasingly popular in fixed fire fighting systems as one of several alternatives to halon. The signing of the Montreal Protocol in 1987 and the subsequent ratification of the protocol by 191 countries around the world regulated the use of halon, effectively banning it for most applications, except for some military, aviation and nuclear purposes.

This brought water mist into focus and since 1991 there has every year been a Halon Option Technical Working Conference in USA, where

water mist has been presented in a number of papers (examples are given in [4-8]). The International Water Mist Association (IWMA), which was founded in 1998, hosts several meetings and a conference every year.

A further impetus to the use of water mist systems came after the fire in 1990 on the passenger ferry "Scandinavian Star" sailing between Norway and Denmark, where 158 persons were killed. In 1995, this prompted the International Maritime Organisation (IMO) to require that all ships carrying 35 or more passengers should have marine sprinklers installed [9]. Water mist has often been chosen instead of traditional sprinkler systems on passenger ships, because of its lower weight and smaller space requirements. Furthermore, a lesser quantity of water used in fire fighting is an advantage, as large amounts of water discharged on an upper deck can jeopardise the stability of a ship.

1.3 Commercial development

Modern day water mist systems were largely developed for marine use but in recent years water mist has also been used on land for protection of buildings, as shown in a recent Norwegian report [10]. Norway has also had focus on the use of water mist systems in the health care sector, where some of the good properties of water mist can be combined with faster activation times [9].

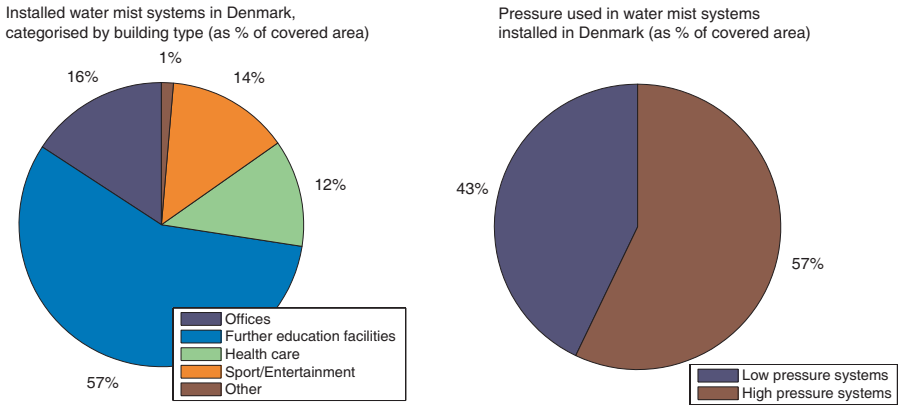

Figure 1. Water mist systems in Denmark under inspection by DBI (January 2007)

In Denmark, water mist was initially installed as a replacement for halon in computer server rooms. Now water mist is seen as an alternative to traditional sprinkler systems. The use of water mist systems has increased in recent years, although the number of water mist systems on-shore is still limited. Less than 1% of the fixed fire extinguishing systems in Denmark which use water are water mist systems (January 2007). These figures are based on inspections of sprinkler and water mist systems carried out by the Danish Institute of Fire and Security Technology, DBI.

The main areas for installation of water mist systems in Denmark are offices, further education facilities, health care and entertainment/sport, see figure 1. There is very little use in industry and for warehouses and transportation. About half of the installed water mist systems are low pressure systems and the rest are high pressure systems. There are currently no intermediate pressure systems installed in Denmark.

In Europe, the use of water mist seems to be greater than in Denmark, and the areas of application are more diversified. For example, water mist has recently been installed in road tunnels in Madrid and in the Alps and also in sports centres [11-13].

According to the International Water Mist Association, the water mist market in Europe grew from € 140 million in 2005 to about € 180 million in 2006 [14], though the market for water mist is still only a small percentage of the sprinkler market. Alan Brinson from the European Fire Sprinkler Network, which is an sprinkler interest group, estimated the European market to be worth € 2500 million [15]. This gives water mist a market share of 5-10%. There are large uncertainties in these figures, but water mists share of the market for land-based use is definitely less than 10%.

1.4 Detection of fires

Regardless if it is sprinklers or water mist that is used in a fixed fire fighting system, the fire has to be detected. It is the size of the fire when the sprinkler or water mist is activated which determines if the fire can be controlled, not the time to activation. Some water mist systems,

typically where sections of water mist nozzles are activated simultaneously, use an electronic detector based on measurement of smoke, heat, radiation or gasses from the fire. The detection of the fire can either be by one of these principles or by a combination, and it is typically fast. When using water mist instead of traditional sprinkler systems, detection is often carried out by a mechanical system such as a glass bulb or a fusible link, both having a somewhat longer response time. This can lead to an uncontrollable fire if the response time is too long, and it is therefore important to be able to predict the activation time of the water mist nozzle. Calculation of the activation time for a glass bulb sprinkler and the influence of draft curtains is discussed in paper 1 [16]. It is shown that for this purpose, relatively simple models give adequate results.

1.5 Problems with dimensioning water mist systems

Due to the growing use of water mist systems, there are several issues which need to be resolved. Currently, a water mist system must be designed for a specific location by carrying out extinguishing tests for a relevant setup. The only standard for water mist systems, NFPA 750, states that a water mist system should be listed for the specific purpose[17]. This is very costly and drastically limits the use of water mist systems, as every new system has to be designed and tested separately. For marine applications, water mist has been used in smaller compartments and full-scale tests have been performed. This is expensive however, and in some cases also unrealistic, especially when it comes to water mist systems for buildings.

Today, there are no guidelines available for dimensioning water mist systems. It would be desirable to obtain enough knowledge in the area to enable performance based design of water mist systems.
Simulations could be carried out using computational fluid dynamics using relevant models to account for the spreading and extinguishing effects of the water mist.

1.6 Complicated physics of water mist systems

The physics behind the water mist systems that must be modelled is relatively complicated, and is briefly described in the following. More details can be found in paper 2 [18].

While sprinklers work due to surface cooling, the effect of surface cooling in water mist systems is negligible for practical purposes [18]. Water mist systems mainly work by flame extinguishing, where the droplets evaporate and lower the flame temperature. The area of surface contact between water and the surrounding hot gasses increases with decreasing droplet size. However, very small droplets are rapidly decelerated, and may have difficulties in penetrating a flame zone.

The water mist will induce a flow in the room as the momentum from the droplets is transferred to the surrounding air. Furthermore, a fire will also create a flow in the room. The interaction of these two flows must be accounted for. Another problem is that water mist droplets, at the size used in most water mist systems, will be stopped by a physical obstacle and therefore cannot extinguish a concealed fire. Andersson and Holmstedt showed that water mist droplets larger than 20 μm would not be able to follow an air stream of 5 m/s and would, due to inertia, hit the obstacle instead [19]. Recent experiments with ultra fine water mist with an uniform droplet size of 10μm have shown promising results, though it is difficult to get the mist distributed and therefore there was only a spacing of 1 m between mist inlets [20].

One-zone models, like the Fire Demand Model and Optimist, are available for calculating the extinguishing effect after flash-over in a room with a uniform temperature [21-24]. In cases where water mist is used in lieu of traditional sprinkler systems, the nozzles are activated before flash-over and the temperature is not uniform. Here there are 2-zone models such as Splash, developed at South Bank University to examine the interaction of sprinklers and fire ventilation, which can calculate temperatures in the smoke layer [25, 26]. In order to model water mist before flash-over, which considers the fire, temperature, water distribution and flows in the entire compartment, and where these

quantities will depend both on location in the room and time, these models can not be used. The only tool available for modelling is Computational Fluid Dynamics (CFD), discussed in paper 3 [27].

Previous attempts have been made to model water mist using the CFD-tools Fluent and FDS [28], but they have been relatively unsuccessful. This is due to both deficiencies in the modelling and also the lack of good experimental data to use for input and verification of the models.

The aim of this thesis is to provide experimental data that can serve as a basis for simulations of the interactions of water mist and a fire and to demonstrate that CFD can predict the performance of a water mist system.

1.7 Readers guide to report

Chapter 2 contains a description of the measurement techniques for measuring velocity and droplet size used for the experiments.

Chapter 3 describes measurement techniques for measuring volumetric water distribution.

Chapter 4 contains results of measurements on spray without and with flames.

Chapter 5 discuss the use of different CFD codes for the simulations of water mist

Chapter 6 discuss the setup of water mist in FDS 4.07

Chapter 7 contains the results of the simulations carried out with FDS 4.07

Chapter 8 conclusion

Chapter 2 Measurement techniques for measuring velocity and droplet size

A number of different techniques are available for measuring particle size of water droplets, including optical and mechanical methods. Mechanical methods can be drop freezing and molten wax techniques but nowadays, optical methods are normally used, as these are non-intrusive techniques where droplet size can be measured without interfering with flow. Optical methods are also predominant in measurement of drop velocities.

In this work, Particle Image Velocimetry (PIV), Phase Doppler Anemometry (PDA) and a high-speed camera have been used for measurements on two high-pressure water mist nozzles. Details of the actual experiments with PIV and PDA can be found in paper 4, [29]. Another commonly used method, but not used here, is laser diffraction. An overview of the ability of the four methods to measure velocity and droplet size is given in table 1. Note that PDA is best suited for measuring both velocity and droplet size at the same time.

Table 1 Methods used for measuring droplet velocity and droplet size – (x) indicates that the method is less suited for measuring water mists

	Droplet Velocity	Droplet size
Particle Image Velocimetry (PIV)	x	(x)
High speed camera	x	(x)
Phase Doppler Anemometry (PDA)	x	x
Laser Diffraction		x

The methods also differ in how large an area they cover in a single measurement. PIV and high-speed camera are carried out in a plane or sheet. Laser diffraction measures along a line, whereas PDA is a point measurement technique.

Measurements on a water mist spray pose several difficulties, as the spray is dense and the droplets small. All the techniques have difficulties taking measurements very close to a nozzle. However, measurements

carried out with PIV and PDA have shown good results from a distance of 50 mm, for both a hollow cone as well as a full cone nozzle.
This chapter gives an overview of the principles of the different measurement methods, along with their advantages and limitations. These are outlined in table 2.

Table 2 Characteristics of the four measurement types

	PIV	**PDA**
Principle	Cross-correlation of two successive images of a light sheet illuminated by a pair of pulsed laser	Phase Doppler Anemometry, based on light scattering interferometry and the Doppler effect
Measure drop velocity	Yes	Yes
Measure drop size	Not in a dense spray like water mist	Yes
Measure in plane	Yes - can capture spray dynamics	Only point measurements
Time resolution	Poor resolution, maximum frequency 4 Hz achieved during the experiments. Specialised high speed options available on the market, up till 10 kHz, but typically only 16 subsequent pictures can be taken	Good time resolution
Processing of measurements	Processing of raw images is carried out subsequently and is very time consuming (in these experiments, up to 12 hours for a single measurement with 1000 double exposures)	Fast -typically online
Advantages	Will give measurements in a plane, and can therefore be used to capture the dynamics of a spray.	Corresponding droplet sizes as well as velocities are determined. Fast.
Disadvantages	The velocity is determined for different sizes of drops that may move at different speeds. Which droplet size this velocity represents is unknown.	Requires spherical droplets. Measurements are made at a point, and therefore difficult to use in unsteady conditions such as at the interaction of water spray and flame. Can give problems at very high droplet density.
Recommendations	PIV should be used further away from the nozzle where the droplet velocities of different sized droplets are more similar.	PDA should be used for steady state measurements, and at a distance from the nozzle to avoid too dense a spray. However, it will work closer to the spray than PIV-measurements
Suppliers	Dantec Dynamics, TSI, Lavision	Dantec Dynamics, TSI

High Speed Camera	Laser diffraction
Photographic imaging of droplets	Uses diffraction of monochromatic light from a droplet to determine droplet size
Yes, but only at the onset of the spray where the velocity of the water front can be found.	No
Not in a dense spray like water mist	Yes
Yes, provided a laser sheet is used for illumination	Measures along a line
Good time resolution	Good: up to 10 kHz
Processing has to be done subsequently, and can be time consuming.	Processing of measurements is fast
Will show formation and break-up of droplets.	Standard measurement technique, where limitations are well known
Cannot be used in dense sprays; however use of a light sheet might improve the situation. Evaluation of data is very time consuming, as this has to be done manually	Cannot measure a very dense spray, as the technique is sensitive to multiple scattering. To get the droplet size in the spray it is necessary to perform several measurements and use a deconvolution technique.
Can possibly be used for studying interaction of water mist and a flame front. However, a light sheet should be tried to show the droplets properly	Easy to set up method for characterising spray
Several	Malvern, Sympatec

2.1 Particle Image Velocimetry

Principle

PIV is basically a pattern recognition technique. Two pulsed lasers are used to illuminate the spray in a thin sheet and two images are taken with a short time interval, synchronised with the laser, see figure 1. The images are typically stored in two different frames in the same picture. The frames are then subdivided into a number of fields, also called interrogation windows. Movement of the droplets is calculated by cross-correlation of the pixel intensity in the interrogation areas from the two frames, as illustrated in figure 2.

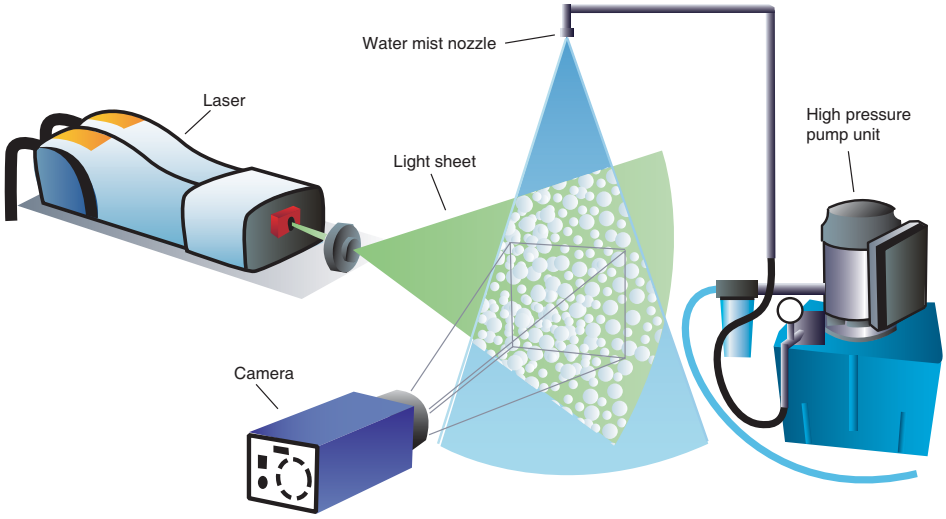

Figure 1 Measurement setup for PIV on water mist with laser, camera, nozzle and high pressure pump unit

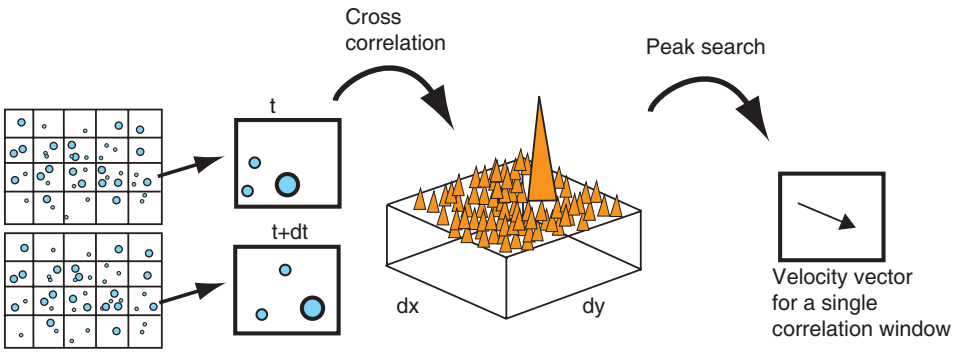

Figure 2. Principle of PIV measurements, using cross correlation between two successive frames

PIV is normally used to measure gas flow velocities. The gas flow of interest is then seeded with small solid particles to allow the necessary imaging. The seeding particles are all nearly the same size. The size and density of the particles are of vital importance for the particles to faithfully follow the gas flow in question. With water mist, the water droplets in the spray are directly used for imaging and velocity calculation of the particles. The surrounding air has not been seeded and air velocity is not directly captured. The basic formula for performing cross correlations is given in (1), where intensities of the single pixels are also considered. The algorithm is therefore sensitive to droplet size, as a larger droplet gives a higher intensity than a small droplet.

$$C(dx,dy) = \sum_{x=0,y=0}^{x<n,y<n} I_1(x,y) \times I_2(x+dx, y+dy) \qquad (1)$$

$$-\tfrac{n}{2} < dx < \tfrac{n}{2}, -\tfrac{n}{2} < dy < \tfrac{n}{2}$$

C is the value for the correlation of all combinations of displacement by *dx* and *dy*
dx, *dy* is the displacement in pixels
I(x,y) is the intensity of a pixel in the local pixel coordinates in the interrogation window
n is the size in pixels of the interrogation window

Processing of measurements

Processing of the raw images (cross-correlations to determine velocities) can be performed by a number of commercial codes (Lavision, Dantec, TSI) and a number of open source codes. Of the open source codes, there are stand-alone programs as Gpiv and mpiv, which are a toolbox to Matlab and thus require this software. The commercial codes are expensive, but they are more robust and stable and they provide good interfaces to different programs. The open source codes are slower and do not have the same user-friendly interface. Decreasing window size and measurement of spray angle are not features of some of the open source codes. According to Greber van der Graaf, one of the developers of the open source Gpiv: ”The main advantage of the Gpiv project is that it is Open Source Software in its widest meaning; it does not use any closed source/commercial software, only Open Source code, like Gpiv.” [30]

Using commercial PIV-evaluation codes for calculating velocities is recommended. However, post processing / viewing and evaluation of data may be more easily done using another tool with greater control over the calculations, for example the free toolbox pivmat for evaluating results from Lavision in Matlab [31].

Advantages, disadvantages & recommendations

The main advantage of using PIV is that velocities of a plane through the spray are determined simultaneously.

The resolution in time is poor; an average of 2 double exposures every second can be taken. This means that turbulence cannot be tracked and compared to modelling results. There are faster PIV-systems on the market, which can take up to 16 or more double exposures in a row with high time resolution. However, this is a relative small sample for turbulence determination and for understanding movement of the droplet in a turbulent spray [32-34].

In measurements of water mist, the aim is to measure the velocity of the water droplets. This poses a challenge, as droplets of different sizes will move at different velocities, especially close to the nozzle. Furthermore, the velocities in the measurements are not linked to specific drop sizes.

When there are equal amounts of small and large droplets, PIV has a bias towards the velocities of the larger droplets, as they reflect more light. Measurements only give one velocity measurement for every interrogation window, and it is not known which droplet size this velocity represents. Outside the immediate spray outlet zone, where droplet velocities are more uniform, results can be more useful. It is recommended that these velocities are used for comparison with simulations. Further details of measurement with PIV are given in Paper 4, [29].

The PIV approach could also be used with a continuous laser and a high speed camera, provided the high speed camera can get sufficient light.

2.2 Phase Doppler Anemometry

Principle

Phase Doppler Anemometry (PDA) techniques measure particle size and particle velocity at the same time. The method only measures at a point, but resolution in time is very good.

The underlying theory for the measurement is based on light scattering interferometry and the Doppler effect. The PDA method was introduced in 1984 by three research groups [35-37]. Measurements are made in the volume of the intersection of two focussed laser beams and are conducted on single particles as they move through the sample volume, see figure 3.

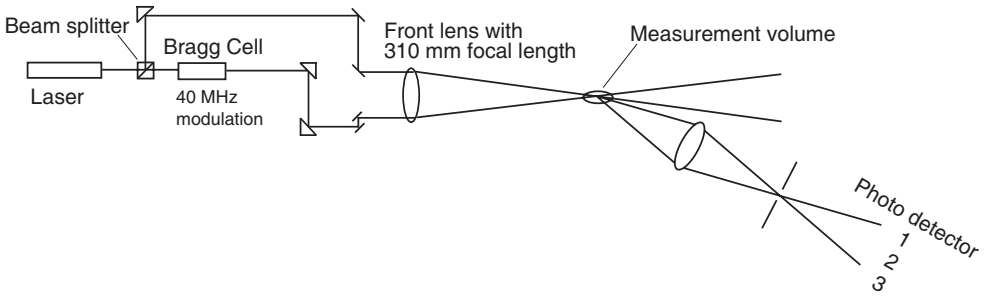

Figure 3 The principle of Phase Doppler Anemometry

Particles scatter light from both laser beams and generate an optical interference pattern. The frequency of the pulsation of light intensity is proportional to the velocity of the particle. Each detector is mounted at different angles and converts the optical signal into a Doppler burst. The phase shift between the Doppler signals from 2 different detectors is a direct measure of the particle diameter

Processing of measurements

PDA is specifically designed for measuring particle size and velocity, with processing of measurements being carried out online. With the 1-dimensional Dantec Classic PDA instrument used in this study, the results can be presented as histograms showing drop sizes and numbers. Furthermore, characteristic diameters of droplets can be calculated as mean diameter, surface weighted mean diameter, volume weighted mean diameter etc., as well as a single mean velocity of all droplets.

For determining the velocity corresponding to a droplet size, more work is involved, as this was not possible in the PDA-software used in this study. Instead, raw data from the measurements, containing droplet number, time, diameter and velocity were exported. A single measurement for one position would typically consist of about 300,000 samples. These data are subsequently imported into a maths program such as Matlab and processed.

Advantages, disadvantages & recommendations

PDA is the only measurement type that provides corresponding values of velocities and droplet sizes. It also has very good time resolution, and processing of data is online. In a very dense spray, there may be more particles in the measurement volume, however in the experiments conducted, this was only a problem very close to the nozzle (25 mm).

PDA measurements require that the droplets are spherical. The Weber number (see equation 2), which is the ratio between inertia and surface tension forces, can be used to indicate droplet shape and eventually break-up.

$$We = \frac{\rho_{air} \times u^2 \times d}{\sigma_{water}} \qquad (2)$$

For water droplets in air, the critical Weber number is about 13, according to Lefebvre[38]. For the largest and fastest drop in the measurements reported in paper 4 [29], which is a droplet of 75 μm moving at 40 m/s, the Weber number is approximately 2.3. Therefore the droplets are expected to be reasonably spherical.

A disadvantage of this technique is that it only provides point measurements.

The one-dimensional Dantec Classic Phase Doppler Analyser that was used for measurements should also be able to measure mass flux. This was attempted, but the mass flux values were very unrealistic. However, Zhang and Ziada have successfully measured mass flux with PDA from the atomisation region of a water jet [39]. The reason for their better results was that they used a Dual PDA system and took great care in calculating measurement volume correctly. More details on this is given in chapter 3.

2.3 High-speed camera

Principle

This is a photographic technique where a number of pictures are taken (up to 8000 pictures per second). Droplet size can be determined directly from pictures. To determine velocity, individual droplets must be tracked between the frames. Jackman has done this to measure the velocity of sprinkler droplets and more details are given below [26].

Processing of measurements

This is not a commonly used technique, and processing of pictures has to be performed subsequently by the user. This can be very time consuming.

Advantages, disadvantages & recommendations

Water mist droplets are small and to detect a droplet and determine its size, a minimum of 4 pixels are required. Thus a droplet 20 µm in diameter will result in a pixel resolution of 10 µm, as shown in figure 4. This means that for a high speed camera having a resolution of 800 x 600 pixels, the area which can be covered is about 10 mm. Furthermore, in a dense spray it is difficult to distinguish between the individual droplets. This makes it impossible to use a high-speed camera to determine droplet size on a larger scale.

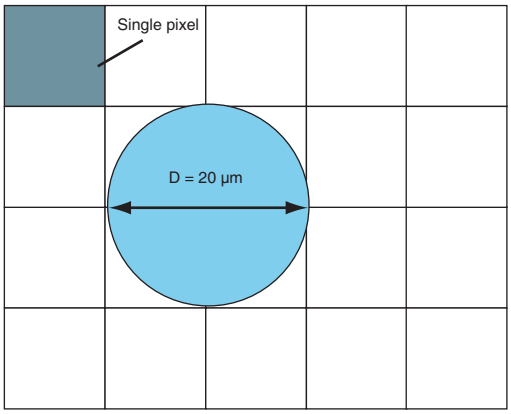

Figure 4. Mapping of a droplet on the camera pixels. If 4 pixels are required to resolve a droplet of 20 µm in diameter, the pixel resolution has to be 10 µm

In this study, it was found that high-speed camera images could only be used to study movement of the bulk volume. This is the case at the onset of the spray, where the velocity of the moving front of water can be found, see figure 5.

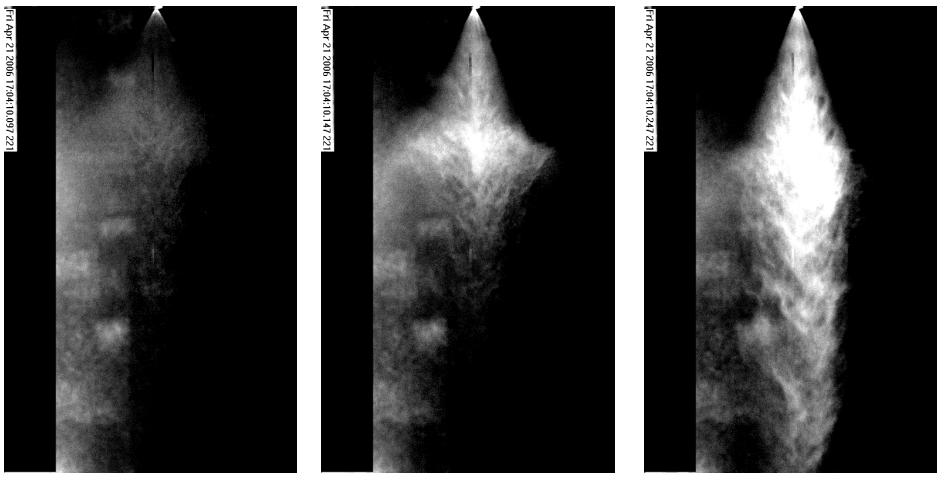

Figure 5. Onset of hollow cone spray, height of window is 0.5 m and time between frames is 50 ms. The front of the spray moves with 0.25m/50 ms = 5 m/s

A further problem for fast moving water mist droplets is in providing enough light for the camera when the number of pictures per second is increased.

In the 1990's, Nolan and Jackman had good results using a high speed camera to measure droplet size and velocity in water spray from a traditional sprinkler head, where the droplets are much larger than water mist droplets [26, 40]. A light sheet from a copper-vapour laser was used to illuminate part of the sprinkler spray, which was captured on photographic film. In spray from a sprinkler head, the individual droplets have greater separation and can be seen clearly on the film sequences in figure 6. Movement of a droplet of about 400μm in diameter is captured in the film sequence on the left and a droplet of about 800 μm in the sequence on the right. It can be seen that the larger droplet in the film on the right is not spherical, whereas water mist droplets are of a smaller size and surface tension will keep them spherical. So high-speed camera

can be an option for studying individual droplets from a sprinkler spray, but is not well suited for water mist.

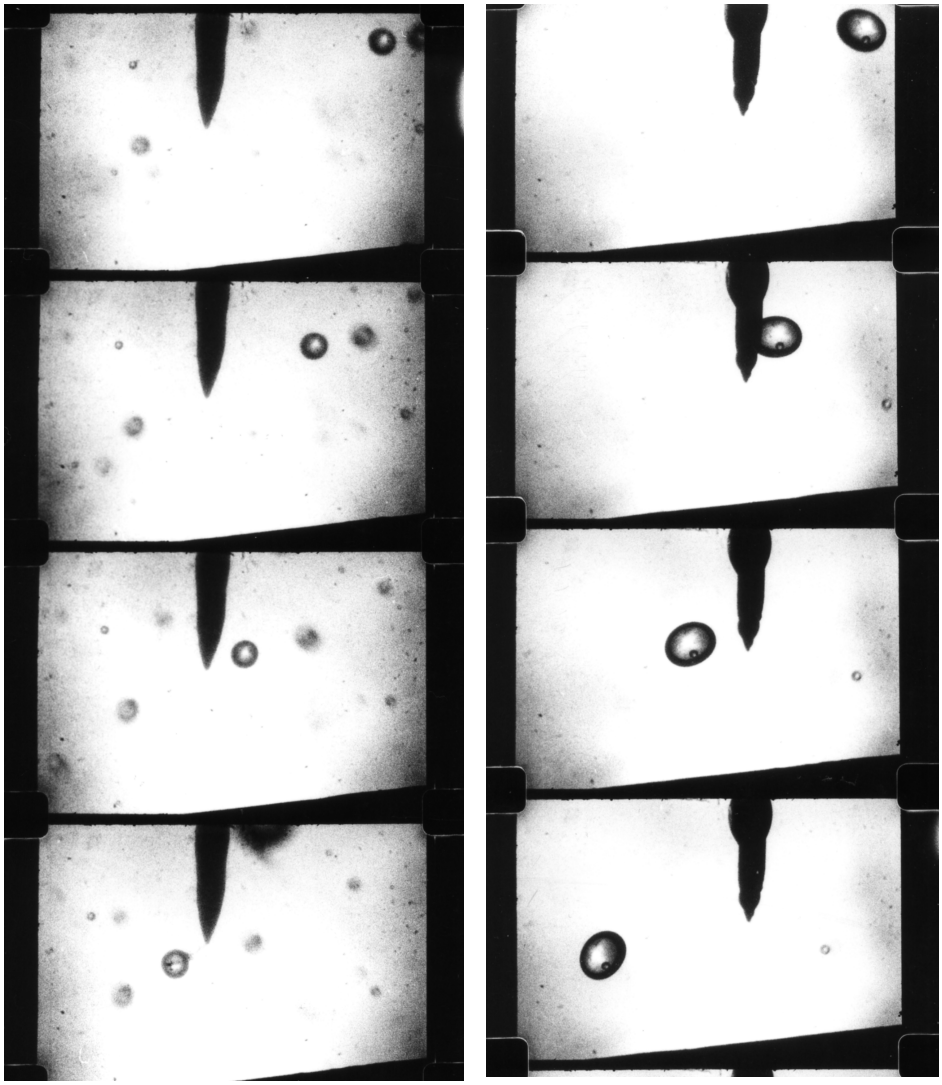

Figure 6. Measurement of size and speed with high speed camera, two different measurements. In the film on the left, droplet size is 400µm and in the film on the right, 800µm. From Nolan [40]

2.4 Laser diffraction

Principle

One of the most widely used techniques for measuring droplet size is laser diffraction [38]. The most well known supplier is Malvern Instruments and therefore it is often referred to as the Malvern particle sizer, see figure 7. Today, there are more suppliers on the market, such as Sympatec in Germany.

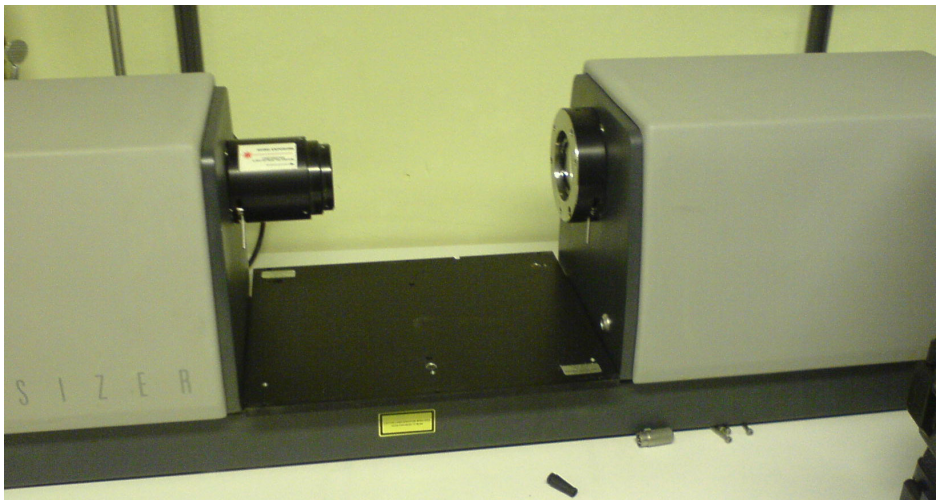

Figure 7. Laser diffraction instrument (Malvern) at Lund University

The Malvern particle sizer uses diffraction from droplets to measure the size of the droplets using the principle shown in figure 8. The diffraction pattern of droplets within the working range of the instrument is projected onto a ring-formed detector through a Fourier lens. This means that droplets of the same size but at different positions, are projected onto the same detector ring and the instrument measures the particle size along the light path of the laser beam. The laser beam is typically 10 mm wide and, for the Malvern instrument, the working distance for a 5µm particle is over 1m, which makes it well suited for water mist.

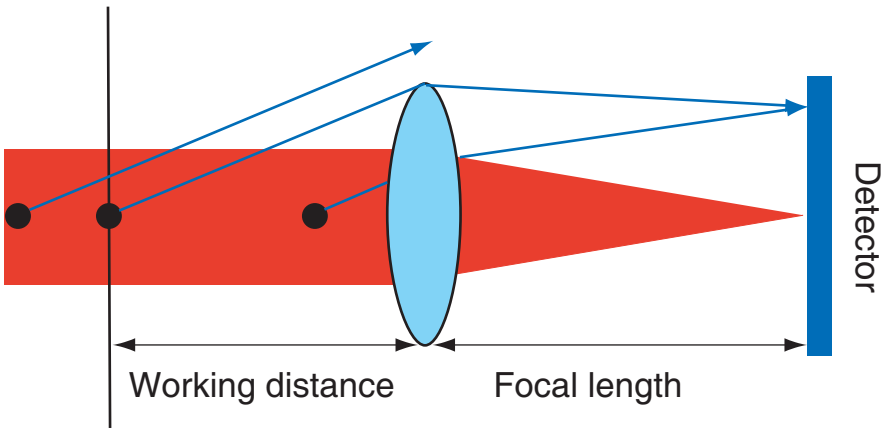

Figure 8. Principle of laser diffraction measurement

Processing of measurements
Data is processed on-line.

Advantages, disadvantages & recommendations
One drawback of the Malvern particle sizer is that it only measures droplet size and does not measure droplet velocity.

Laser diffraction is sensitive to multiple scattering errors due to dense sprays, but normally this error can be ignored if less than 50% of the light is attenuated by the spray. There are algorithms available which can compensate for multiple scattering and with these algorithms it is possible to measure with extinction of light as high as 95% [38]. Triballier et al. found in a recent study with the Spraytec from Malvern that these compensating algorithms cannot satisfactory correct for large and inhomogeneous sprays [41]. The algorithm worked best in spray which was dense, homogeneous and small. In the present study, both water mist nozzles attenuated the light less than 50%, so measurement on these sprays using laser diffraction should be possible.

Lefebvre has mentioned that variations in detector responsivity could lead to variations in the measurement of drop size, and Hirleman et al. found differences up to 27% in mean droplet size when doing a round robin test between several laboratories [38, 42]. These problems should

have been solved in the late 90's through improvements in detector technology [43].

Another factor is the maximum sampling frequency, which for the Malvern instrument is 10 KHz. This means a time delay between every measurement of 100 μs. A droplet moving at 30 m/s would cross a 10 mm laser beam in 300 μs and the maximum velocity of the droplets is then 100 m/s. This makes it difficult to measure very close to a high-pressure nozzle, where droplet speeds can exceed 100 m/s.

Finally, there is the phenomenon called beam steering, caused by Schlieren effects due to density differences in the air. This could occur when measuring at elevated temperatures, for example when measuring the interactions of water mist and a fire. Turning the inner detector rings on the instrument can minimize this problem.

There can also be problems related to the way the measured data is processed in the instrument. Teipel found that laser diffraction measurements can have problems in determining the size of small particles with a median diameter of 20 μm, if the Fraunhofer approximation is used instead of the full Mie theory [44]. Use of the Fraunhofer approximation leads to the counting of fictitious particles and thereby a bias towards smaller particles. A diameter of 20μm is in the size range for water mist droplets, and therefore it is desirable if the instrument uses the full Mie theory to determine the droplet size.

The Malvern has been compared with PDA in a study by Dodge et al. [45]. The authors found that there was excellent agreement, when the laser diffraction data was deconvoluted and transformed to point measurements, so that these could be compared with the PDA results.

Chapter 2 Measurement techniques for measuring velocity and droplet size

Chapter 3 Measurement technique for measuring water mist distribution (volumetric)

The volumetric distribution of water m''' (kg water /m³ air) is crucial to the extinguishing capabilities of a water mist system. Measurements have been made to find the volumetric distribution for a free spray, and for a spray that interacts with a fire.

Three different methods have been used: Phase Doppler Anemometry (PDA), laser tomography, and an enhanced version of the water density apparatus, developed by Andersson and Holmstedt [46]. The measurement with PDA and the water density apparatus were made by this author. The measurement with laser tomography was made by Almén and Irvert as described in [47]. Additional measurement with the laser tomography method where made by this author to clarify some of the uncertainties in the setup. Table 1 shows the main characteristics of the three measurement types.

Measurements have been carried out with all three methods, but trustworthy data was only obtained with laser tomography. However, this method gives only a qualitative measurement, due to the sensitivity to droplet size. But if the droplet distribution is known, quantitative values are given with reasonable accuracy. Measurement with PDA is the most used of the three techniques, although the available instrument provided faulty data. The water density apparatus is a relatively new concept. It could prove a relatively inexpensive alternative, for measuring the water content directly. However the current prototype has several inherent problems that must be solved.

Table 1. Characteristics of the 3 measurement types

	PDA	Laser Tomography	Water density apparatus
Principle	Phase Doppler Anemometry, based on light scattering interferometry and the Doppler effect	Determination of mass density by measuring attenuation of laser light.	Humidity measurement of heated sample, where air and water mist is sucked from a point in the spray.
Spatial resolution	Point measurements	Can give 3-D image.	Point measurements
Time resolution	Good time resolution	Slow, gives average values, possible to get better time resolution if more lasers and detectors were used	Slow, response time > 10s
Processing of measurements	Fast, typically online	Time consuming, but could possibly be automated	Fast
Advantage		Possibility of a 3-D image	Inexpensive, easy to setup, independent of drop size
Disadvantage	Requires spherical droplets. Measurements are made in a point, and therefore difficult to use in unsteady conditions like interaction of water spray and flame. Can give problems with very high droplet density.	Result strongly dependent on droplet size. To get a result, a representative droplet size must be assumed.	Intrusive method which can disturb the spray pattern. Very sensitive to flow direction on sampling probe. Requires isokinetic sampling. The humidity meter used only works up till 180°C.
Recommen-dations	PDA to be used for steady state measurements, and at a distance from the nozzle to avoid to dense a spray.	Measurement is mainly qualitative, due to the sensitivity to droplet size.	Additional work on the sampling system
Suppliers	Dantec Dynamics, TSI	Constructed at the Department of Fire Safety Engineering, Lund University	Constructed at the Department of Fire Safety Engineering, Lund University

3.1 PDA for water density measurements

Principle

The principle of Phase Doppler Anemometry (PDA) and its primary function to determine droplet size and velocity is explained in chapter 2. PDA can also measure the volumetric distribution of water as well as mass flux. This measurement is based on knowledge of particle numbers, sizes and velocities as well as size of the measurement volume, which the droplets pass, as shown in figure 1.

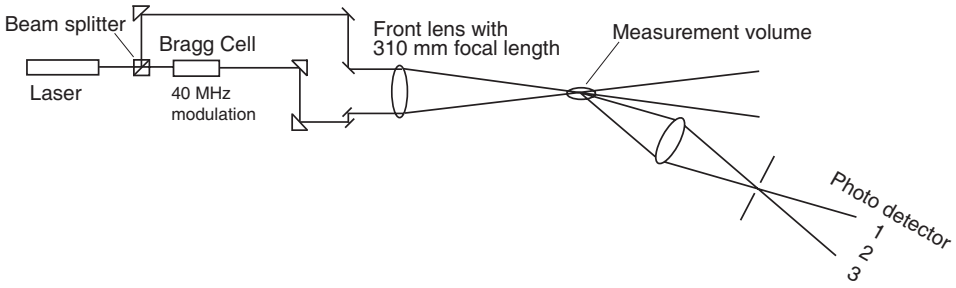

Figure 1 The principle of Phase Doppler Anemometry

Processing of measurements

The processing of measurements is done online, and is therefore easy.

Advantages, disadvantages & recommendations

The one-dimensional Dantec Classic Phase Doppler Analyser that was used for measurements of velocity and droplets size should also be able to determine the mass flux. This was tried, but the mass flux gave very unrealistic values. This might be due to an incorrect determination of the measurement volume, which according to Dantec is an inherent problem with single PDA systems, where the receiving optics is in one plane. Zhang and Ziada have discussed this in detail and obtained better mass flux measurement with a DualPDA system (Dantec), where an extra measurement plane is added [39]. Similar Wang et al. in a recent article used DualPDA to measure volume flux and their results seemed consistent [48].

3.2 Laser Tomography

Principle

Laser tomography can be used to determine the water concentration of a spray by measuring the light attenuation through the spray. The principle is shown in figure 2 with a laser on one side of the spray and a detector at the opposite side of the spray. Further, the distance between laser and detector is shown and the approximate width of the spray is given for the no fire case. Figure 3 shows the actual experimental setup, where the light attenuations were measured at different heights simultaneously. There are a row of lasers on one side of the water mist spray and a row of detectors on the other side of the spray.

This actual experimental setup has earlier been used by Andersson for measuring soot volume fraction in flames [49]. However, the use of the setup for measuring water mist is based on other physical phenomena, and therefore the data treatment is different.

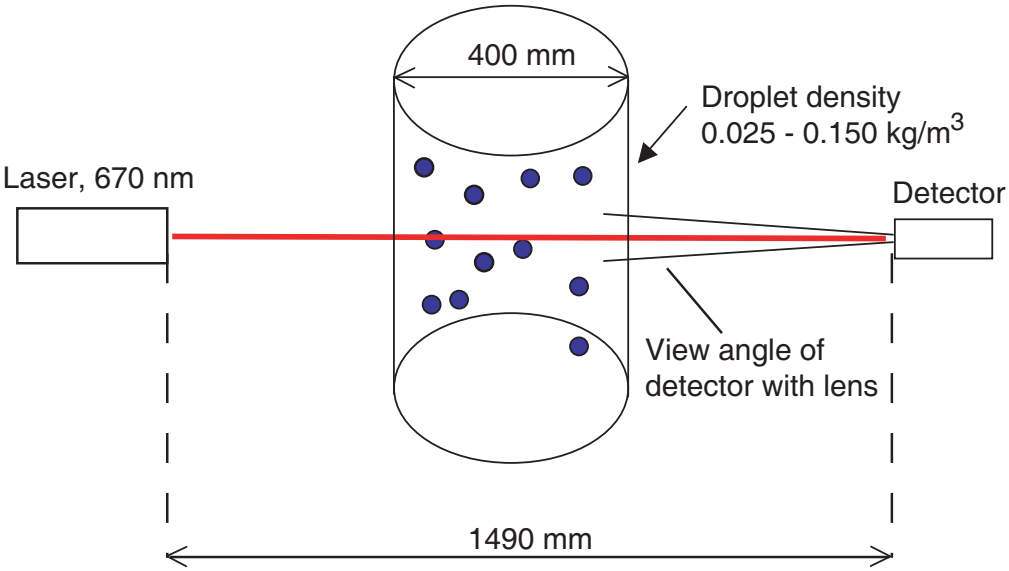

Figure 2 Principle for measuring light attenuation though water mist spray

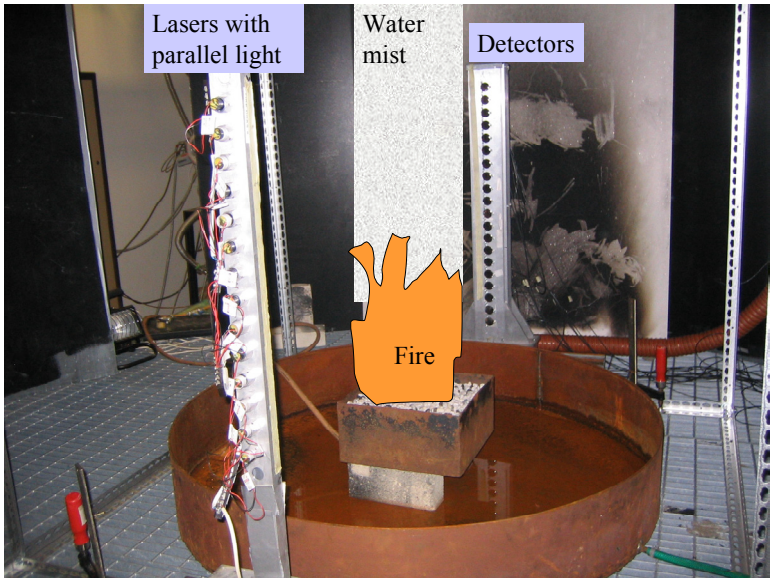

Figure 3 Experimental setup for measuring with Laser Tomography

Light attenuation and scattering

For a parallel light beam, the intensity incident on the spray (I_0) to the intensity traversing the spray (I) can be determined by measurements without spray and with spray. Lambert-Beer's law below describes the relation:

$$K_{ext} = \sigma_e \cdot L = \ln\left(\frac{I_0}{I}\right) \qquad (1)$$

Measurement allows direct determination of the extinction $K_{ext} = \sigma_e \cdot L$, where σ_e is the extinction coefficient (fractional loss of intensity per unit length) and L is the path length through the spray [m]. In the following, the calculation of the water mist concentration based on the extinction coefficient σ_e is discussed.

The attenuation of light is due to the scattering by the water mist droplets, whereas absorption is very small. This follows from the refractive index of water in air. At a wavelength of 670 nm, delivered by

the laser in the experiments, the complex refractive index of water with a temperature of 15°C is 1.33 + 2.34E-08i (value from the program MiePlot, [50]) . The imaginary part of the index is the absorption and it is much smaller than the real part and can therefore be ignored.

The scattering of light from a single particle and the interaction with incident light can be divided into 3 different ranges based on the value of the Mie parameter ε according to Teipel [44].

$$\varepsilon = \frac{\pi \times d_p}{\lambda} \qquad (2)$$

ε << 1	Range of Rayleigh scattering
0.5 < ε < 10	Range of Mie scattering
ε >>1	Range of geometric optics

Table 2. Size of the Mie parameter ε as a function of droplet diameter at a wavelength of 670 nm

Diameter of droplet [µm]	0.01	0.10	1	10	75	100	300
ε	0.05	0.47	4.7	47	352	469	1407

For the water mist droplets, which varies from 1 µm to 75 µm in size and a wavelength of a laser of 670 nm, ε will be in the range from about 5 to 350 as shown in table 2. This is mainly outside the immediate Mie region, but is it still covered by the Mie theory. There are a number of different computer programs freely available, which can be used to calculate the Mie scattering. They are all based on the same theory and differ only in user-friendliness. The program MiePlot written by Philip Laven has been used in this study [50]. It can calculate the scattering from a single droplet, but also from a distribution of droplets. MiePlot does not calculate the effect of multiple scattering, but single scattering is a reasonable assumption when less than 50% light attenuated [38], which was the case in the experiments.

Droplet size and Mie scattering

The scattering in the Mie region is dependent on droplet size of the actual measured droplet distribution for the nozzle. Figure 4 shows the number droplet distribution for the raw measured data and for a log-normal distribution, which is fitted to the data. The data is measured with PDA 500 mm below the hollow cone nozzle and details for this measurement can be found in chapter 4 and in paper 4, [29]. Note that scattering of light is based on the number of droplets, where as extinguishment is based on the amount of water and in that case a volume-based distribution is more appropriate to describe the spray.

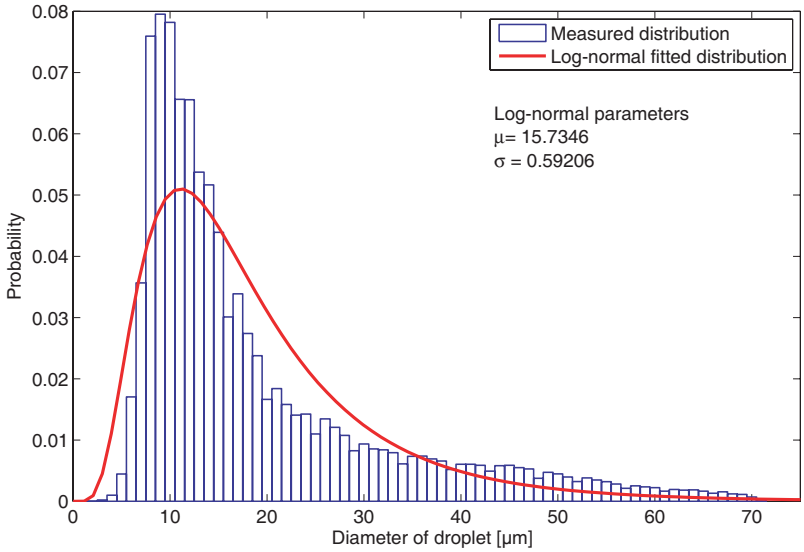

Figure 4. Number distribution of droplets, 500 mm below hollow cone nozzle

With a known droplet distribution the Mie scattering has been calculated using MiePlot. Figure 5 illustrates the effect of Mie scattering and the intensity of scattered light from a light source located at 180° with the droplet distribution shown in figure 4. The calculations are made as single scattering, a reasonable assumption provided light attenuation is less than 50% [38]. It can be seen that the main part of the light is scattered in the forward direction and that the scattering pattern is complicated.

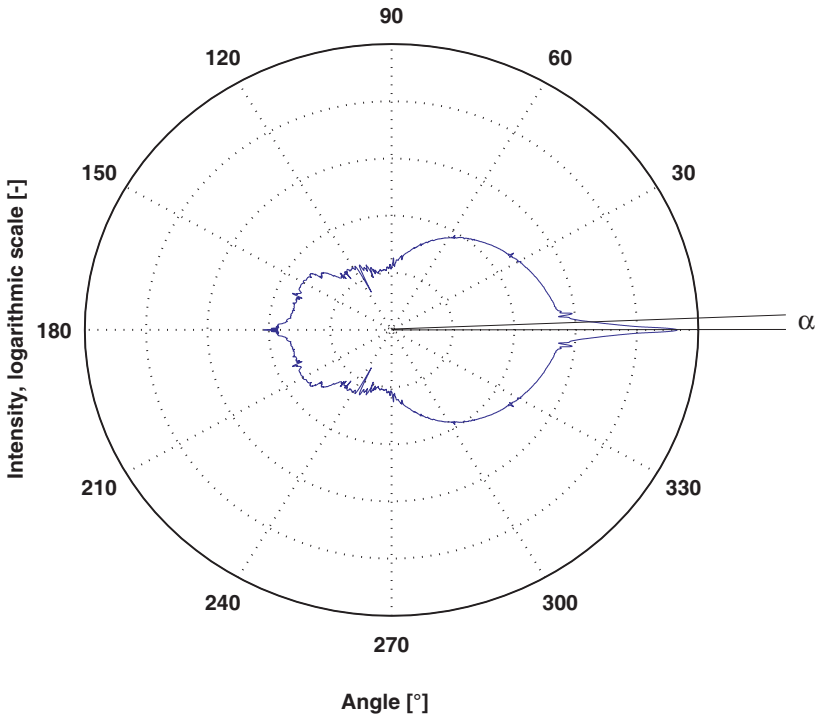

Figure 5. Logarithmic intensity versus angle due to Mie scattering of an actual measured droplet distribution (500 mm below the hollow cone nozzle used in the experiments). The light source is located at 180° and has a wavelength of 670 nm (red light). α is the viewing angle of the detector as illustrated in figure 6.

Calculation of water concentration

The principle of the detection of a single droplet is shown in figure 6. The laser beam is coming from the left side and illuminates the droplet. The droplet is much smaller than the width of the laser beam, so the main part of the light will hit the detector. The light that hit the droplet will scatter according to the diagram shown in figure 5 and the scattering is also shown on figure 6 as red arrows. The scattering is three-dimensional and the angle α form a cone on a sphere with the droplet situated in the middle of the sphere. This angle is also shown on figure 5. The light within this cone will be collected by the lens and also be detected. The light outside the cone and within the angle β will not be detected. The total intensity scattered can be found if the "miss fraction" f_{miss} is known. The "miss fraction" is the fraction of scattered light that

misses the detector compared to the total amount of scattered light. It is dependant on droplet size and can be determined by integrating intensities within the angle 0° to α and comparing them to the total intensity as shown in formula (3).

$$f_{miss}(\alpha) = 1 - \frac{I(\alpha)}{I(\pi)} = 1 - \frac{\int_0^{\alpha} I(\theta) \times \sin(\theta)\, d\theta}{\int_0^{\pi} I(\theta) \times \sin(\theta)\, d\theta} \qquad (3)$$

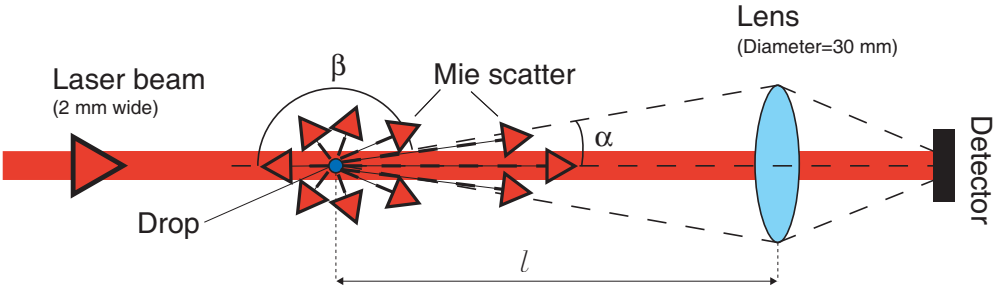

Figure 6. Principle of measurement of a single droplet

When light hits a droplet it will be scattered. However even light that pass in the vicinity of the droplet will be scattered, - this is referred to as the extinguishing efficiency, Qe [51]. In this case a little more than twice the light intensity incident on the droplet is scattered.

From the earlier considerations it can now be seen that the extinction coefficient σ_e is proportional to the number of droplets pr unit volume, area of droplets, extinction efficiency and fraction of scattered light not hitting detector.

$$\sigma_e = N \cdot A_p \cdot Q_e \cdot f_{miss} \qquad (4)$$

where:

N: number of droplets pr unit volume [m^{-3}]

A_p: area of the droplets [m^2]

Q_e: extinction efficiency [-]

f_{miss}: "miss fraction" [-]

The water concentration m''' can be described as:

$$m''' = N \cdot V_p \cdot \rho \qquad (5)$$

where:

N: number of droplets pr unit volume [m^{-3}]
V_p: volume of the drop [m^3]
ρ: density of water [kg/m^3]

This leads to the following relation for particle density m''':

$$m''' = \frac{2 \cdot d_p \cdot K_{ext} \cdot \rho}{3 \cdot Q_e \cdot f_{miss} \cdot L} \qquad (6)$$

d_p: diameter of the water drop [m]
K_{ext}: extinction, measured value [-]
ρ: density of water [kg/m^3]
Q_e: extinction efficiency [-]
f_{miss}: "miss fraction" [-]
L: width of spray [m]

There is considerable uncertainty with regards to the conversion constants and the chosen constants are explained in the following.

To find a representative droplet diameter, d_p, a droplet is required that will give the same miss fraction as the whole droplet distribution. In figure 7 the miss fraction is shown for a solid angle α, from 0 to 2°. The view angle of all the detectors, α_{mean}, have been measured to be about 1°, which is indicated as the vertical line in figure 7. This assumes that the droplet is in the centre of the spray, but if the droplet is further away or closer to the detector, this value can vary between 0.8° and 1.4° (α_{min} and α_{max}). These two values are also shown as vertical lines.

The overall miss fraction for the distribution of droplets is shown with the red line, dot and hyphen, which is relative close to the solid line, where the droplets have been fitted to a log-normal distribution.

Furthermore the miss fraction is shown for a droplet size of 20, 30 and 40 µm. For a detection angle of 1° it can be seen from the graph, that a droplet between 20 µm and 30 µm will give about the same miss fraction as the distribution of droplets. Therefore the representative droplet size has been chosen to be 25 µm.

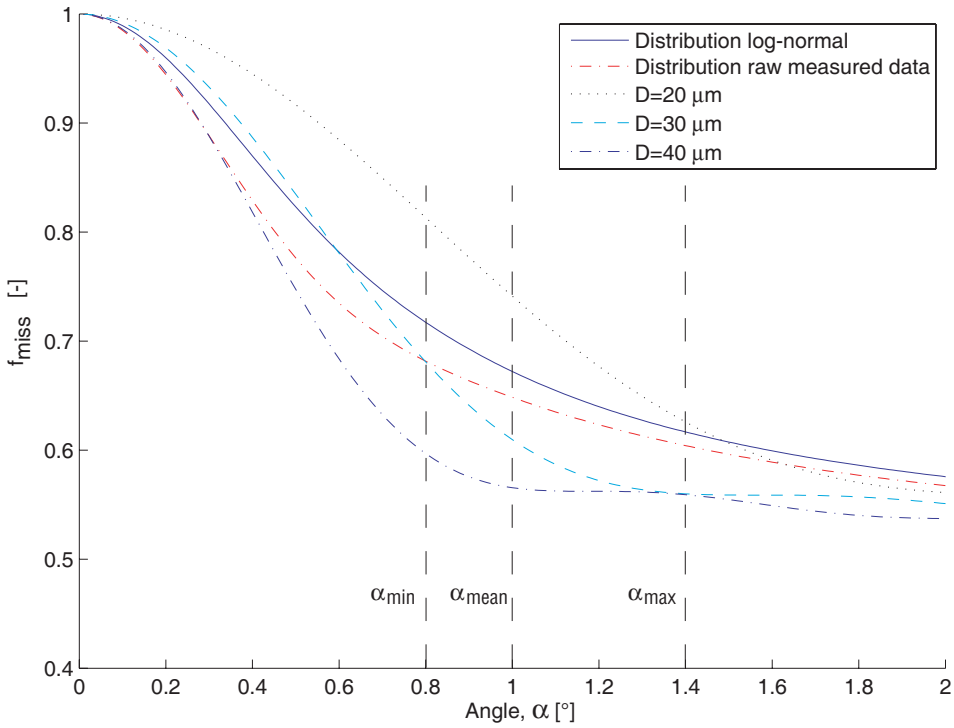

Figure 7. Miss fraction: fraction of scattered light missing detector.

Note that f_{miss} is very sensitive to the angle α in the range around 1° and had a detection angle of 1.8° been used instead, the dependence of f_{miss} on droplet diameter would have been reduced. The polarisation of the light has also be been accounted for, but this does not have any effect for angles below 10°.

The extinction efficiency, which is the light intensity scattered and absorbed by the drop to light intensity incident on the geometrical area of the drop, can be determined based on the drop diameter of 25 µm and

the wavelength of the laser (670 nm) by using MiePlot. It has been found to be 2.1 for this case – but it only varies slightly with droplet diameter.

The length L is the width of the spray and based on the traversing of the spray is was found to be approximately 400 mm in the middle. This value changes if measurements are made outside the centre line.

Transversing of spray and deconvolution

In order to create a 2D image of the water density at a given distance below the nozzle, the spray was moved horizontally in steps of 25 mm though the laser and detector array. This is shown schematically in the first part of figure 8.

In the experiments conducted, axial symmetry has been assumed and radial values of the water density have been found from intensity measurements through the spray. Several methods are available to reconstruct the 2–D image based on the measurements of the spray. The method by Bockasten (1961) is one of the first methods [52], but now modern algorithms used for Computerized Tomographic scanning can be used. These methods are outlined by Born & Wolf and in the principles of computerized tomographic imaging by Kak et al. [53, 54]. In the present study the method of Shepp and Logan has been used [55].

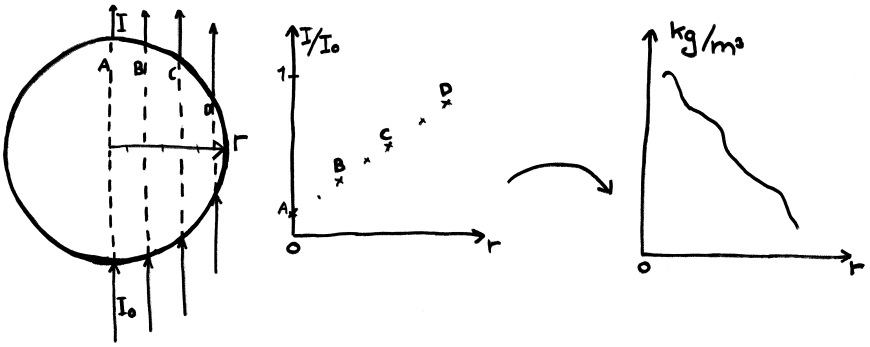

Figure 8. Conversion of measurement through spray to radial values of water concentration in [kg/m³]

Accuracy of tomography method

Almén and Irvert found that the accuracy of the method could be expected to be within ±25% [47], but in order to check that the values are within the right range the mass flow has been calculated and compared with the measured mass flow from the nozzle.

Assuming that the spray is circular and axis symmetric the total mass flow can be calculated by integration over the surface area shown in figure 9.

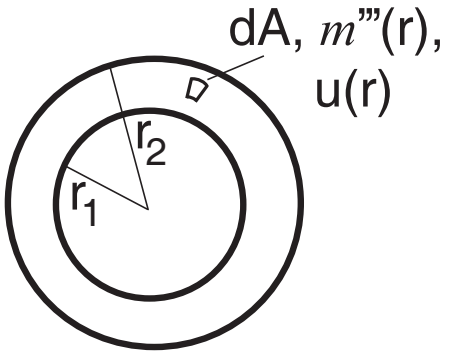

Figure 9. Integration of mass flow of water

$$d\dot{m} = m'''(r) \cdot u(r) \cdot dA$$

$$\Downarrow$$

$$\dot{m} = 2 \cdot \pi \int_{r_1}^{r_2} m'''(r) \cdot u(r) \cdot r \cdot dr \qquad (7)$$

$m'''(r)$: water concentration at radial distance r [kg/m^3]

u(r): velocity of water droplets at radial distance r [m/s]

For the integration in formula (7) the water concentration values are taken from the tomograhpic measurement and the velocities are taken from the PIV measurements. The PIV measurements are very symmetrical at the distances below the nozzle, where the water

concentrations were measured and therefore the values from the centreline to one side can be used.

Figure 10 shows a comparison of the measured nozzle flow (±1%) and the mass flow based on the tomographic technique combined with the PIV measurement. The error bars indicate the uncertainty of ±25% as found by Almén and Irvert [47]. It can be seen that from about 900 mm to 1300 mm below the nozzle the tomographic technique gives reasonable close results to the measured flow from the nozzle.

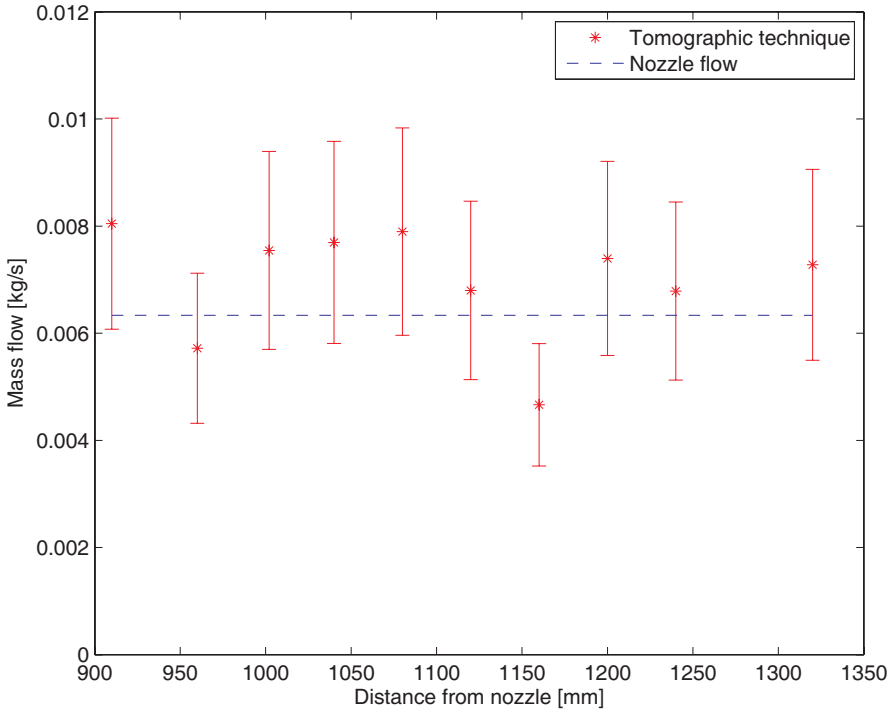

Figure 10. Calculated mass flow based on PIV and tomographic measurements compared with the actual nozzle flow at 10 different distances below nozzle in the no fire case.

Advantages, disadvantages & recommendations

Measurements with tomograhpic technique can give a 3-D picture of the water distribution in the spray. A qualitative picture of the spray is given, but if the droplets distribution is known also quantitative values can be given. By integration of the volumetric distribution with the velocity measurement (PIV) reasonable agreement with the mass flow from the nozzle was found. With the setup used here, axial symmetry is assumed, but it is not required by the method

3.3 Water density apparatus

Principle

The principle of the measurement relies on measuring humidity of air, which is a standard procedure. An air sample is continuously taken and heated to make the water in the air evaporate so that the relative humidity becomes less than 100%. Temperature and humidity is then measured, and from those the water concentration in [kg/m^3] can be determined.

Andersson and Holmstedt has given a detailed description of the instrument [46] and a brief summary is given here, based on figure 11. The air sample is taken in through a coiled electrical resistor filled with stainless steel wool (in the following referred to as the oven). The heated sample then passes a humidity meter, where the measurements can be made. A pump pulls the air through the instrument and to protect the pump, a cold trap and silica gel desiccant is placed before the pump as seen in figure 11.

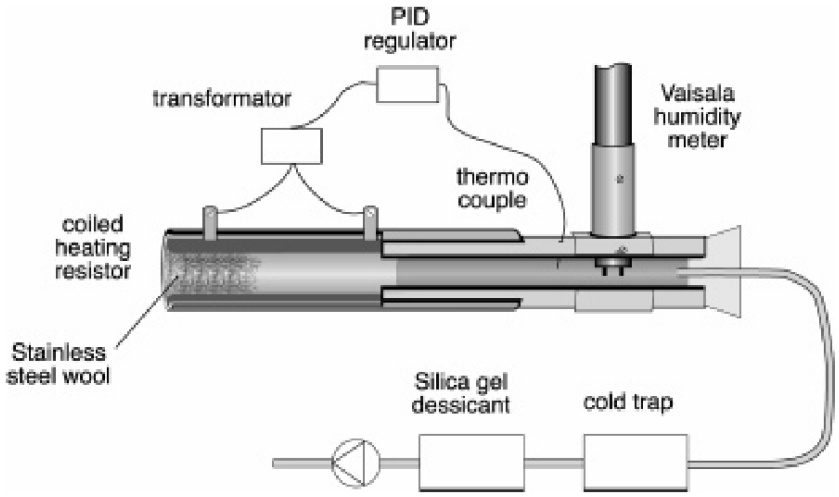

Figure 11. Water density apparatus used by Andersson and Holmstedt [46]

The instrument has previously been used to measure the water concentration in a fire room, away from the direct spray [46, 56]. In these experiments "total flooding" water mist systems were studied. The measured concentrations were around 50 g/m^3, and in this area the instrument performed well. The instrument was orientated horizontally as shown in figure 11.

In the present experiments the instrument was aligned vertically directly under the spray in order to measure the water concentration in the spray. Andersson and Holmstedt has recommended that the instrument is used outside the direct spray [46]. It was difficult to get reliable results and even during calibration the instrument gave very varying results. The reasons and possible remedy will be discussed below.

Isokinetically sampling

In order to collect a representative amount of droplets the probe should be located parallel with the gas flow streamlines and the velocity in the probe opening should be the same as the gas velocity [51]. Andersson and Holmstedt studied this for water droplets and found that water mist droplet are sensitive to the sampling velocity [46]. Too low sampling velocity overestimates the larger droplets and too high sampling velocity overestimates the smaller droplets.

Therefore when measuring directly in the spray, where the velocities are higher, the air flow has to be increased. This requires a pump with a higher capacity.

Higher water concentrations

For the instrument to perform well at higher water concentrations and higher flow rates, an oven with a higher heat input is necessary. This ensures that a constant temperature can be kept in the oven and the system remains stationary.

Orientation of instrument

Another important factor is the orientation of the instrument. If the instrument is orientated horizontally, the sides of the oven will help evaporation of the water. If the instrument is orientated vertically, as was the case for present experiments with high pressure water mist system,

most of the heat transfer occurs between the steel wool and the water droplets. Thereby the evaporated amount of water is dependent of how well the heat is transferred from the side of the cylinder to the wool in the middle of the cylinder.

New design

A new design of the instrument has been proposed, where water sampling is carried out through a longer tube and the instrument is placed horizontally as shown in figure 12, in order to measure directly in the spray. One problem is the amount of water, which is collected during the measurement. To avoid water entering the pump, it is necessary to cool the piping after the water content has been measured. Further an extra water collected container was added and shown in figure 12.

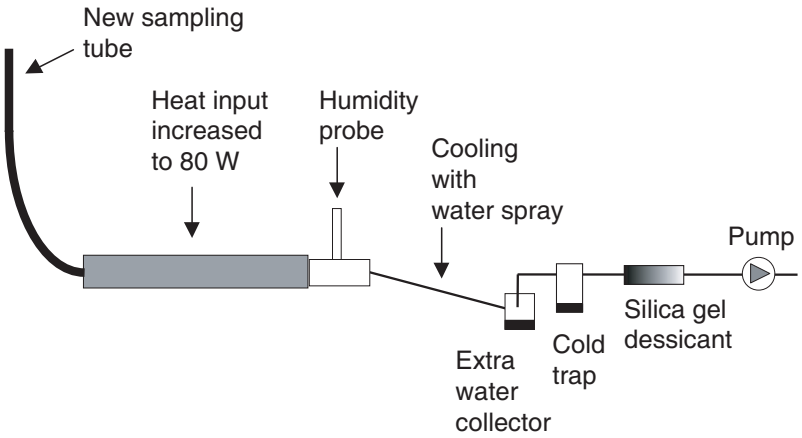

Figure 12. New design of water measuring instrument

Processing of measurements

Temperature is known and with humidity measured, the water density is easily determined.

Advantages, disadvantages & recommendations

The method directly samples the water, and is not dependant on assumptions of droplet size. It has the potential of becoming a relatively

inexpensive and robust instrument. However, due to the higher water contents compared to Andersson and Holmstedt, there were problems evaporating all the water. Furthermore, correct sampling can be difficult.

The prototype needs more work to address the above issues. Issues to examine are

- Higher power to evaporate all the water
- More time in the heater to evaporate all the water. Sampling should perhaps not be continuous.
- Ways of determining size of suction rate
- Ways of determining direction of sampling probe
- Closer study of sampling probe and hole size
- Isokinetic sampling

Chapter 3 Measurement technique for measuring water mist distribution (volumetric)

Chapter 4 Measured data from experiments

A series of measurements has been performed to provide an understanding of the spray pattern of water mist and subsequently examine the interaction with a fire. The data has relevance as a basis for simulations of the interactions of water mist and fire. The measurement setup involving the water mist interaction with a fire is shown in figure 1.

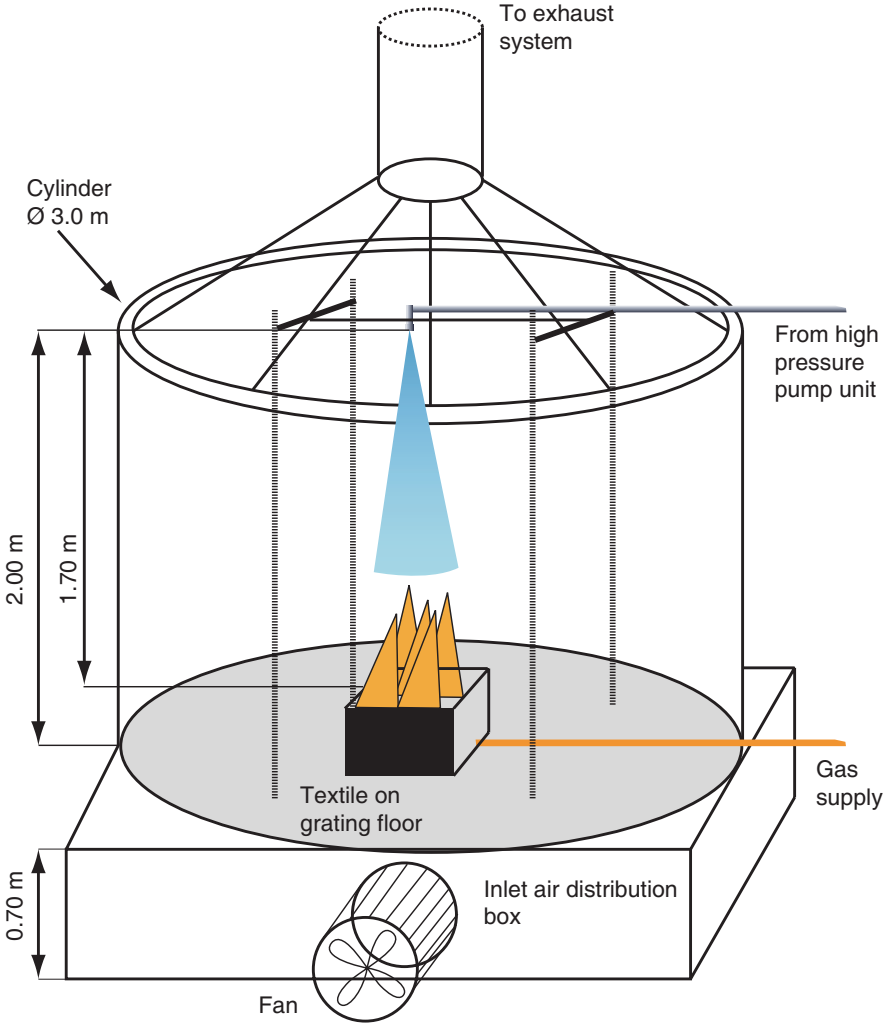

Figure 1. Experimental setup for measuring the interaction of water mist and fire used for PIV and tomographic measurements.

The fire size was chosen so that steady state conditions without extinguishment were achieved.

Measurements have been carried out on a hollow cone water mist nozzle and a full cone water mist nozzle, as shown in table 1.

Table 1. Details of hollow cone and full cone nozzle used in experiments

Spray type	Manufacturer and type	Spray generation process	Spray cone angle	Measured flow rate [l/min] @ 100 bar	Pressure (bar)	Water temperature
Hollow cone	Danfoss 1910	Atomisation	56°	0.38	100 bar	15°
Full cone	Lehler 212.085	Atomisation	72°	0.132	100 bar	15°

More details on measurement setup and methodology can be found in Paper 4 [29].

Several methods have been used for the measurements (see chapter 2 and 3). Results obtained by high speed camera, PDA, PIV and tomography are shown in table 2, which gives an overview over the conducted experiments.

Table 2. Overview over experiments with the positions that were measured

	Hollow cone, no fire	Full cone, no fire	Hollow cone with fire
High speed camera	Picture of spray	Picture of spray	
PDA	Velocity and diameter 25 to 500 mm below nozzle	Velocity and diameter 25 to 150 mm below nozzle	
PIV	Velocity 25 to 1400 mm below nozzle		Velocity 600 to 1400 mm below nozzle
Tomography	Water density 910 to 1320 mm below nozzle		Water density 910 to 1320 mm below nozzle

4.1 Hollow cone nozzle: Start up of spray

A series of pictures have been taken with the high-speed camera at the start-up of the hollow cone spray. The pictures are shown in figure 2b where the numbers indicate the distance below the spray nozzle in mm. The pictures show the development of the spray as the water is turned on. The pressure in the pipe is build up within 100 ms as shown in figure 2a, however there is no significant spray after this time and therefore this pressure build up has little influence. Initially the throw length is limited as the momentum from the water drops is transferred to the air and the droplets are decelerated. After 250 ms very little water is visible and after 300 ms the spray has only reached 300 mm. By now the momentum has been transferred and a downward air jet has been created. Therefore the water droplet can now move relatively fast down to 500 mm.

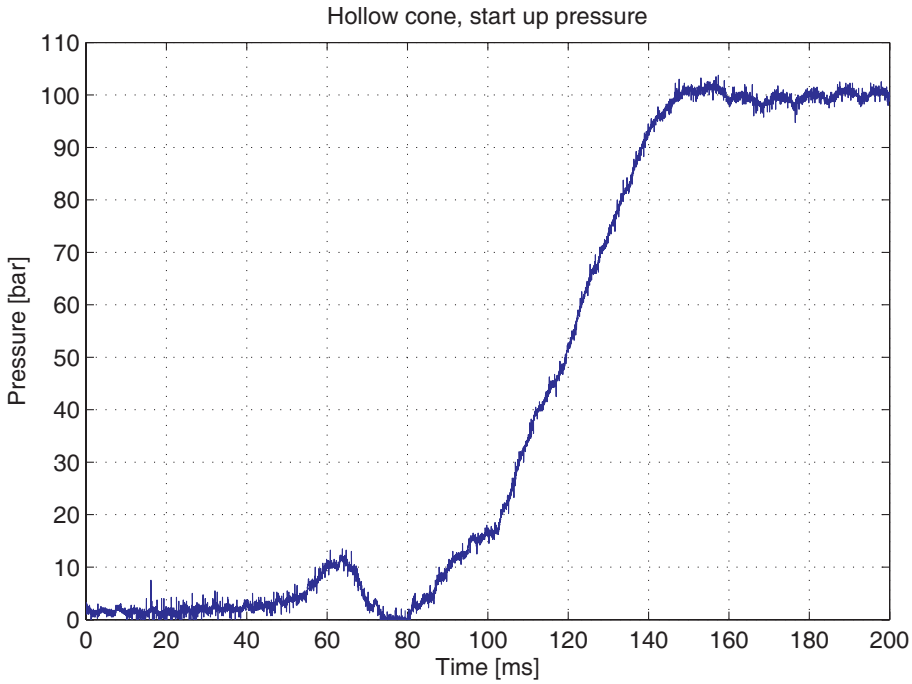

Figure 2a. Start of hollow cone spray, time for pressure build up

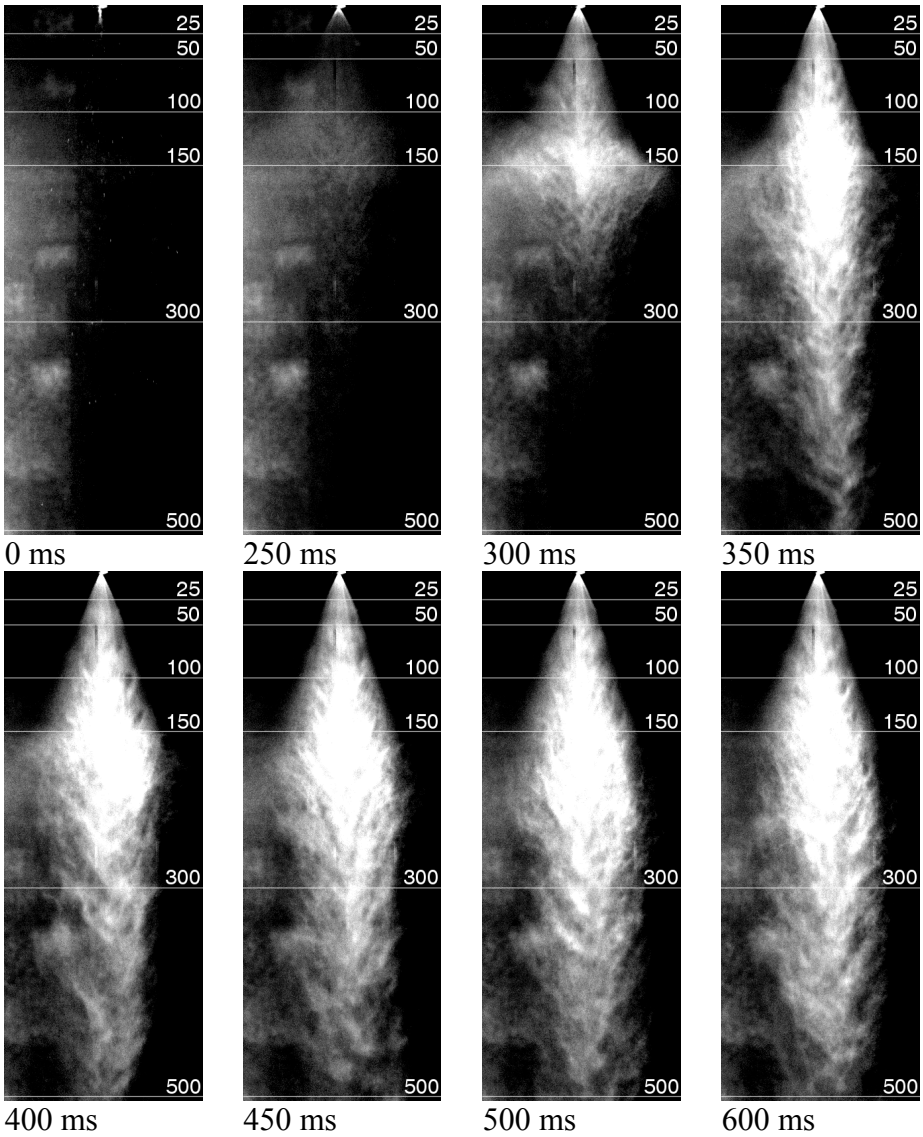

Figure 2b. Start of hollow cone spray. Exposure time 500µs. Numbers on figure are distances below nozzle in mm and the frames are 190 mm wide.

4.2 Hollow cone nozzle: Continuous spray

Pictures were also taken with the high-speed camera of a continuous spray of water mist from the hollow cone as seen in figure 3. It is interesting for the understanding of the physics involved in the water spray to look at the shape of the spray and the level of instability. It can be seen that the water comes out in a cone. Up to 50 mm from the nozzle, the cone is stationary and the patterns shown in all the pictures are very similar. Around 100 mm there are slight variations and from 100 mm to 150 mm there are pronounced variations, the cone collapses and the spray continues down vertically. It can be seen that flow from 150 mm and downward is quite turbulent with large variations. An angle has been drawn to help the visual inspection of the cone shape. It is not the spray cone angle and closer inspection of the area around the nozzle shows that the cone starts to bend slightly inward already at 50 mm.

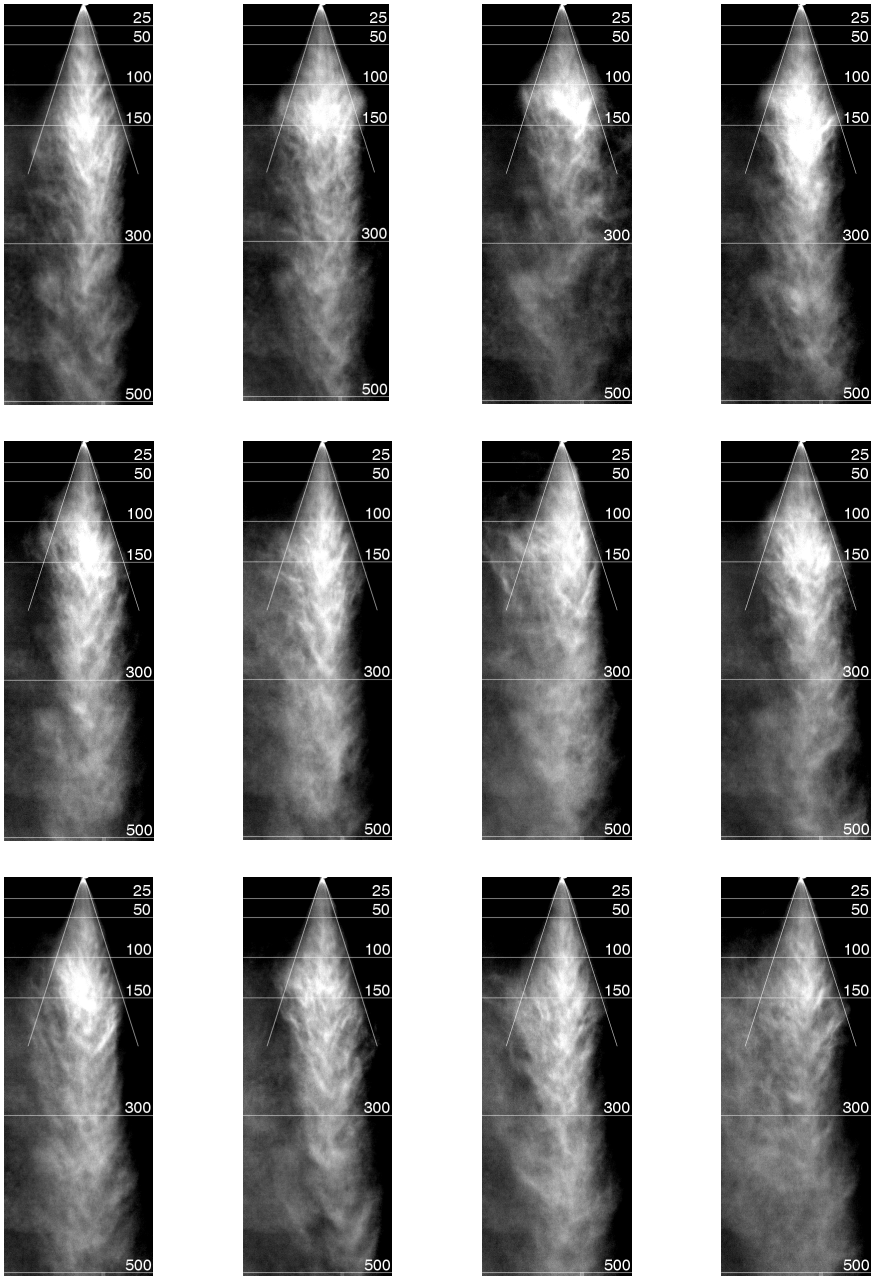

Figure 3. High-speed photography. Continuous spray, 1 s between every frame. Exposure time 500 µs. Numbers on figure are distances below nozzle in mm and the frames are 190 mm wide.

4.3 Visual inspection of the spray by characteristic droplets

To provide a better overview of the data obtained in the PDA measurements a methodology has been developed for drawing the spray pattern of a water mist spray. Here characteristic droplets are illustrated as circles, with diameters to scale. Furthermore, velocities are illustrated with arrows that are also drawn to scale, as illustrated in figure 4 below.

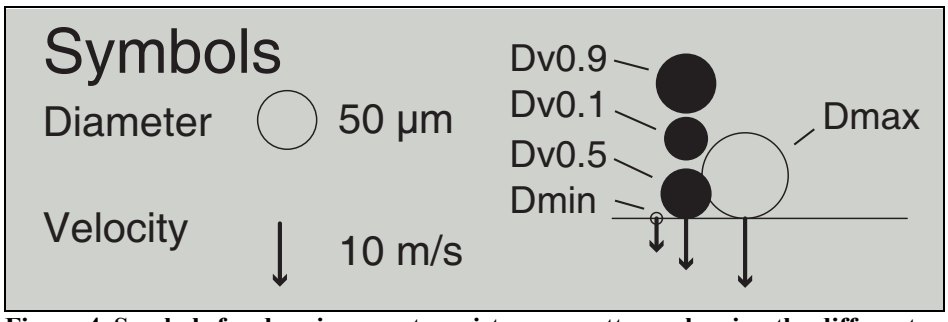

Figure 4. Symbols for drawing a water mist spray pattern, showing the different droplets characteristic. D_{min}, $DV_{0.1}$, $DV_{0.5}$, $DV_{0.9}$ and D_{max}. The velocity of the D_{min} droplet, $DV_{0.5}$ and D_{max} is shown with the arrow. The size of the droplet and the length of the velocity vector are to the scale shown to the left.

There are many different representative diameters that can be used to characterise a spray.
They help to describe different phenomena, for example, for surface area cooling the surface mean diameter is used. In the case where the amount of water determines the extinguishing capabilities, volume-weighted diameters are relevant. One problem in using a single value is that it doesn't describe the droplet distribution. A spray with a very wide distribution in droplet size may give the same volume weighted diameter as a spray where all droplets are of the same size.

Droplet size distribution has therefore been characterised by using the three representative diameters.

$D_{0.1}$: is the drop diameter where 10% of the liquid volume is in drops of smaller diameter

$D_{0.5}$: is the drop diameter where 50% of the liquid volume is in drops of smaller diameter, the mass median diameter (hereafter referred to as the mean droplet)

$D_{0.9}$: is the drop diameter where 90% of the liquid volume is in drops of smaller diameter

By using these diameters, both distribution as well as volume of drops, which for this application is the most important factor, are described.

Two other droplets are illustrated in figure 4, the maximum measured droplet, that varies in size from 33 to 70µm and the minimum droplet size from 3 to 8 µm. Droplet size of the largest droplet is illustrated whereas all the minimum droplets are all drawn with size 10 µm for practical purposes.
The velocities are illustrated for the minimum, maximum and mean droplet. In most cases, they will describe the relevant velocity range.

Figure 5 shows the results for the scan of spray and a point measurement 100 mm below the nozzle, where the mass mean diameters are nearly the same, but the distribution is very different. The scan of the whole spray shows that there is a large spread in droplet size, whereas in the point measurement the majority of droplets have the same size.

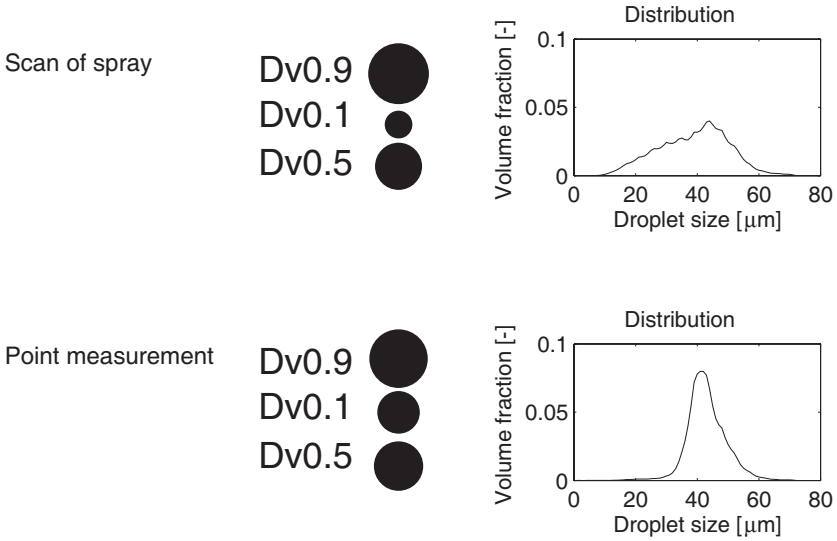

Figure 5. Two measurements on hollow cone nozzle with the same mass median diameter but different droplet distributions. (100 mm below nozzle, scan and 40 mm from centre)

The small droplets quickly transfer their momentum and adapt to the velocity of the surrounding air. In the graph in figure 6, it can be seen that a 10 µm droplet moving at 20 m/s in 10 m/s air flow decelerates to the air speed over a distance of only 10 mm. This means that the smaller droplets can be used to indicate the velocity of the air in the spray. The larger droplets of 70 µm will travel a distance of more than 200 mm before they have experienced the same slowdown. It is interesting to also look at this droplet and in particularly its velocity in comparison to the smaller droplets to see the spray pattern.

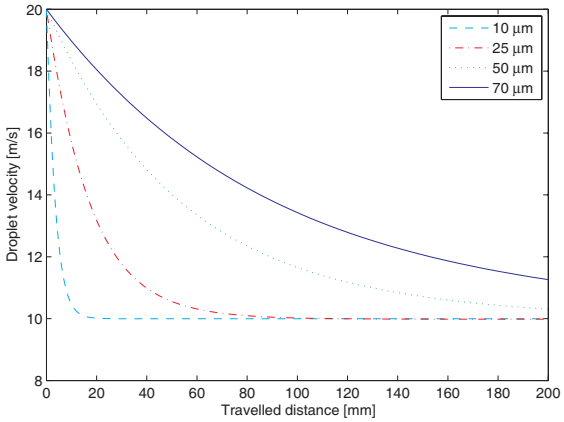

Figure 6 Calculation of slowdown of single droplets with initial speed of 20 m/s in an airflow of 10 m/s (Paper 4)

4.4 Hollow cone: Spray description

The characteristic patterns of the spray can be seen in figure 7. It has been found that the spray can be divided in 4 characteristic zones. These are described in broad terms here, with a more detailed analysis in the next section.

1) In the initial conical zone, the bulk of the water is in a stable cone around the nozzle. Here the largest droplets move at very high speeds. In the centre of the spray are very small droplets at slightly lower speed.
2) In the inflow zone, the large droplets at the edge of the spray have lost their momentum due to drag and collisions and have slowed down and increased in size. Some mean size droplets have moved from the edge of the spray to the centre, where the small particles move at high speeds. This happens as air is being sucked into the low pressure zone in the centre of the spray through the water sheet.
3) Around the transient zone, the spray collapses due to the low pressure zone in the centre of the spray. This results in a larger spread in particle sizes in the centre of the spray and a wider sheet with uniformly sized droplets moving at very slow speeds at the edges.
4) In the turbulent zone, there is considerable mixing and spray instability, which eventually causes droplet distribution and velocity throughout the spray to be the same. There are large and small droplets throughout the spray moving at the same velocity.

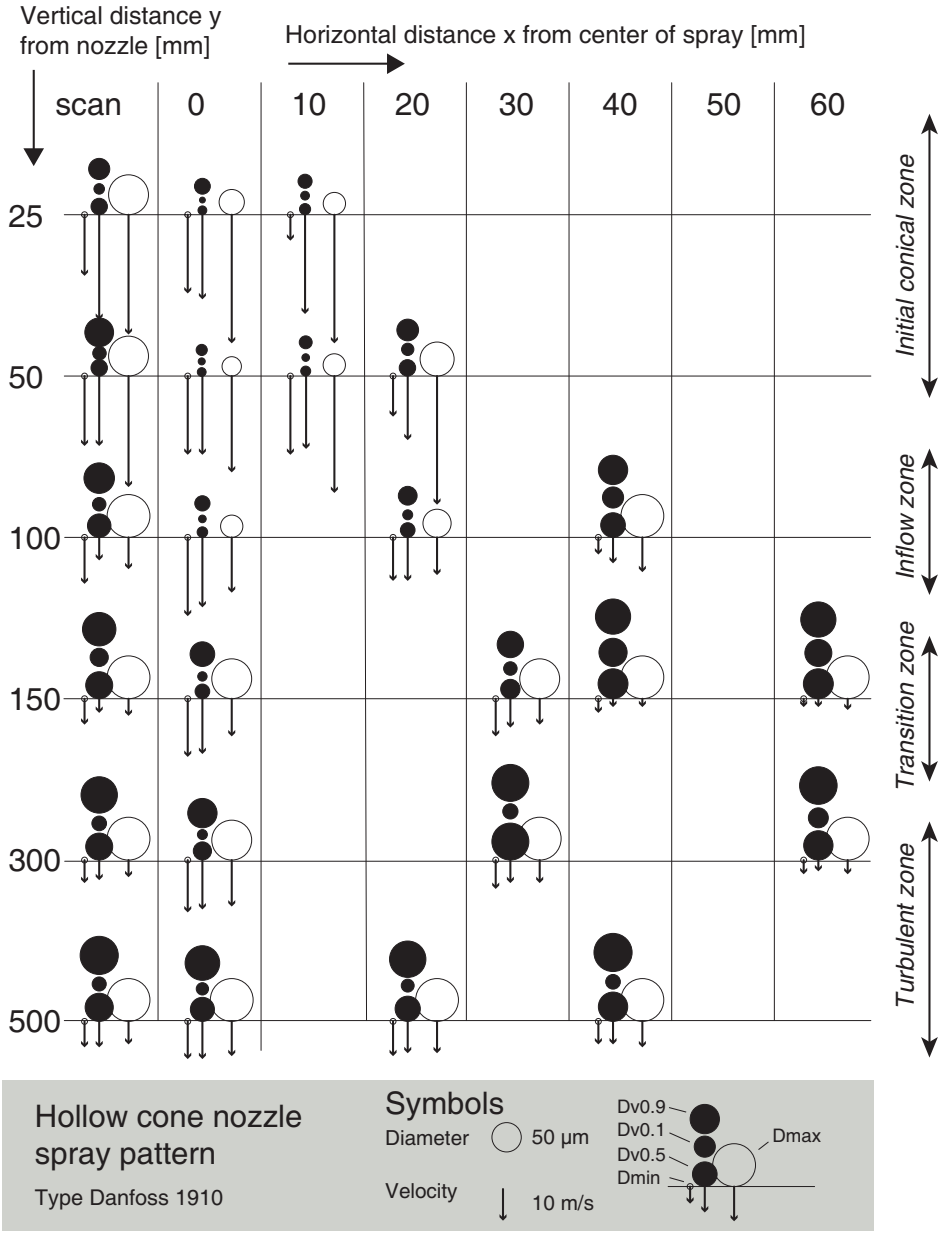

Figure 7 Droplet velocities and sizes for hollow cone spray (PDA measurements)

Initial conical zone: 25 mm & 50 mm

The initial conical zone is characterised by a stable shape, where the bulk of the spray is in a cone around the nozzle. The scans compared with the point measurements at 25 and 50 mm below nozzle indicates that the bulk of the water is in a cone, which consists of the largest droplets.

In figure 8 the velocity profile from the PIV measurements also indicates that the spray at 25 mm is wider than the PDA point measurement at 10 mm from centre. The same is the case for measurements 50 mm below the nozzle. Note that the velocity profile from the PIV measurements indicate that the spray pattern is not completely symmetrical.

The larger drops in the cone have the highest speed as they are decelerated slower than the smaller drops. In the centre of the cone are very fine drops moving at high speeds. A low pressure at the centre of the cone can be expected to be created by the fast moving water curtain.

The mean droplet size for the entire plane increases from 28 µm to 35µm as the faster large droplets catch up with the smaller. The speed of the mean droplet reduces from 35 m/s to 23 m/s over this distance, due to drag and possibly energy lost in drop collisions.

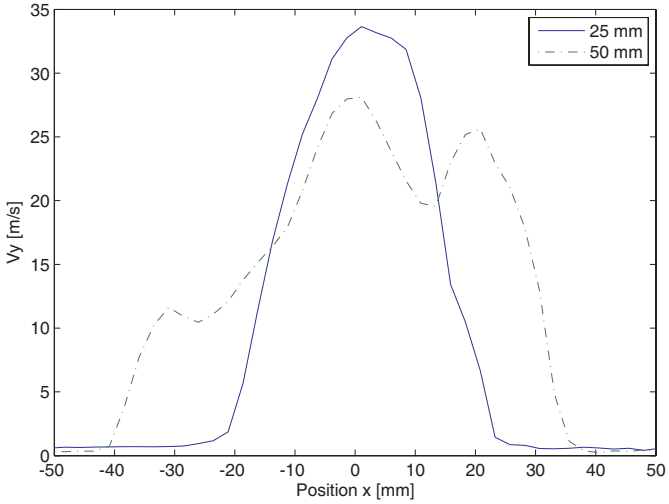

Figure 8 Velocity profile for hollow cone nozzle at 25 mm and 50 mm below nozzle

Inflow zone: 100 mm
At the edge of the spray, droplets have now been decelerated and move much slower at only 8 m/s, whereas in the centre, the mean drops are moving at 26 m/s.

At this stage a change happens so that the largest particles in the centre of the spray start moving slower than the smaller. Furthermore, the size distribution in the centre is changed and there are more larger droplets. It is likely that these drops have come from the edge of the spray. Due to the lower pressure created in the centre of the spray, air could be sucked in through the water sheet and this air will transport small to middle size droplets from the edge to the centre of the spray.

The edge of the spray is now dominated by relatively evenly sized larger particles. Only smaller droplets have been sucked to the centre and the majority of the spray is still at the edge.

Droplet size for this level has increased again so that the mean droplet is now 40 μm and moving at 7 m/s.

Transition zone 150 mm:
Around 150 mm below the nozzle, the cone collapses, as was seen on the high speed pictures.
At 40 mm and 60 mm from the centre, large drops around 50 μm appear. Drop sizes here are quite uniform, and the speed is very low, only a few m/s.

The bulk of the water is no longer only in the edge of the spray. The scan shows that drops within dv0.1 and dv0.9 must originate from the centre as well as from the sides of the spray.

In the middle of the spray, 0 mm and 30 mm from the centre, larger droplets now appear (dv0.9~45 μm) and there is a wide spread in drop diameters here. The larger drops move at slower speeds than the air velocity, which is around 19 m/s (the speed of minimum droplets).

Turbulent zone 300 mm & 500 mm:

In the high speed pictures, it can be seen that the spray is quite turbulent, changing in size as well as placement at these locations. At 300 mm from the nozzle, the spray pattern now changes so that there is a wider spread in droplet sizes throughout the spray. There is however still a tendency to larger, slower drops at the sides and smaller, faster drops in the centre. Drop speeds level out so different sized drops at the same location move at approximately the same speed.

At 500 mm from the nozzle, the spray is fully mixed and drop distribution is the same in the centre and at the sides of the spray. Drops at the same location move at the same speed. The velocity profile has levelled out, as droplets in the centre have decelerated to only 12 m/s.

The mean droplet size in this fully developed spray is 48μm and 10 % of the volume consists of droplets smaller than 24 μm whereas 90 % consist of droplets smaller than 65 μm.

4.5 Full cone nozzle: Start up of spray

The pictures in figure 9b show the development of the spray as the water is turned on. The water flow of this spray is only a third of the hollow cone nozzle and the pressure in the pipe builds up more slowly (200 ms) as seen in figure 9a. In spite of this, water spray moves faster downwards, probably because the water droplets are more concentrated in the middle. Within 300 ms the spray has nearly reached 500 mm. The spray cone stops at approximately 100 mm and droplets continue downwards in a slightly slimmer jet.

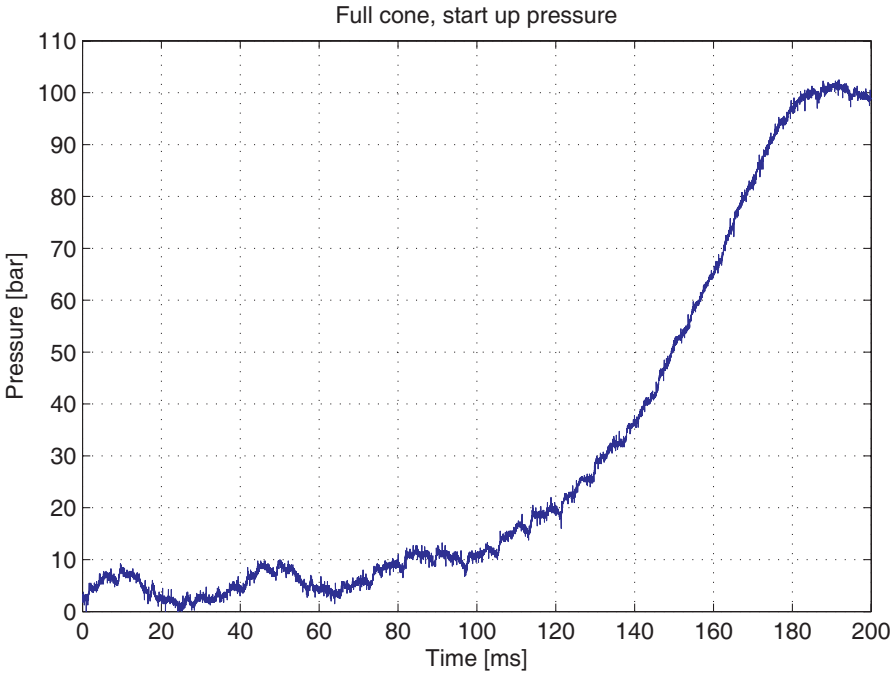

Figure 9a. Start of hollow cone spray, time for pressure build up

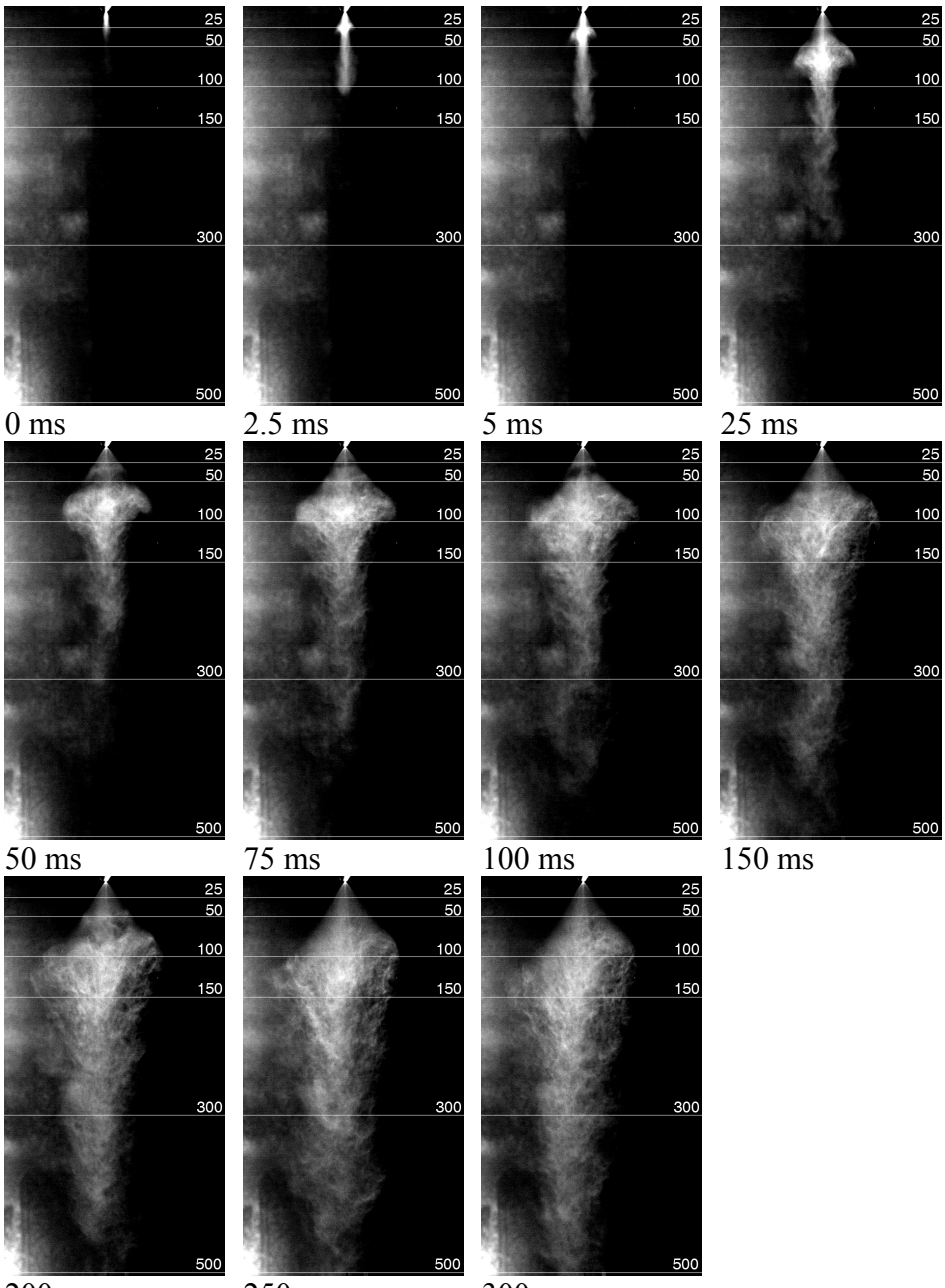

Figure 9b. Water mist spray from full cone nozzle. Numbers on figures are distances below nozzle in mm and the frames are 275 mm wide.

4.6 Full cone nozzle: Continuous spray

The pictures of the full cone nozzle spray in figure 10 are not as clear as those for the hollow cone nozzle, as they were taken with a shorter exposure time. Furthermore, they have been taken over a short time period. However, it can still be seen that the spray is wider than for the hollow cone. Furthermore, the change from outwards to downwards direction happens earlier. It appears this already takes place at 100 mm.

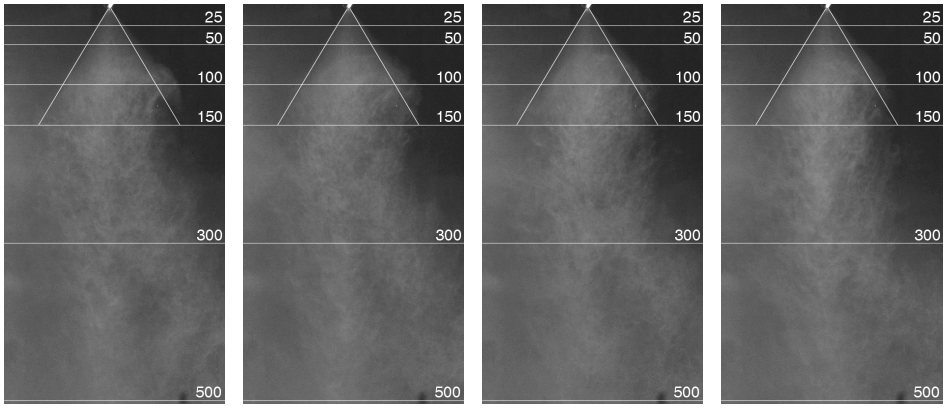

Figure 10. High speed photography. Continuous spray, 0.1 s between every frame. Exposure time 250 µs. Numbers on figure is distance below nozzle in mm and the frames are 275 mm wide..

4.7 Full cone: Spray description

Measurements of full cone spray with PDA have only been conducted down to 150 mm below the nozzle, as shown in figure 11. The same four zones as in thehollow cone can be observed, however the break-up happens closer to the nozzle, around 100 mm.

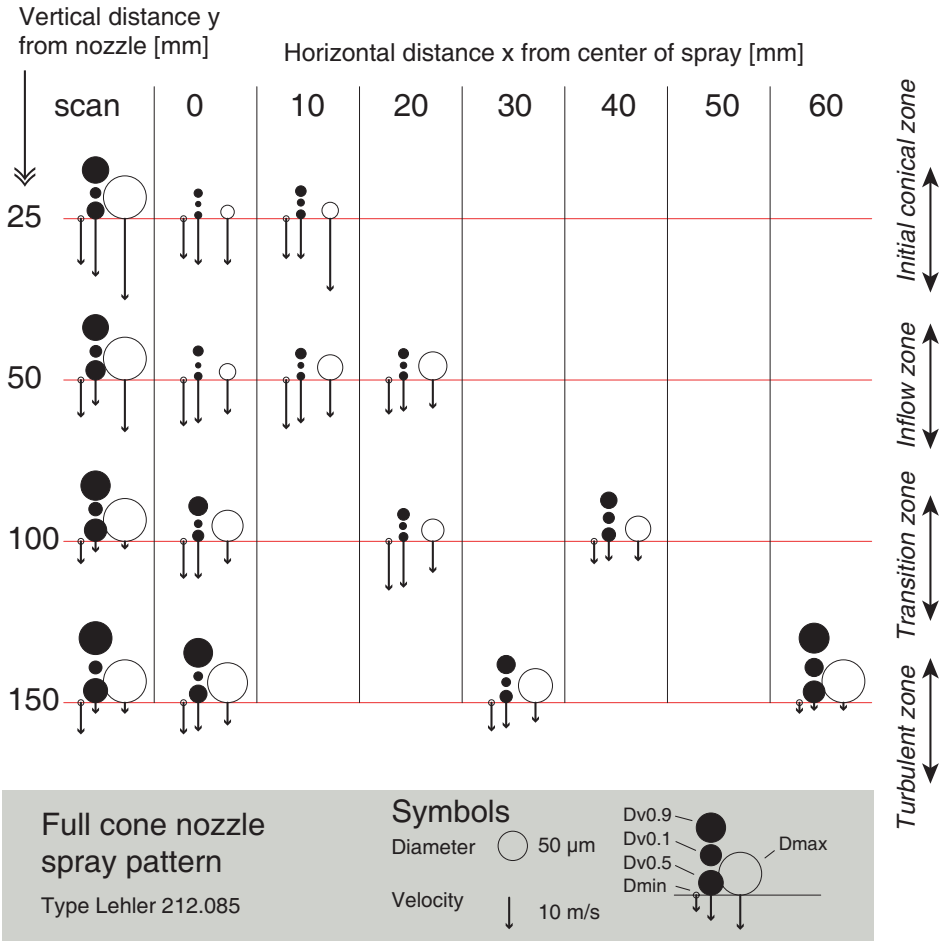

Figure 11 Droplet velocities and sizes for full cone spray (PDA measurements)

Initial conical zone: 25 mm

Even though it is a full cone spray, the scan indicates that the bulk of the spray is in a cone around the nozzle. The larger droplets that appear in the scan are not found in the centre and 10 mm from centre.

The larger drops in the cone have the highest speed, as they are decelerated more slowly than the smaller drops. There are very fine drops in the centre of the cone. The PIV measurements in figure 12 show very high velocities in the centre approximately 25 mm from centre, where no PDA point measurement was made.

The mean droplet is 29 µm and moving at 19 m/s. It is the same mean droplet size as for the hollow cone, but the velocity is lower.

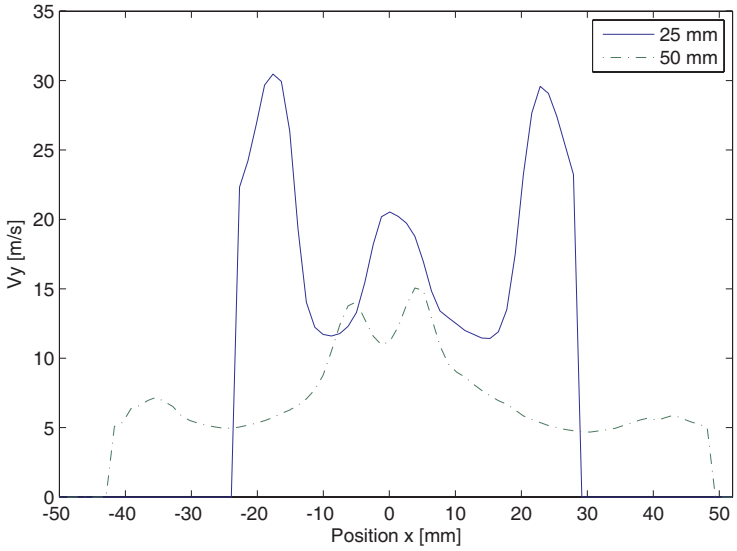

Figure 12 Velocity profile for full cone nozzle at 25 mm and 50 mm below nozzle

Inflow zone 50 mm:

At this stage, mean sized particles in the measurements start moving slower than the smaller particles. The few very large particles of 73µm still have a high momentum and move fast at the edge of the spray. Size distribution in the centre is very even, but the maximum particle size has increased, possibly because a few larger drops have moved inwards.

At the edge of the spray, droplets have now been decelerated and move much slower, only about 10 m/s. The edge of the spray is presumably still dominated by relatively larger particles (see scan). Hence it is likely that only smaller droplets have been sucked to the centre and the majority of the spray is still at the edge. Droplet size has increased, so the mean droplet is 33 μm moving at 8 m/s.

Transition zone 100 mm:
Around 100 mm below the nozzle, the cone collapses, as was seen on the high speed pictures. In the middle of the spray, 0 mm and 20 mm from the centre, larger droplets now appear and there is a slightly wider spread in drop diameter here. The larger drops move at slower speeds than the air velocity, that is at around 12 m/s (the speed of minimum drops).

The edge of the spray has become wider. The largest drops in the bulk of the spray still cannot be seen in the point measurements. However, the scan shows larger droplets.

The mean droplet has increased to 38 μm, moving at only 3 m/s.

Turbulent zone 150:
In the high speed pictures, it can be seen that the spray is quite turbulent, changing here in size as well as placement. The spray pattern now changes so that there is a wider spread in droplet sizes throughout the spray. There is however still a tendency to larger, slower drops at the sides and smaller, faster drops in the centre.
Interestingly, it can be seen that the smallest drops were found at a distance of 30 mm from the centre. Drop speeds level out, so different sized drops at the same location move at approximately the same speed.

To get measurements at a fully mixed spray where the droplet distribution was the same across the spray, observations would have to be made further down in the spray.

4.8 Hollow cone: Velocity measurements in spray with no fire versus spray with fire.

The vertical velocity profiles have been measured with PIV from 600 mm to 1300 mm under the hollow cone spray both with and without a fire present. Figure 13 shows the interaction of the water mist and the fire during, when conducting the PIV measurement.

Figure 13. Interaction of water mist and fire during PIV measurements

The results can be seen in figure 14.

It can be seen from the measurements that the velocity is highest in the centre of the spray, where the velocity difference between droplets and air is small and inflow of surrounding air is limited. The velocity profile becomes broader further away from the nozzle. The spray bends slightly to the right. Maximum velocity reduces from 5.5 m/s at 600 mm to 2.5 m/s at 1300 mm below nozzle.

The influence of a fire on the velocities can be seen from the dotted lines. It influences velocity all the way up to 600 mm below nozzle, 1100 mm above the fire. Here the fire reduces the maximum downward velocity to nearly half, from 5.5 m/s to 2.5 m/s.

The neutral plane, where the water mist is in balance with the fire, is about 1100 mm below the nozzle. Below this plane, water droplets are moving upwards instead of downwards, due to the buoyancy of heated gasses. At 1300 mm there is an upward velocity of approximately 0.5 m/s

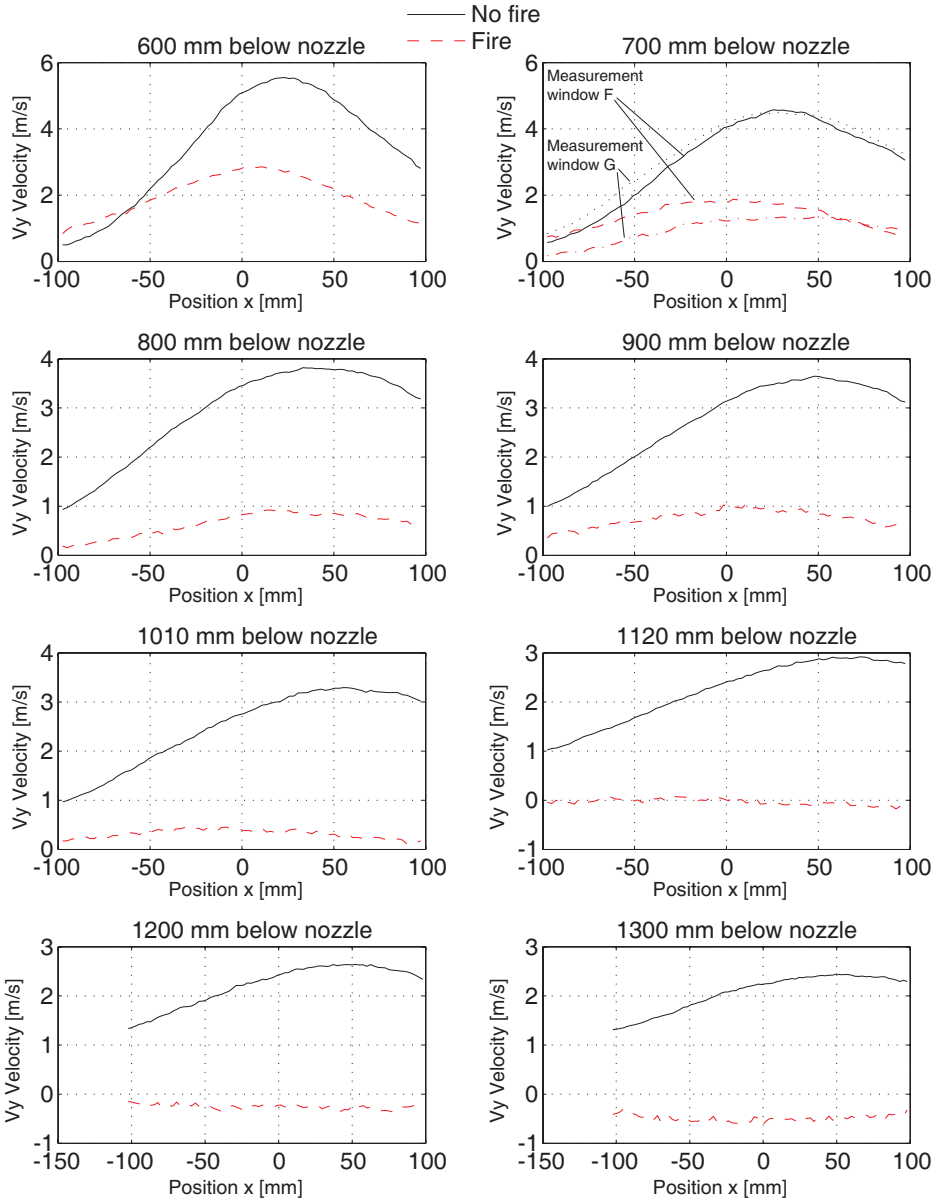

Figure 14. Comparison of average velocity profiles of water mist measured with PIV, with and without fire below the nozzle.

Velocity vector fields from PIV measurements with fire

Figure 15, 16 and 17 shows the averaged measured vector field at different distances below the nozzle. It can be seen from the experimental results that where the buoyant plume and water mist jet interacts that the velocities goes horizontal outward. Further it can be seen that the plume is not symmetric and the velocities points to the left in figure 17. The cause could be that the velocities were measured outside the centre plane.

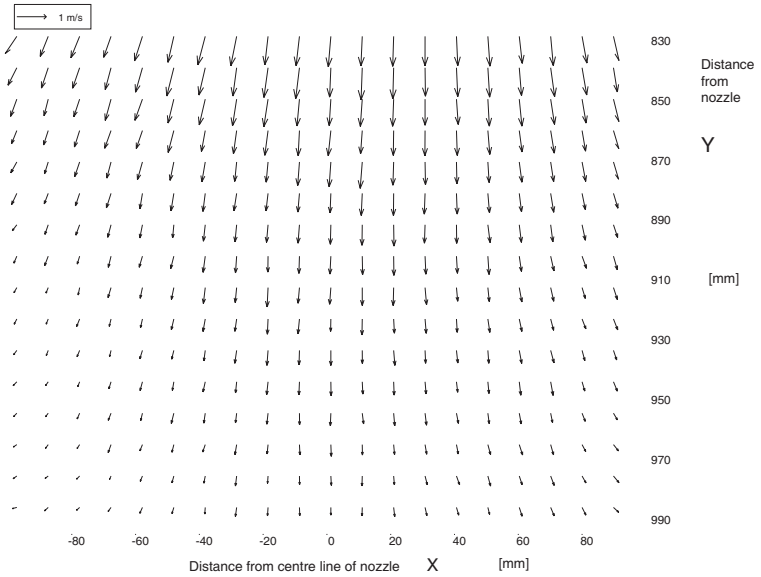

Figure 15. Vector field from measurement with PIV, fire, 830 mm to 990 mm below nozzle

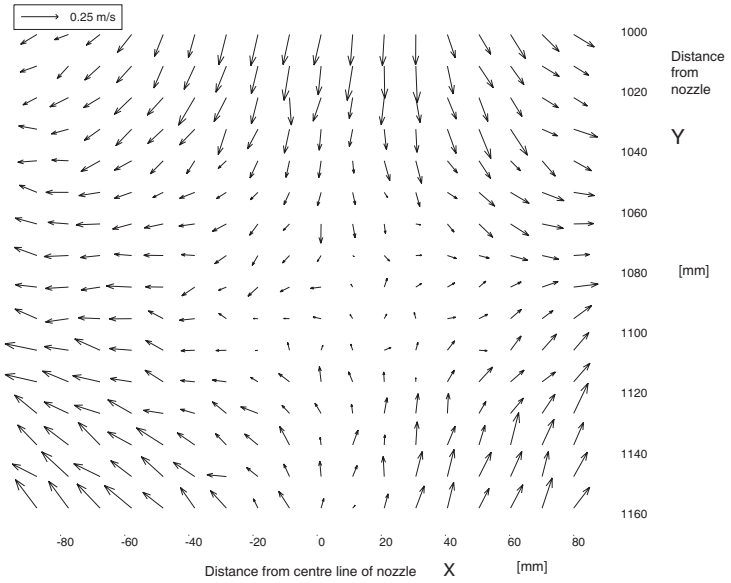

Figure 16 Vector field from measurement with PIV, fire, 1000 mm to 1160 mm below nozzle

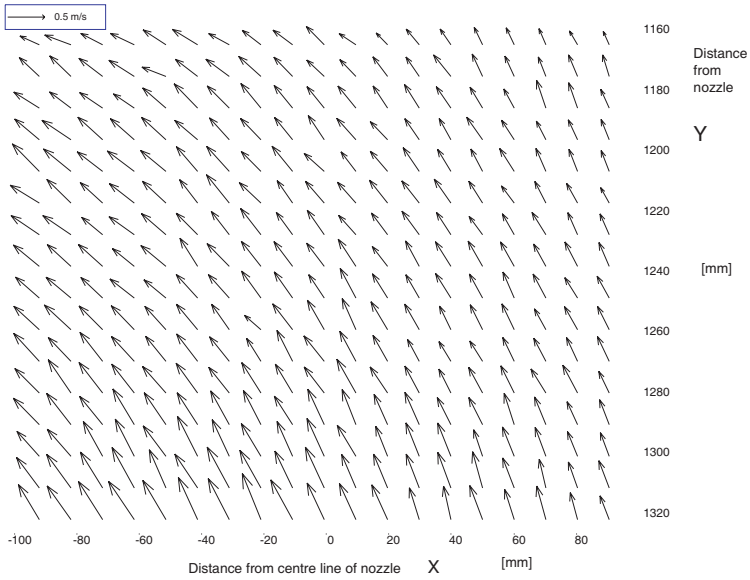

Figure 17 Vector field from measurement with PIV, fire, 1160 mm to 1320 mm below nozzle

4.9 Hollow cone: Water concentration measurements in spray with no fire versus fire

The water concentration of the spray has been measured with tomography at distances from 910 to 1320 mm below nozzle, as shown in figure 18. The results show large variations and some measurements, such as zero water contents in the centre, are clearly not true. Despite the large uncertainties with this measurement method, control calculations of the total water flux have shown results within 25%, as shown in chapter 3.

The water concentration in the spray with no flame shows that water concentration at the centre reaches a maximum of around 0.1 kg/m³. Moving down the spray, the water concentration profile levels out and water becomes relatively evenly distributed over the area, as can be seen in the graph of water concentration at 1320 mm below nozzle.

The water concentration in the spray with flame already reduces at 900 mm below nozzle. And, with some minor variations, there is a general trend of lower water content, down to 1240 mm where the water is nearly gone. Thus no water will reach the surface of a fire situated 1700 mm below the nozzle. No surface cooling will take therefore place and all extinguishment will be as flame cooling. Furthermore, it can be seen that fire extinguishment is not possible, as the water content is below the required 160 g/m³ for flame extinguishment of a diffusion flame [6, 19, 57].

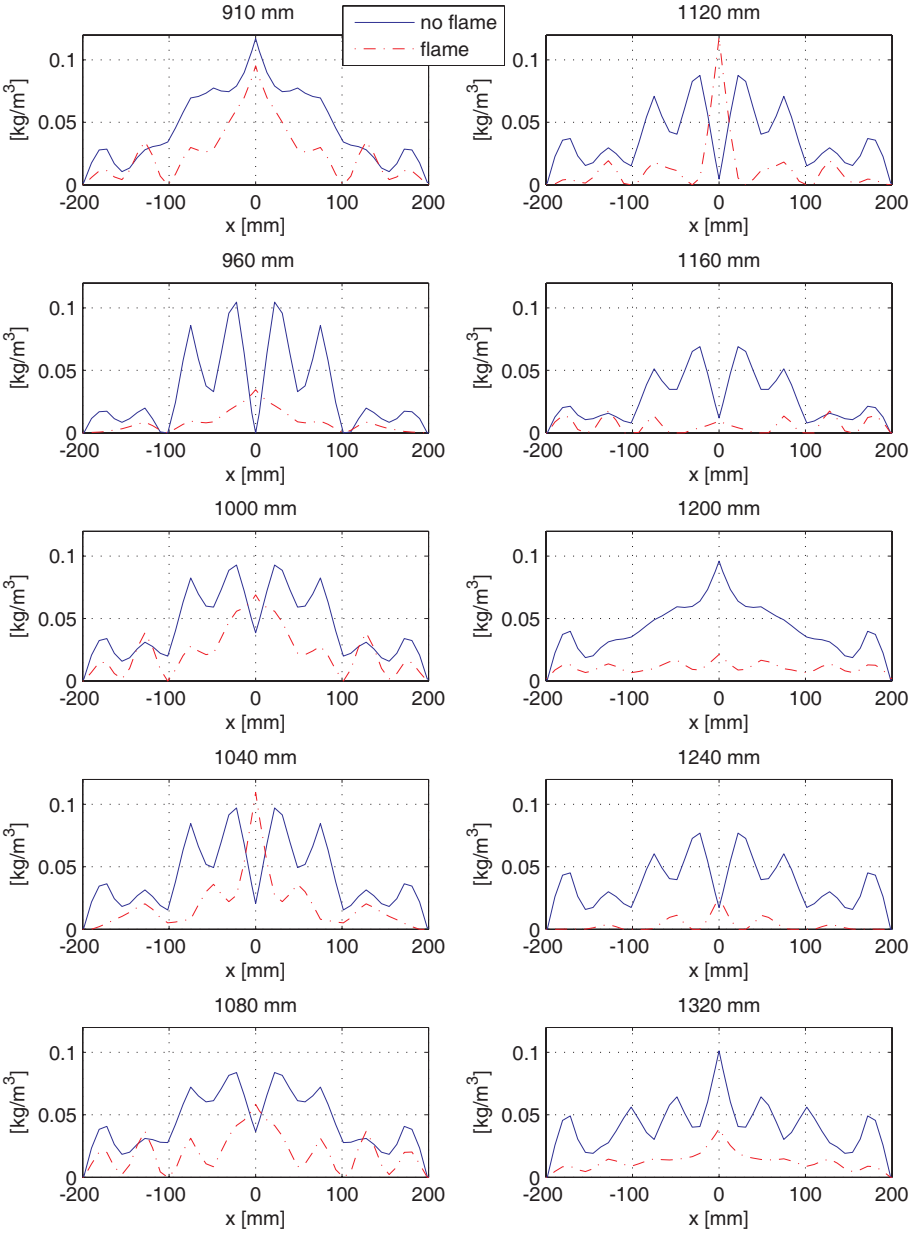

Figure 18. Distribution of water in hollow cone spray at different distances below nozzle

Chapter 4 Measured data from experiments

Chapter 5 Modelling of water mist with CFD

In the introduction simple models for modelling water mist was introduced, but the general recommendation for the calculation of water mist is to use CFD-models that solve the momentum equations, as the flow in the room can be crucial on the effect of the water mist system. This flow is influenced by the outlet conditions at the nozzle, the fire and the physical layout of the room. Several codes for CFD simulations of fires are available such as Fire Dynamics Simulator (FDS), CFX and SOFIE (Simulation of Fires in Enclosures) [58-60]. The various programs have some differences with regards to the models available for modelling turbulence, particles, fire and heat transfer. Some of the key differences will be discussed in the following with emphasis on FDS 4.07. FDS 4.07 has been the primary tool for simulation of water mist in this work.

5.1 Modelling of turbulence

CFD codes can grossly be divided in three groups based on the way they model turbulence: Reynolds Average Navier Stokes (RANS), Large Eddy Simulations (LES) and Direct Numerical Simulation (DNS). In general LES and DNS puts higher demands on the computer and have mainly become accessible for fire simulation within the last 10 years. Paper 3 has a more thorough discussion of this subject [27].

Most commercial CFD codes are RANS models, where the velocities are split into a mean velocity component and a fluctuating part. One such code is CFX with its primary focus on RANS modelling, - though there is a LES model available in the code as well [59]. However, the LES model in version of CFX (10.0) used in this study cannot handle particle transport [59]. SOFIE, which has been widely used for fire modelling, is a non-commercial code and it also uses the RANS approach [60].

The Fire Dynamic Simulator (FDS) developed at National Institute of Standard and Technology is a freeware program that is specifically developed for fire modelling [58, 61]. It is widely used by fire consultants in Denmark and Sweden and has in some way become a sort of a de facto standard for fire modelling. The turbulence models in FDS

are either LES or DNS, but for larger scale application only LES is a feasible option, as DNS requires a very fine resolution of the grid. In the LES model in FDS the transient larger eddies are modelled directly and the eddies smaller than the grid are modelled in a subgrid model using the Smagorinsky model [58]. Ideally the LES model should overcome some of the problems with RANS models, where the turbulence is modelled using empirical relations (like the k-ε model), which is sensitive to the scenario. In practice some of the problems are retained, when doing full scale fire modelling, as the grid has to be coarse due to limitations in computer capacity. The consequence is that a large amount of the turbulent energy is handled by the empirical subgrid model instead of being modelled directly.

5.2 Modelling of particle transport

The modelling of particles transport can be done in two different ways with CFD. Either the Euler-Euler method suited for very dense sprays. Here the particles are modelled as a gas phase, which have the properties of a given particle size. Therefore in order to model a distribution of droplets sizes several gas phases of droplets needs to be used.

The other approach is the Euler-Lagrangian method, where the trajectories of a representative number of droplets are modelled and the momentum is transferred between the two phases using the particle-source-in-cell method [62]. The handling of large momentum exchange between the gas phase and the particulate phases are treated in paper 5, [63].

The Euler-Lagrangian model is used in FDS. The lagrangian particle tracking model in FDS do not include droplet collision or break-up of droplets, but it includes a semi-empirical model for the evaporation of the droplets[58].

FDS has built-in sprinklers, where the initial droplets velocity has been measured for a number of sprinkler heads. This surpassed the models, which are available in more simple models. David Sheppard have in his Ph.D. thesis [64] measured the droplets characteristics of a great number of sprinklers, which are available as separate files in FDS.

Water mist calculations has in this work been carried out in FDS and compared to the experimental results. In the following the models used in FDS is described, and this description based on version 4.07 of FDS [58].

5.3 Fire modelling in FDS

The release of fuel can in FDS be controlled by a fixed amount of fuel leaving a unit area or be controlled by the heat of vaporization [58]. In the first case there is no feedback from the flames on the fuel surface, where the feedback from the flames is considered in the later case.

The combustion model in FDS is a mix is burnt combustion model [58]. This model leads to immediate combustion, if fuel and oxygen are present in the same cell. This can lead to, that too much energy is released in a single cell. Therefore FDS uses an approach where excess energy is distributed across the entire flame zone. In some cases this will lead to an unrealistic temperature distribution in the flame, which again influences the calculation of radiation, which is highly temperature depend. McGrattan et al. specifically specifies that care must be taken, when trying to model suppression, like water mist [61]. In this work the amount of water has been too low to suppress the fire and the above-mentioned problems are of lesser concern.

5.4 Heat transfer model in FDS

Below is a brief description of the heat transfer models in FDS 4.07 based on the FDS reference guide [58].

Radiation model
: Solves the Radiative Transport Equation (RTE) using the discrete ordinance method

Convection
: Uses empirical correlation to model the heat transfer, as the grid at the surfaces is not resolved sufficiently.

Conduction

Uses the full transient Fourier one-dimensional heat transfer equation to model the heat transfer in the wall. The walls can only consist of a single material.

5.5 Simulations of water spray by other researchers

The majority of researchers uses the Lagrangian approach for simulation of water mist, but Grant has in a recent study demonstrated that both approaches are feasible [65].

Studies by other researchers have mainly been feasibility studies, which demonstrated that it is possible to model sprinklers spray. Lesser attention has been given to the validation of the models with experimental results. A few examples are given below.

In the study by Sinai et al., CFX version 4.3 was used to study the interaction between a spray and a pool fire [66]. They used the k-ε turbulence model (RANS) and the Lagrangian method was used to model the particle motion. The start parameters for the droplets, were taken from experimental results. They concluded that the results were sensitive to the grid size, but no comparison was made with experimental results.

In the study by Hua et al. a Lagrangian model was used to study the interaction of a single water spray and a fire, but no comparison was made with experimental results [67].

Trelles et al. reported good results when comparing a high pressure nozzle with experiments using a LES model [68]. They did an isothermal calculation with FDS 4.0, where the droplets were injected perpendicular to a sphere having a radius of 0.20 m. The sphere was divided into 1056 solid angles and 56 had non-zero flows. The flux at a distance of 1 m below the nozzle was compared with experimental results and a grid having a resolution of 75 mm adequately reproduced

the measured results. Using a grid having a coarser resolution of 150 mm and 300 mm could not reproduce the results.

Another problem is the lack of detailing in both the modelling and the experimental work, when numerical results are compared with experimental results. In an initial report, which this author was involved in, a concealed fire was modelled in FDS and compared to experimental results [28]. The modelling of the nozzle was crude and the water would not reach the concealed fire, - further the combustion model did not take into account the evaporated water. This resulted in an over prediction of the smoke layer temperature as seen in figure 1.

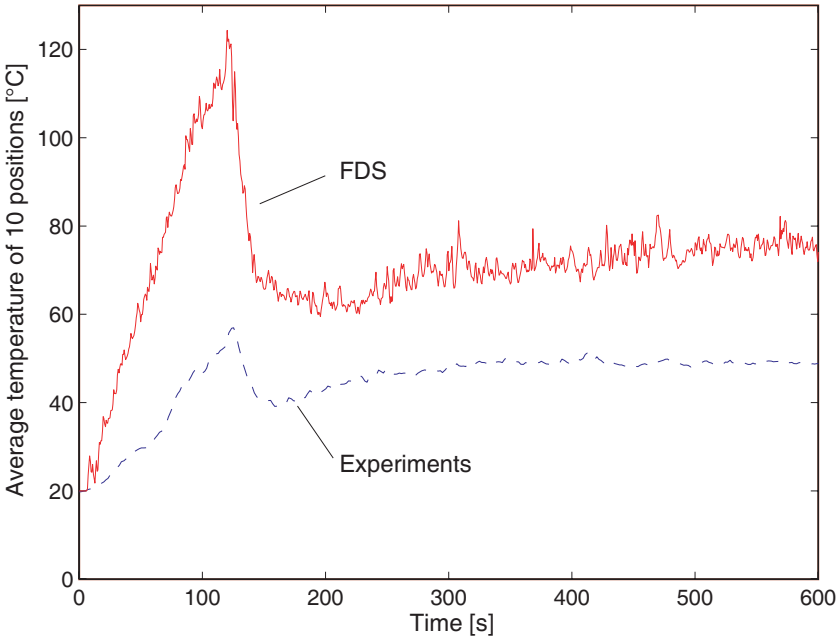

Figure 1 Comparison of temperature calculated in FDS with experimental data, from [28].

It is important to stress that good results using CFD have been produced on smaller scales, e.g. LES of sprays into crossflow [69], but the focus in this thesis is on full scale fire scenarios.

5.6 Problems with modelling of water mist

There are some problems modelling water mist. If the droplets enter at a high velocity the momentum of the droplets need to be transferred to the fluid. The way the coupling of the momentum is handle can have profound effects on the shape of the spray as mentioned by Nordin [70].

The water mist spray, as described in the section on the experimental results in chapter 4, is a jet spray where the momentum is transferred from the droplets to the air over a very short distance. The dominating flow direction of the droplets is downward. The water cone breaks up after about 150 mm and the spray is very turbulent. The flow pattern in the spray is very complex; involving collision and coalescence of the droplets, collapse of the spray and transfer of momentum from water droplets to the air. Failure to simulate this properly will result in drops that continue in a radial direction and in too low air velocities.
Often simulations are carried out by inserting droplets very close to the nozzle. However, none of the RANS codes used in this work, CFX 10.0 and SOFIE have a coalition model for the droplets. Furthermore, to get correct calculation of momentum transfer, very small time steps have to be used. This approach has therefore been relatively unsuccessful so far. A simulation with this approach using the CFD-codes CFX 10 and SOFIE gave a radial pattern of droplets from the spray, which is undesirable.

An alternative approach to model the area in the vicinity of the nozzle correctly, using the k-ε model in steady state in CFX 10.0 has also been tried. The geometry was modelled exactly as the experimental setup described in chapter 4, - CFX using unstructured meshing, enabling the meshing of a cylinder. The droplets are directed vertical downward though an opening, which have the same shape as the spray. This is not the correct shape of the spray for the first 150 mm, but it ensures that the water is kept within the cone. The droplets were given the maximal velocity, which based on the measurement of the reaction force from the nozzle is about 130 m/s. Furthermore the droplet size distribution for the scan of the spray, 500 mm below the nozzle was entered as a Rosin-Rammler distribution, which is shown as the lower formula in equation

(1) in chapter 6. Details on the fitting of a distribution can also be seen in chapter 6. Turbulent dispersion was turned on, which means there is a coupling between the turbulent energy in the gas and the droplets.

The results of the simulation are shown in figure 2 below, where the streamlines of the droplets are coloured with the droplet velocity. The cylinder being 2 m high and the droplets released at the top they are very quickly retarded for both the coarse and the fine grid. The velocity in the spray was about 2 m/s at about 500 mm below the nozzle, where the experiments showed that they would move at about 7 m/s.

Turning turbulent dispersion off, did not significantly change the results as can be seen from a similar simulation as shown in figure 3. When turbulent dispersion is on, the spray gets wider and the droplets do no move in straight lines, but the difference in droplet velocity is very small.

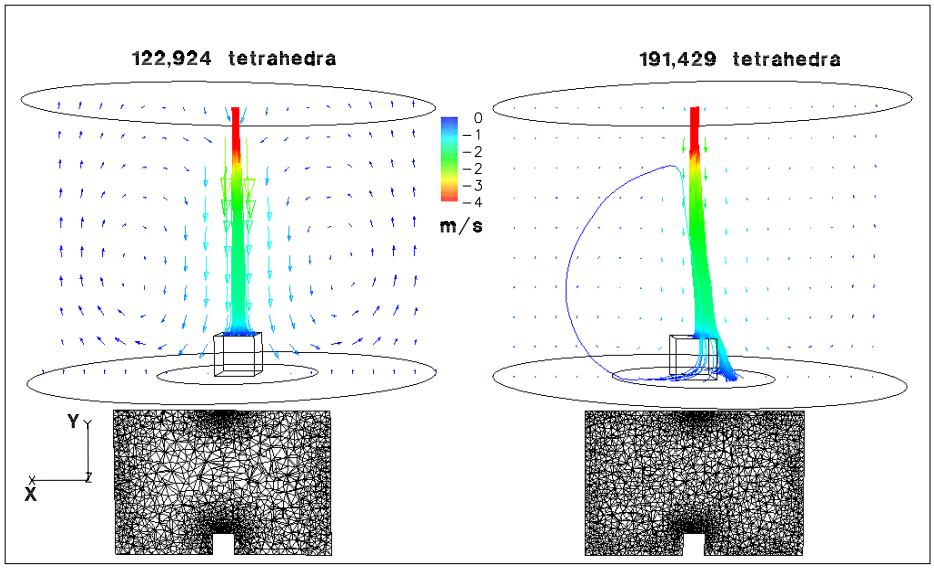

Figure 2. Modelling of hollow cone spray in steady state using CFX 10 with unstructured mesh with 122,924 tetrahedra and with 191,429 tetrahedra. The height of the cylinder is 2 m. The grid through the centre is shown in the underneath the geometry.

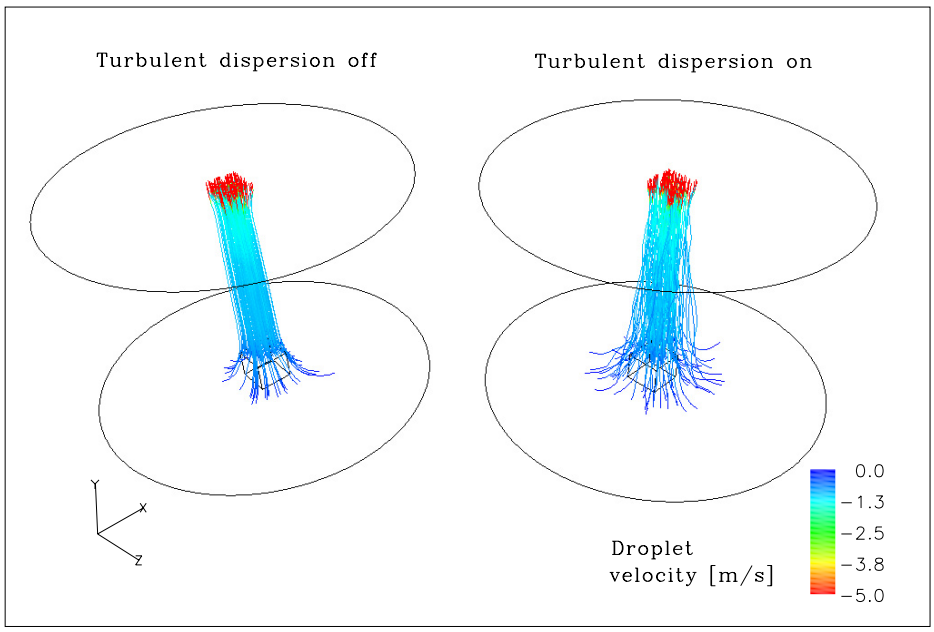

Figure 3. Influence of turbulent dispersion on droplet velocity and paths using a steady state k-ε model in CFX 10.

5.7 Size of droplets and modelling problems

The reasons for these problems in modelling are the strong coupling between particle phase and gas phase. For sprinkler droplets there is a weak coupling as they are larger and less influenced by the movement of the gas. For water mist droplets the coupling is stronger. This can be studied by calculating the terminal velocity of a free falling droplet in air as shown in table 1. A typical sprinkler droplet will fall with 4.6 m/s and tend to be less influenced by the air, where a smaller water mist droplet of 100 µm only will fall with 0.3 m/s. This is the reason for fairly successful modelling of sprinkler droplets as described by Gant [65]. One of these models is the one described by Walmsley [71].

Table 1. Terminal velocity of a free failing droplet calculated after [19]

Droplet size [µm]	10	20	40	80	100	200	300	500	1000
Terminal velocity [m/s]	0.003	0.012	0.050	0.20	0.31	0.80	1.20	2.0	4.6

Chapter 6 Setup of model for hollow cone water mist nozzle in FDS

Based on the experiments already performed and presented in chapter 4, modelling of a hollow cone spray without and with fire was chosen. For this nozzle experimental results are available. The droplets sizes and velocities measured with PDA without the fire can be used as an input in the model.

For the no fire case the results can be compared with velocities measured with PIV and PDA. Furthermore the simulation result can be compared with the concentration of water droplets measured with the tomographic method.

For the fire case the velocities were measured with PIV and the water concentration was measured with the tomographic method and these results can be compared with the simulations results.

Table 1. Details of hollow cone nozzle used in experiments

Spray type	Manufacturer and type	Spray generation process	Spray cone angle	Measured flow rate [l/min] @ 100 bar	Pressure (bar)	Water temperature
Hollow cone	Danfoss 1910	Atomisation	56°	0.38	100	15°C

6.1 Geometry and fire scenario

In FDS 4.07 the Large Eddy Simulation (LES) turbulence model was used [58]. FDS has a built-in transient heat transfer model for walls and the default wall material was set to concrete. The reaction (fuel) was set to propane and the heat release rate was set to 45 kW with a heat release rate per unit area of 500 kW/m^3, based on the measured gas flow during the experiments and the size of the fire area. The radiation model in FDS was also used and the radiative fraction was set to 30% based on Tewarson [72]. For the other parameters in the radiation model the default values in FDS were used as given in the FDS User's Guide [61].

Two different grids were used for the simulations and to reduce the total number of cells, the actual grid was modelled as 5 grids as shown in figure 1. The interface between these grids was set at a distance from the water mist and flame area in order to avoid any influence on the results. In the central area where the water spray and the flame interact, a grid with 20 mm grid size in all directions was used. The coarser central grid consists of 396,000 cells, surrounded by an additional 243,595 cells and it hereafter referred to as the "20 mm grid", see figure 1 and table 2. For the finer grid, hereafter referred to as the "10 mm grid" the cell size in the central grid was divided by two in the horizontal plane. The cells in the vertical plane were kept at 20 mm and the number of cells in the surrounding grids (grid 2-5) were the same as for the coarser grid, see table 2.

Initially the whole setup was symmetrical, but this resulted in that the spray would lean to one side, which seemed to be a result of the modelling rather than the actual physics. Therefore the geometry has been modelled asymmetrically and 80 mm has been cut of the geometry on two sides as can be seen in figure 1. The footprint of the geometry is 2.92 m x 2.92 m instead of 3 m x 3m. This is likely to result in a more stable spray, which was confirmed by the simulations.

Table 2. Number of cells in simulation for "20 mm" grid and "10 mm" grid

	"20 mm" grid	**"10 mm" grid**
Grid 1	396,000	1,584,000
Grid 2	92,345	92,345
Grid 3	37,950	37,950
Grid 4	80,300	80,300
Grid 5	33,000	33,000
Total number of cells	639,595	1,827,595

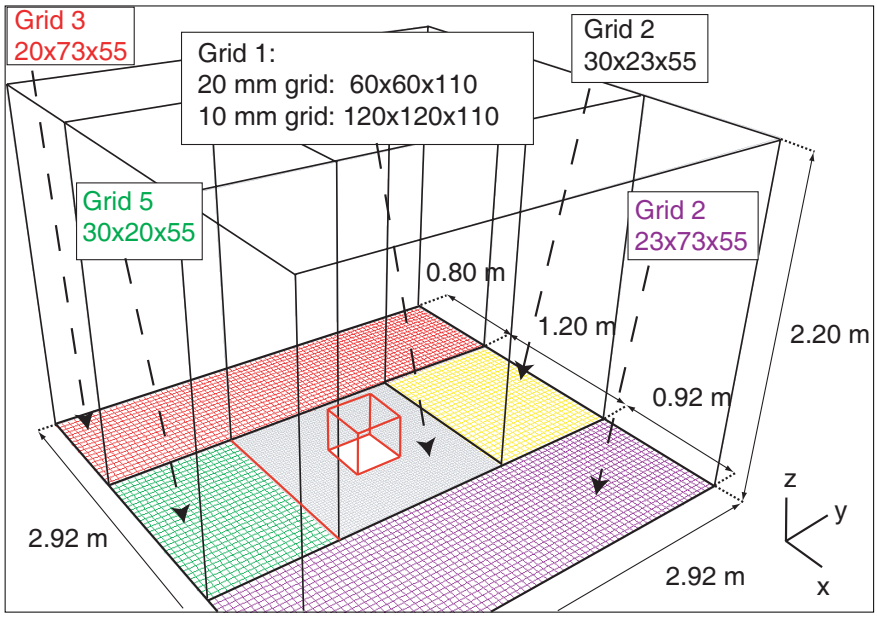

Figure 1 Number of cells in "20mm" and "10 mm" grids used for simulations in FDS

As FDS is a LES model, which resolves the variables in time, the results need to be averaged over a period in order to enable comparison with the experimental results.

Simulations were carried out over a total time period of 30 s as follows:

0-5 seconds	Only fire is modelled
5 seconds	Water mist turned on
10 –30 seconds	Time period used to get average results

6.2 New modelling approach for water mist

The present simulations are based on a new approach, where the droplets are inserted in the flow at a distance from the nozzle where the flow is less complex. The experiments show that in the turbulent zone, after break up of the spray, there will be a uniform drop size distribution across the spray and different sized drops at the same position will move at the same speed. The droplets will have a relatively low velocity here, as they have already transferred most of their momentum to the air at this stage. Therefore it is necessary to add the lost momentum to the spray. One way of doing this is to add an extra inlet with air having the momentum, which the droplets have lost. The new approach is illustrated in figure 2 showing the position of the nozzle and the water drops entering the domain 300 mm further below. The extra air inlet is placed above the nozzle.

The requirement is that momentum is conserved and species are conserved. The total momentum is the momentum of the air and the water and the species are the mass flow of water and the mass flow of air. In the following the setup of the boundary conditions of water and air will be discussed.

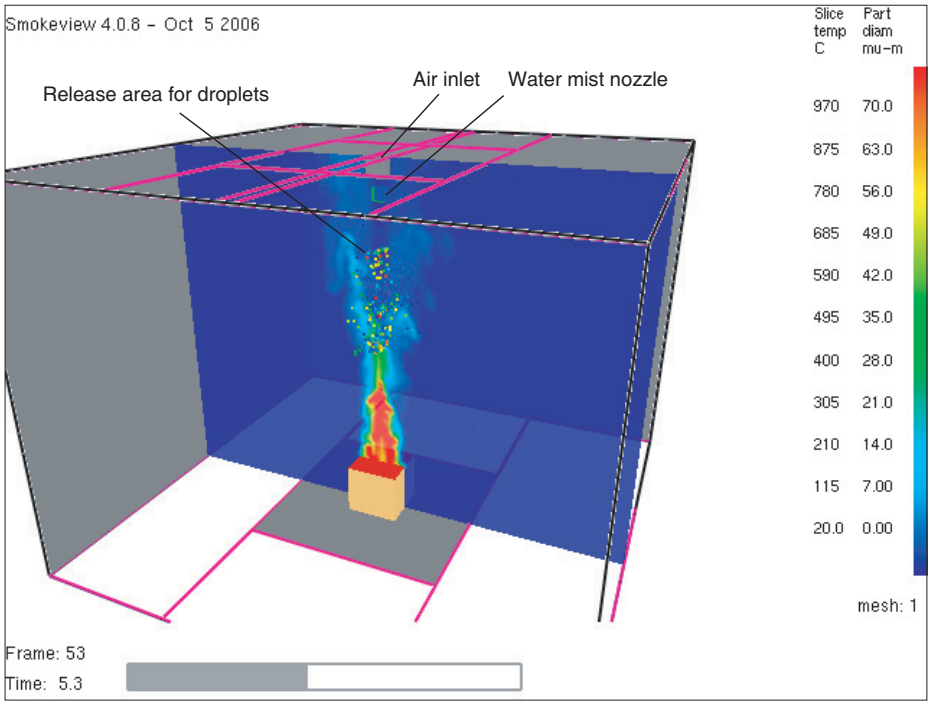

Figure 2. New approach for modelling water mist with release of droplet in the turbulent zone and introduction of an air jet.

6.3 Input parameters for water mist droplets

To insert the water mist droplets the following parameters must be determined:

- Distance for inserting water droplets
- Width of spray
- Drop size distribution
- Drop velocity distribution

Distance for inserting droplets

The new boundary conditions for water droplets should be somewhere outside the zone where the water cone has collapsed (i.e. 150mm) to avoid complex calculations involving collapse of spray, collision and coalescence as described in chapter 4. However it is also desirable to have the water injected as close to the nozzle as possible, as the velocity induced by the fire will have less influence on inlet boundary conditions of the spray. The fire will have greater influence on the spray velocity further away from the nozzle as shown in figure 3.

To simplify simulations, it is also desirable that different sized droplets at the same positions have approximately the same velocity. The velocity of the droplets evens out with increasing distance from the nozzle. At a distance of 500 mm below the nozzle, the different sized droplets have the same velocity, but insertion of droplets this far from the nozzle will prevent simulation of the correct velocities if a fire is present as shown in figure 3. Without a fire the maximum drop velocity is about 6 m/s and with a fire the maximum velocity is 3.5 m/s. It was therefore chosen to insert water droplets at a distance of 300 mm below the nozzle. This is the first position after the collapse of the spray at 150 mm, where the drop size distributions was measured with PDA. At this position, as shall be show below, drop velocities are up to 15 m/s and are therefore less likely to be influenced by the fire.

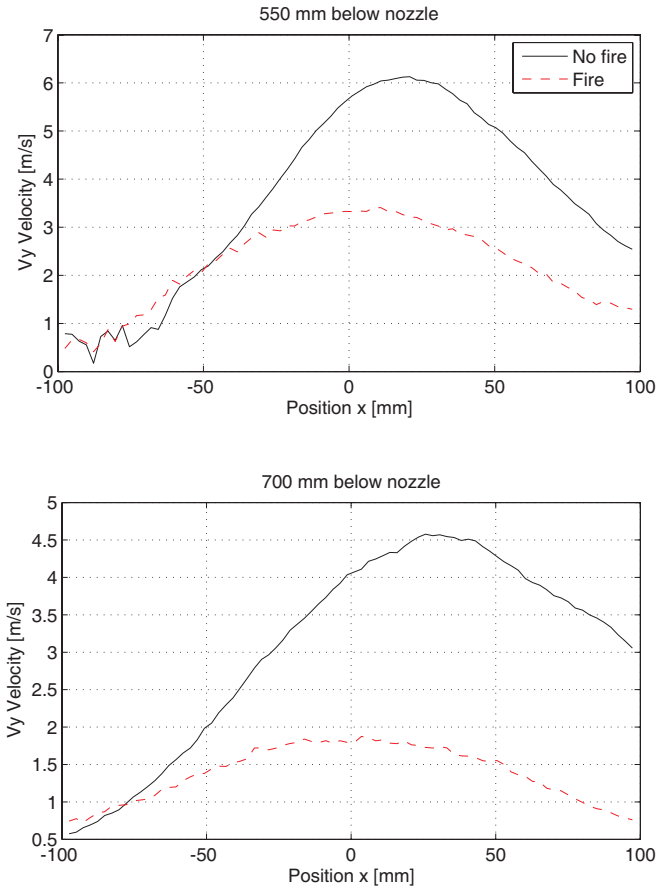

Figure 3. Velocity distribution at 550 mm and 700 mm below nozzle without fire and with fire (from PIV measurements)

Width of spray

To insert the water droplets in the calculation, the diameter of the spray at 300 mm below the nozzle must be determined. Ideally, this could be done based on measurements of mass flux. However, the water distribution has not been measured closer than 900 mm to the nozzle exit (with tomography). At this distance of 900 mm below the nozzle, the majority of mass is within a diameter of 400 mm.

To determine the spray diameter at 300 mm below the nozzle, PIV images have been used. The spray diameter has been determined by

measuring the spray width from a sample of 20 images giving a mean diameter of 130 mm.

Drop size distribution

In order to treat water mist in numerical simulations, it is important to be able to describe particle size distribution in a simple way. Lefebvre [38] has given an overview of the different distributions and a very good recent overview of different particle distribution is given by Verheijen [73]. Tak-Sang Chan found that droplets from sprinklers could be described by a combination of the log-normal and the Rosin-Rammler distribution [74]. This approach has been adopted by McGrattan et al. in FDS and the formula for the combined cumulative distribution based on mass is given in equation (1) below.

$$F(d) = \begin{cases} \dfrac{1}{\sqrt{2\times\pi}}\displaystyle\int_0^d \frac{1}{\sigma\times d'}\times e^{-\frac{[\ln(d'/d_m)]^2}{2\times\sigma^2}}\,dd' & (d \le d_m) \\ 1-e^{-0.693\left(\frac{d}{d_m}\right)^{\lambda}} & (d_m < d) \end{cases} \qquad (1)$$

There are several methods for fitting the data of the distribution. Maximum likelihood estimator, (MLE) uses the probability density function (pdf) to fit all the data to the distribution. Another method is to use the cumulative distribution function (cdf) and use the sum of square error (SSE) method to find the variables. Van Zandt reviewed both method and found the MLE to be the best, but the SSE method was nearly as good [75]. Here the SSE method has been used and a general routine for fitting drop size according to the FDS definition given in equation (1) was developed in Matlab [76].

Figure 4 shows the drop size distribution 300 mm below the nozzle as well as the fitted distribution according to equations (1). The input data to FDS is chosen to be those of the scan of the entire spray, where the parameters are σ=0.43107, γ=3.9609 and d_m=46 μm. The scan fairly well represent the distributions at 30 mm and 60 mm from the centre, but overestimates the droplet size in centre of the spray. In FDS in the

present version 4.07 it is only possible to have one distribution function for a nozzle.

In the simulation, the overall size distribution will be right, but there will be slightly more large droplets in the middle. This can lead to too high drop velocities in the middle of the spray. It will be assumed that mass flux will be evenly distributed over the spray, as there are no flux measurements available at 300 mm below the nozzle.

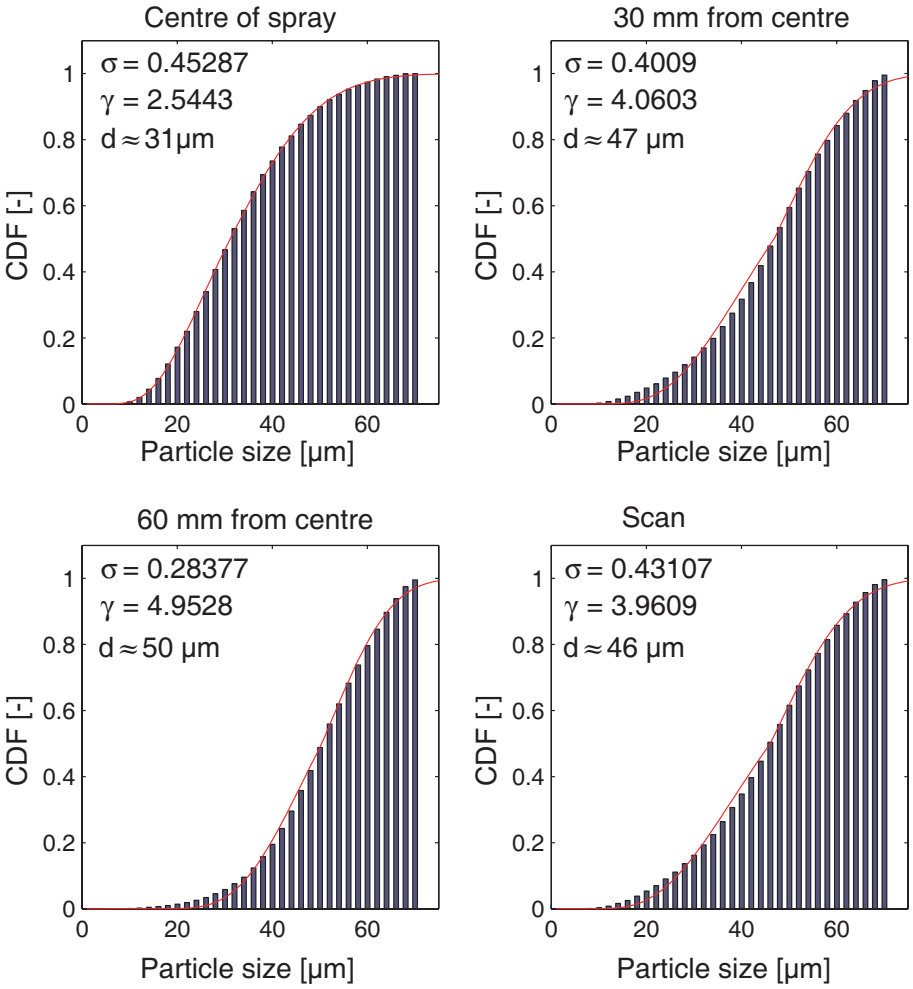

Figure 4 Drop size distributions at 300 mm below nozzle, based on mass. The red curves show the fitted distribution using equation (1). (From PDA- measurements)

Drop velocity distribution

When inserting droplets into simulations, they must be given an initial velocity, dependent on their radial position. As seen in figure 6 in chapter 4, the droplets at the same radial positions have nearly the same velocities, although in the centre of the spray, the smaller droplets are slightly faster than larger droplets.

Figure 5 shows the velocities in the spray measured with PIV and PDA at 300 mm below the nozzle. The velocities from the PDA measurement were used in the simulations, as these were measured together with the drop size. The velocities are linearly interpolated between measured points to define the radial velocity distribution.

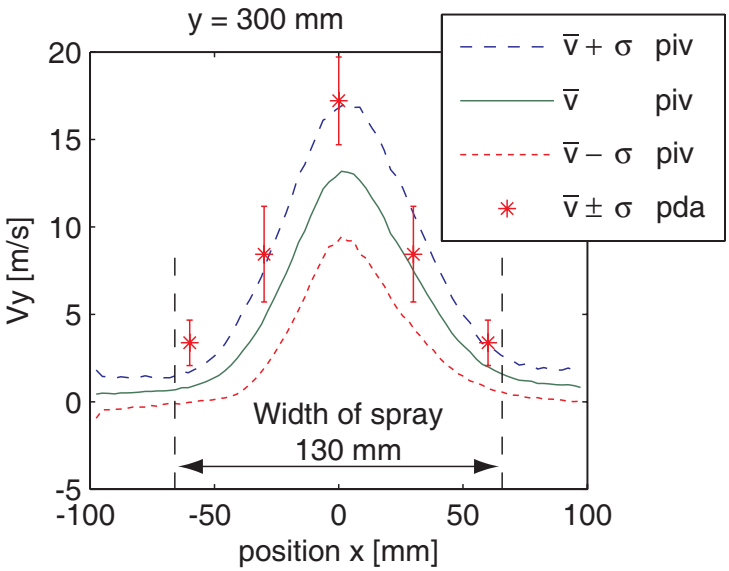

Figure 5 Mean velocity of droplets at 300 mm below nozzle (lines PIV , points PDA)

6.4 Input parameter for air flow

When droplets are inserted at 300 mm below the nozzle with their actual velocities, it is also necessary to include the momentum that they have transferred to the air and the mass flow of the air. This is done by creating an air jet and adjust the flow, so that the correct mass flow at 300 mm below the nozzle is achieved. Furthermore the size of the momentum is controlled.

To simulate momentum transfer to the air by the new modelling approach the following parameters must be set for the air jet:

- Position of air jet inlet
- Mass flow through air jet inlet

Simulations has been performed until the correct values were achieved for

- Mass flow of air at 300 mm below nozzle
- Momentum of air jet at 300 mm below nozzle

Position of air jet

It was chosen to place the inlet 100 mm above the water mist nozzle and inject the air through a rectangular duct with the size 80 mm x 80 mm, so that a velocity profile could be developed over the distance of 400 mm.

Inlet mass flow of air

To simulate the water mist jet correctly, the air jet at 300 mm must have the correct mass flow. The smaller droplets in the spray have a velocity similar to the air velocity. At 300 mm below the nozzle, all droplets at the same position move at nearly the same velocity. Therefore the mass flow of air can be calculated from the PIV measurements, even though this method biases the velocity of the larger droplets, as seen in paper 4, [29]. Figure 6 shows the calculation of mass flow based on PIV measurements, giving approximately 0.08 kg/s at 300 mm below the nozzle.

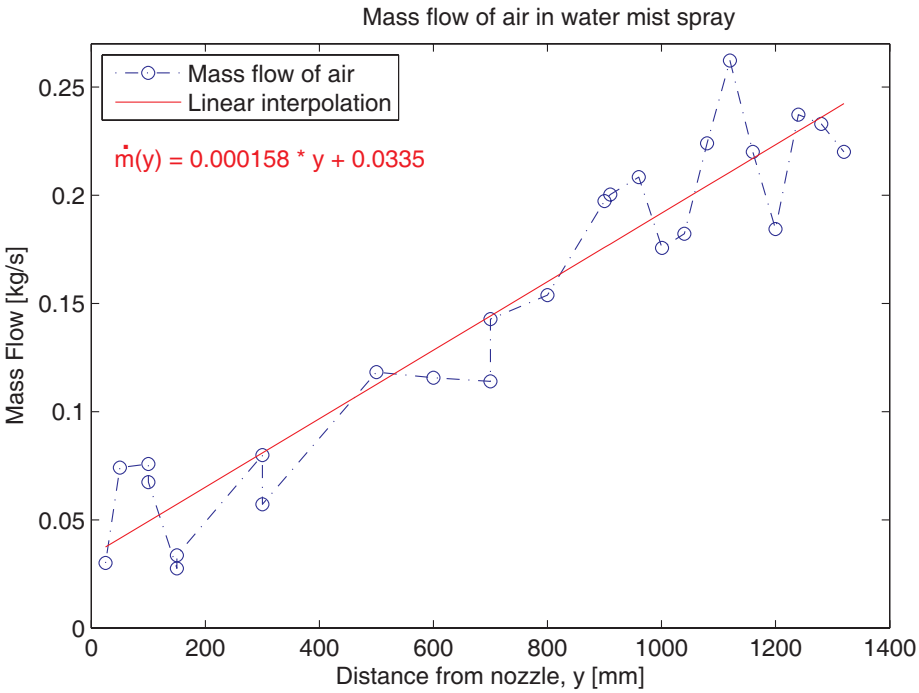

Figure 6. Mass flow of air in water mist spray based on integration of PIV measurement at different distances below the nozzle.

Mass flow of air 300 mm below the nozzle

Several FDS simulations were carried out to achieve the approximate mass flow of air of 0.08 kg/s at 300 mm below the nozzle. A mass flow of air of 0.054 kg/s at the inlet gave the desired results 400 mm further below as seen in figure 7. The width of the air jet is approximate 200 mm, - a bit wider than the width of the water jet of 130 mm, but it can be seen that the bulk of the flow is within 150 mm.

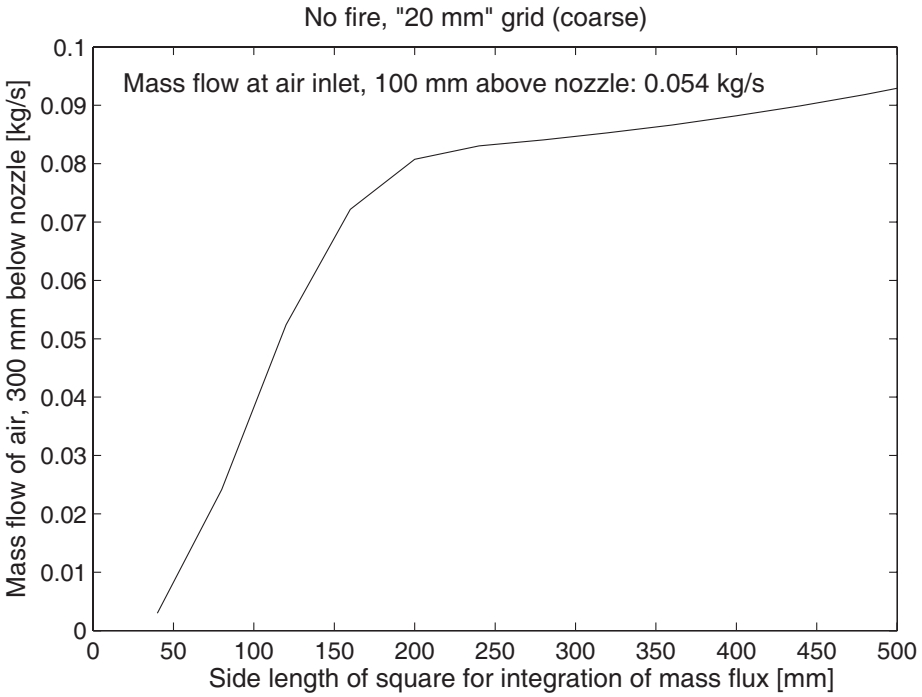

Figure 7. Mass flow of air calculated in FDS at 300 mm below the nozzle

Momentum of air jet

Similar to the calculation of the mass flow of air from the PIV measurement the momentum of the air jet has been calculated as shown in figure 8. At 300 mm below the nozzle the droplet velocity is so low that the main part of the momentum is in the air jet and the momentum of the droplets is negligible. It can be seen from figure 8 that the momentum is at the same level from 150 mm to 1400 mm below the nozzle. If the inlet mass flux of air in the FDS simulations is 0.054 kg/s over an area of 80 mm x 80 mm then the average velocity becomes 7.0 m/s and the resulting momentum 0.38 kg m^2/s^3. This is of the same order as the experimental results and momentum has been conserved in this approach of the setup of water mist boundary conditions for the FDS simulations.

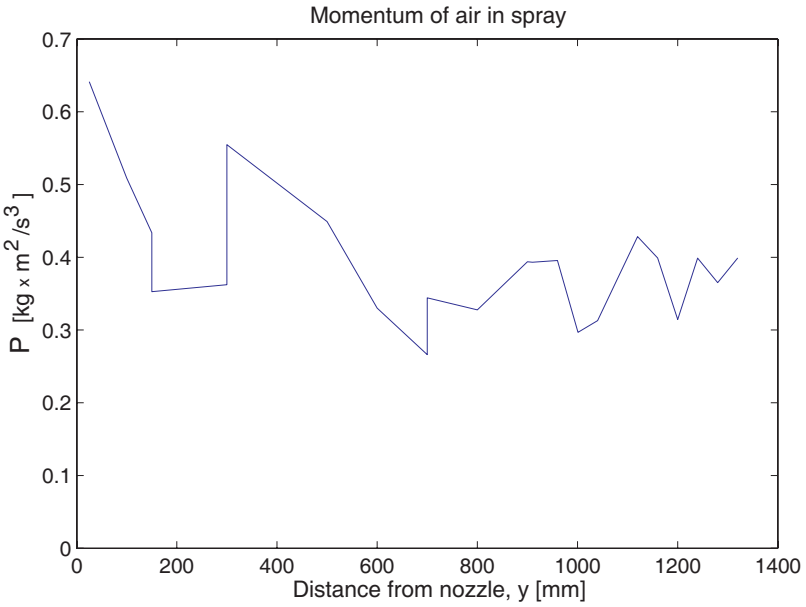

Figure 8. Momentum of air in water mist spray based on integration of PIV measurements at different distances below nozzle.

6.5 Numerical considerations of modelling the release of water droplets in FDS

When using the Lagrangian particle tracking method a representative number of droplets should be inserted and this has been investigated.

In the centre grid where the water drops are inserted the grid has the following dimensions, where z is the vertical component.

Cell dimensions in coarse grid: 20mm x 20mm x 20mm (x,y,z)
Cell dimensions in fine grid: 10mm x 10mm x 20mm (x,y,z)

The maximum droplet inlet velocity is according to figure 6, 15.7 m/s and the droplets are moving downwards. In order to always have a drop present in an inlet cell, the maximum time between the droplets is determined by the following equation, where l_z is the cell height and $v_{d,max}$ is the maximum droplet velocity:

$$t_{\max} = \frac{l_z}{v_{d,\max}} = \frac{0.020\ m}{15.7\ m/s} = 1.3\times10^{-3}\ s \approx 1\times10^{-3}\ s \qquad (2)$$

Furthermore, to model the water spray, it is desirable to seed the inlet with at least one particle per cell. With an area of the droplet inlet of 130 mm x 130 mm and using the coarse grid, this gives 42 inlet cells, whereas use of the fine grid gives 169 inlet cells.
Therefore to seed with a minimum of 1 particle pr cell at the given t_{max} of 1 ms giving a frequency of 1000 Hz, the following droplets released per second are required:

Coarse grid: 45,000 droplets/s
Fine grid: 170,000 droplets/s

Simulation with fewer drops will result in a spray with patches of high water concentration as seen in figure 9 for the coarse grid, when 1000 droplets per second are released with an interval of 0.05 s. This is the default in FDS and can be adequate for slower moving sprinkler drops,

for which the FDS particle model was originally developed. It can further been seen that 45000 droplets/s released with 0.001 s interval gives a smoother picture and increasing the number to 200000 droplets/s with 0.001 s interval smoothes the water concentration further as shown in figure 9.

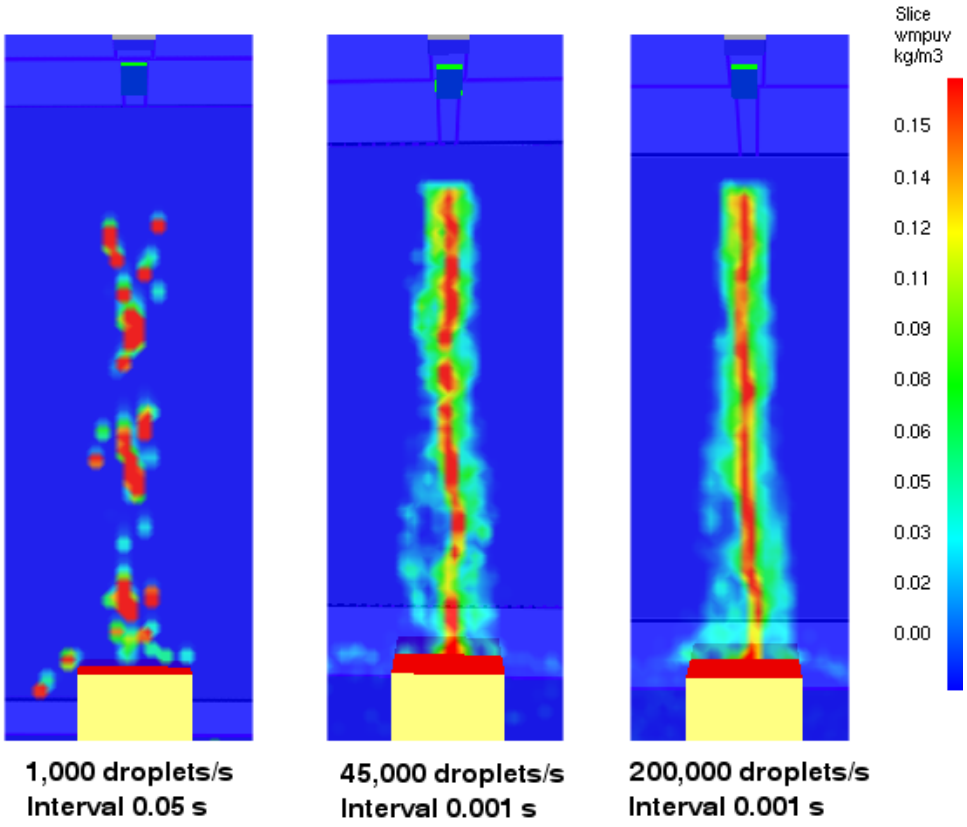

Figure 9. Simulation of water mist spray without fire on the coarse grid. The number of water droplets release per second have been varied and the colour indicates the water droplet concentration in kg/m^3. (The default setup in FDS uses 1000 droplets pr. second released with an interval of 0.05 s, left picture)

6.6 Integrating amount of water and error in FDS.

In order to check that the right amount of water is released from the nozzle, the mass flow of water at 500 mm below the nozzle was calculated. This is done by taking an area below the nozzle and integrating the mass flux calculated in FDS that passed through this area. The validation showed that the mass flux 0.5 m away from the nozzle was 5 times higher than the mass flux from the water mist nozzle, when releasing 45000 droplets/s with an interval of 0.001 s.

It was confirmed that the setup of the sprinkler file in FDS was not the cause, neither was the number of particles from the nozzle.

The cause of the error is the variable called DTSPAR, - the time interval between the release of droplets. If this variable is changed from its default value of 0.05 s to 0.001s, then the mass flow of water changes. The mass flow should be independent of this variable. The correct amount of water was achieved by changing the pressure of the water mist nozzle from 100 bar to 4 bar, thereby reducing the flow by sqrt(100)/sqrt(4) = 5. The pressure at the nozzle is only used to determine the flow, so this does not influence the droplet velocities. The result of the integration of the mass flux calculated in FDS is seen in the figure 10. When the integration area is about 200 mm x 200 mm most of the water is captured and the results are close to the desired mass flow.

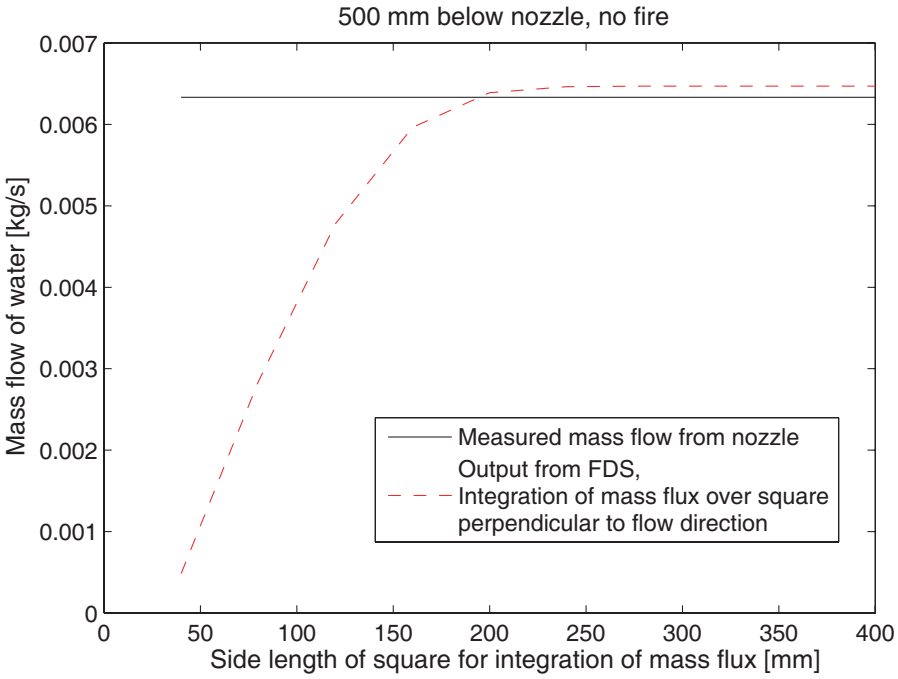

Figure 10. Mass flow of water calculated in FDS at 500 mm below the nozzle

Chapter 7 Simulations in FDS compared with experimental results

Simulations of hollow cone water mist have been carried out in two stages, without fire and subsequently with fire, with the setup described in chapter 6. The simulations were carried out with a coarse grid (20 mm) and a fine grid (10 mm) to study the influence of the grid size on the simulations results. Unless otherwise stated all profiles shown in the following are averaged results. The average for the FDS simulation were done over of a period of 20 s (as described in chapter 6) and the average for the PIV measurements were typically done over a period of 300 s as described in paper 4, [29]. The average of the tomographic measurement were done over a period of 10 s as described by Almén and Irvert [47].

7.1 Simulations of water mist spray on hollow cone, no fire

Generally there are big discrepancies between the simulated and experimental velocity and water density profiles for the no fire case, as shown in figure 1 and 2.

Comparison of velocities

The simulations show virtually the same velocity profile for both the 20 mm grid and 10 mm grid, regardless of the distance from the nozzle, as seen in figure 1. This does not coincide with the experimental results as seen in the graph to the right in figure 1. It is expected that further below the nozzle, maximum velocity would be reduced and the air jet will be broader due to drag and entrainment of air from the sides of the jet, as described in chapter 4. The maximum simulated velocity for both the 20 mm grid and 10 mm grid is nearly constant at 6.5 m/s. In the experiments the maximum velocity at 340 mm below the nozzle has been measured to be 12 m/s, and at 600 mm below the nozzle the velocity is roughly 5.5 m/s. This has been further reduced to 2.5 m/s at 1300 mm below the nozzle, as seen in the measured profile to the right in figure 1.

The simulated velocity profiles are more uniform for the finer grid than for the coarse grid, although it was expected that the finer grid would increase the mixing and result in larger differences between the velocity profiles for the 10 mm grid.

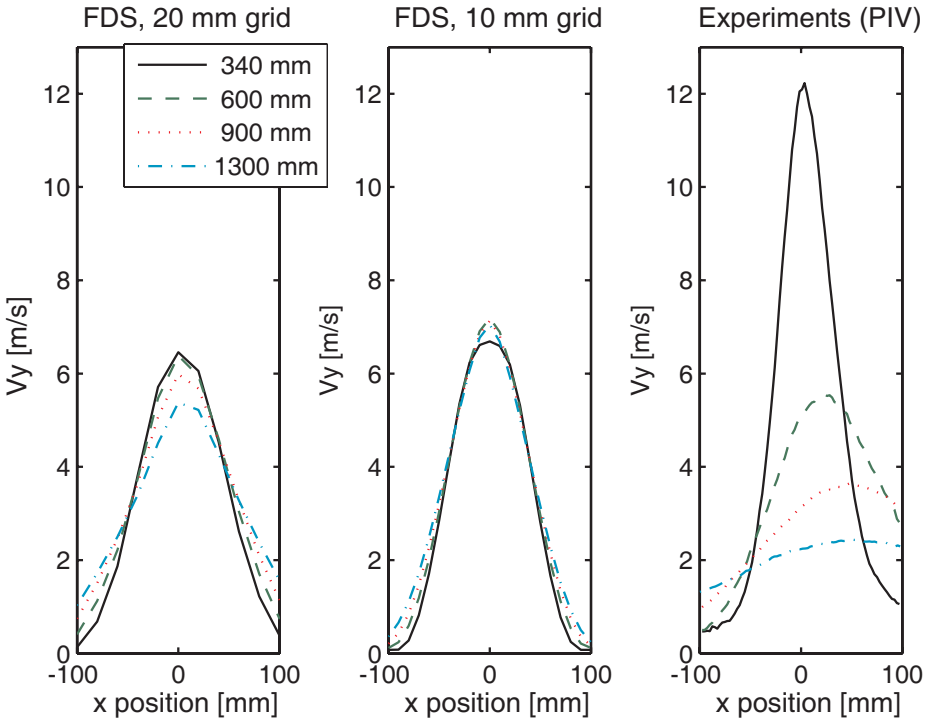

Figure 1: Downward velocity profile for simulation on hollow cone spray compared with experimental results. Scenario with only water mist.

Comparison of water concentration

The simulations using the 20 mm grid show a water concentration of up to 0.14 kg/m³ with a sharp peak in the middle and with water spread over a radius of 60 mm, as seen in figure 2. This radius corresponds to the area of the input data. However, this distribution remains the same at all distances below the nozzle. As can be seen from the tomography measurement to the right in figure 2, at 900 and 1300 mm below the nozzle, the water is evenly distributed in a spray with a radius of 200 mm and with a concentration of 0.05 kg/m³ to 0.10 kg/m³. Simulations using the 10 mm grid in both directions in the horizontal plane were even further away from the experimental results. Here the water concentration in the middle of the spray reaches 0.35 kg/m³.

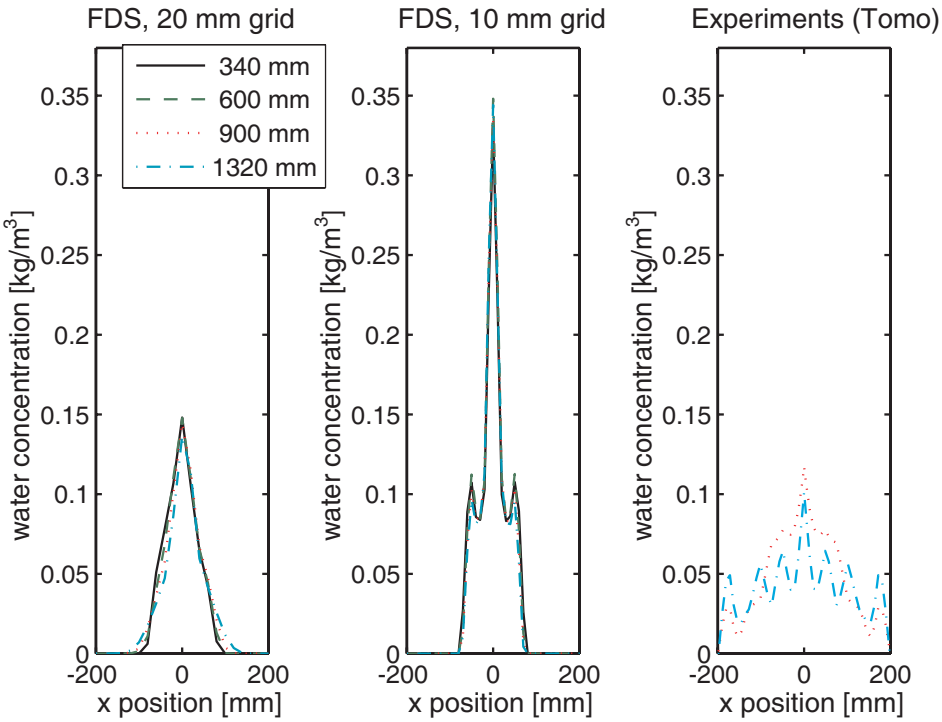

Figure 2. Water concentration for simulations on hollow cone spray simulated compared with experimental results using tomography. Scenario with only water mist.

7.2 Simulations of water mist spray on hollow cone above a fire:

When simulating with a fire underneath the water mist nozzle, there is better mixing and higher turbulence levels due to the interaction of the water mist jet and the buoyant fire plume. The simulated velocity results changes with distance to the fire for both the 20 mm grid and the 10 mm grid as seen in figure 3. The simulations show that the water jet and the fire plume are in balance (vertical velocity is zero) at about 850 mm below the nozzle for the 20 mm grid and at 750 mm below the nozzle for the 10 mm grid as seen in figure 3. The corresponding PIV measurements show that the two flows are in balance at around 1100 mm below the nozzle as seen to the right in figure 3.

Comparison of velocities

Generally the variations in velocity are much larger for the simulation results for both the 20 mm and the 10 mm grid than for the measured results. The simulated vertical velocities varies from about 4 m/s at 600 mm below the nozzle to –4 m/s at 1300 mm below the nozzle (400 mm above the fire) as seen in figure 3 for both the 20 mm and 10 mm grid. The measurements show that the maximum velocity is around 3 m/s at 600 mm below nozzle and the minimum velocity is –0.5 m/s at 1300 mm below the nozzle as seen in to the right of figure 3. FDS seems to overestimate the velocity of water mist jet.

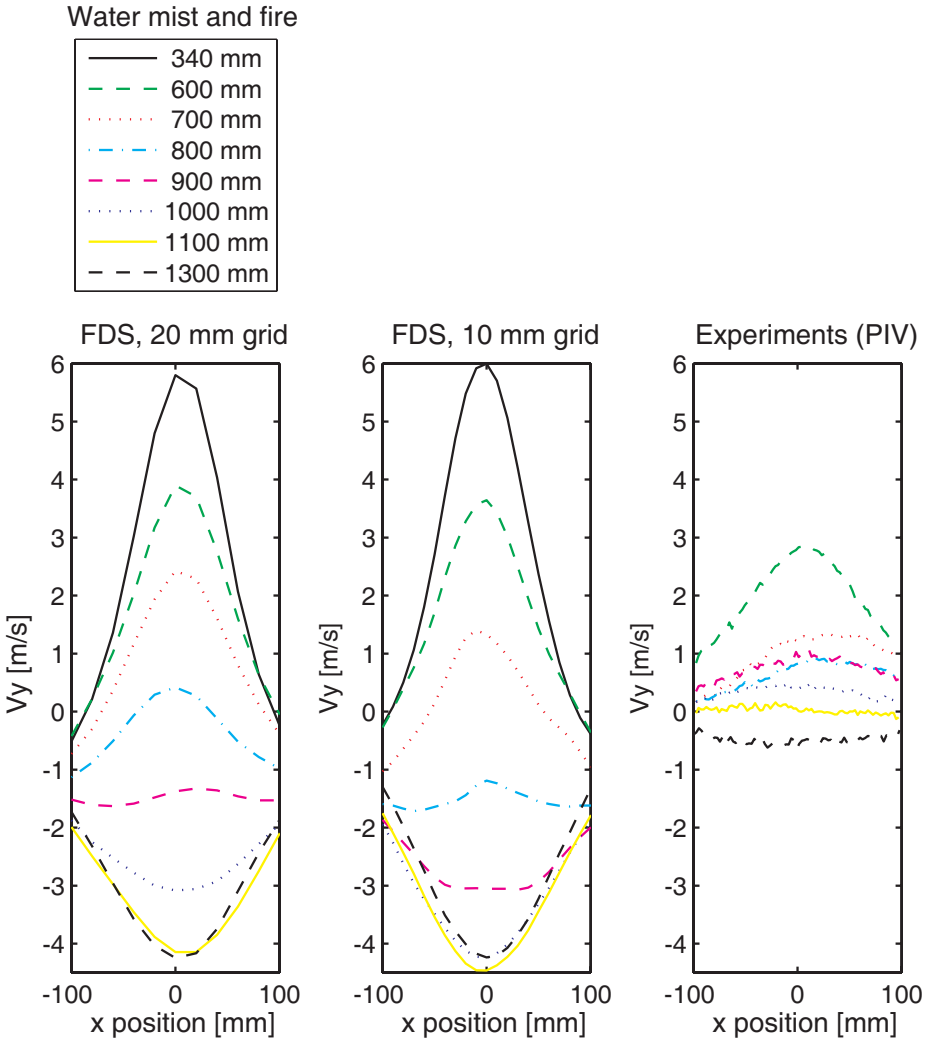

Figure 3. Downward velocity profile for simulation on hollow cone spray compared with experimental results. Scenario with interaction of water mist and fire plume.

Comparison of water concentration

The simulated water concentrations for the fire case are shown in figure 4 and at a distance of 340 mm below the nozzle the water concentration are not influenced by the fire, which can seen by comparison with figure 2 for the 20 mm grid and the 10 mm grid. At 600 mm below the nozzle the maximum value for the simulated results drops to about 0.15 kg/m^3 for both the 20 mm grid and 10 mm grid. The reason for this can be increased horizontal movement of the water mist jet, which lowers the average values. Another reason could be increased vaporisation of the water droplets.

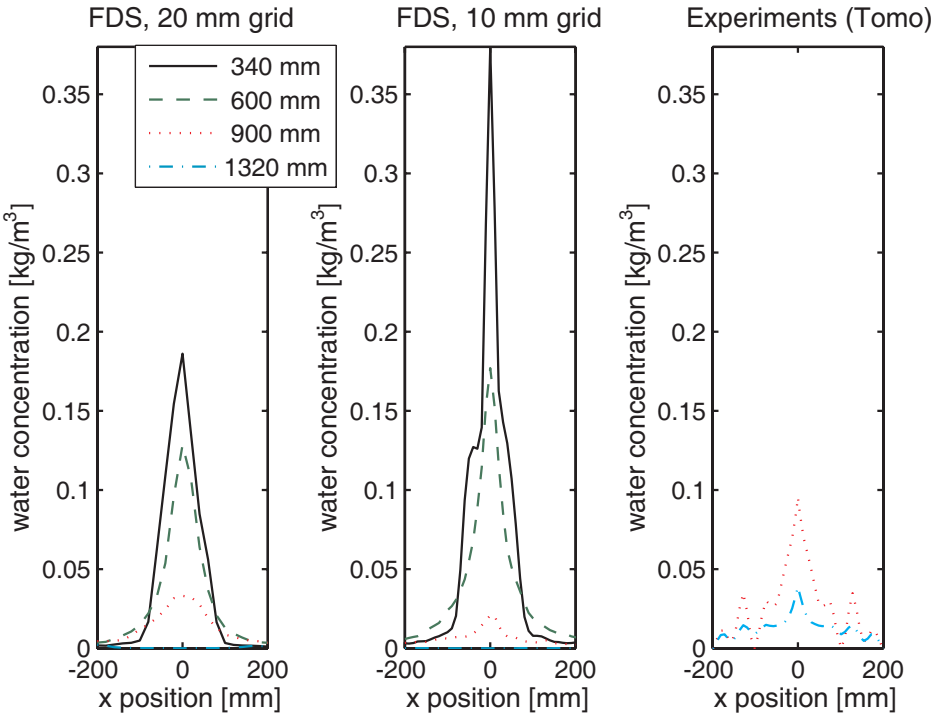

Figure 4. Water concentration for simulations on hollow cone spray simulated compared with experimental results. Scenario with interaction of water mist and fire plume.

At 900 mm below the nozzle the water mist concentration calculated in FDS can be compared with the experimental results as shown in figure 4. The simulated values for both the 20 mm grid and the 10 mm grid are smaller than the experimental results, where the finer grid shows lower levels.

This can be explained by studying the flame height and droplets distribution as shown in figure 5, where the instantaneous values at t=20s are shown.

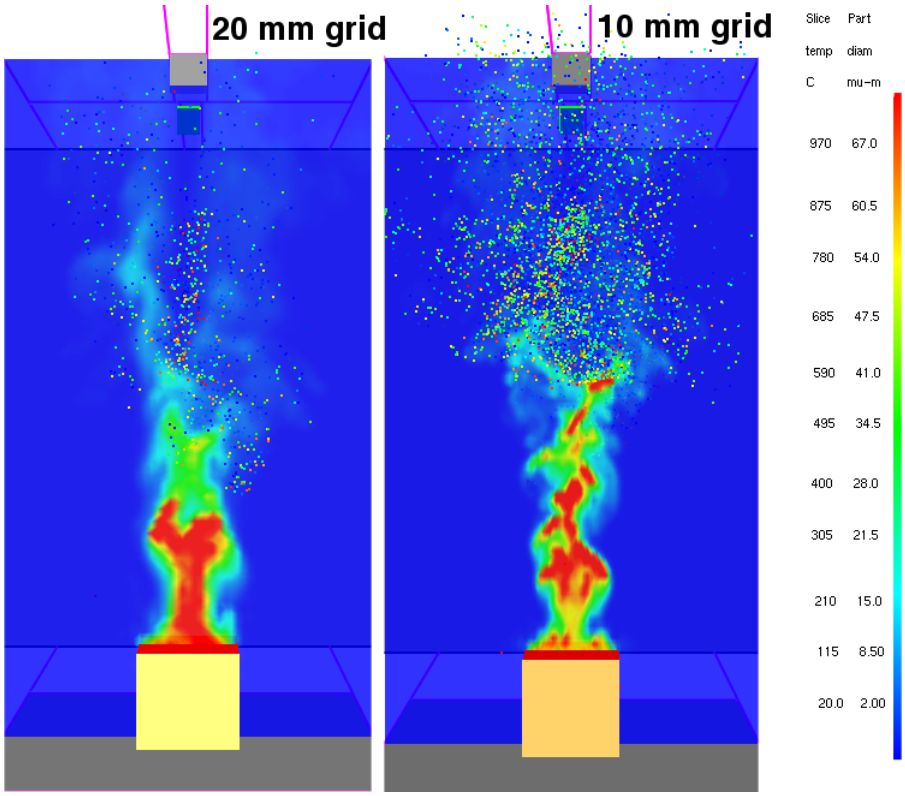

Figure 5. Instantaneous temperature field and droplet distribution for the 20 mm grid and 10 mm at t=20 s. The colour shows the temperature in Celsius and the droplet size in µm.

In general for all time steps in the FDS simulations, the flame is higher for the finer grid than the coarser grid and prevents the droplets entering the flame area. 1300 mm below the nozzle the simulation results do not show any presence of water droplets for both grids according to figure 4, which is also confirmed by studying figure 5. The experiments showed that there was water present at this position, 400 mm above the flame, as shown to the right in figure 4.

Wen et al. has in a recent study validated FDS (version 4) for a medium scale pool fire and found that FDS with reasonable accuracy could predict the axial velocity profile above the fire plume, when using a grid with a cell size of 13 mm [77]. Therefore the discrepancies found between the simulated and experimental work in this study is likely to be due to the modelling of the particles, rather the modelling of the fire. The velocity flow field shall be further investigated in the following paragraph.

Comparison of vector fields from measured results and simulated results with fire

The transient visualisation of the simulated velocity vectors show a very turbulent fire plume and a more steady state water mist jet as illustrated in figure 6. There is very little fluctuations in the water mist jet and as a result there is limited mixing.

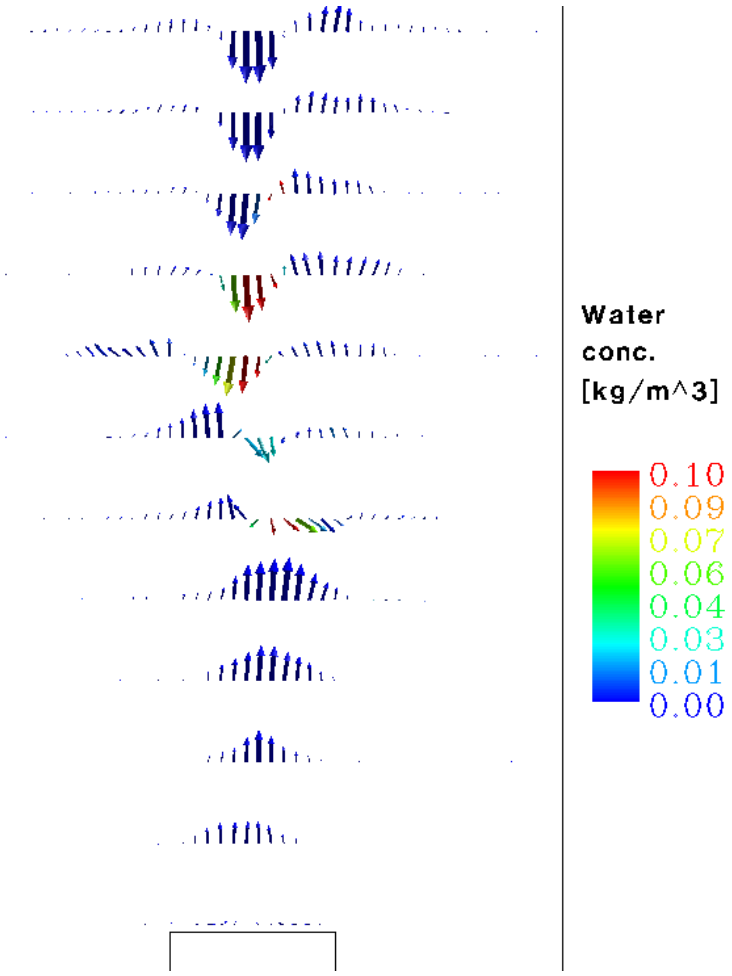

Figure 6. Instantaneous vector field from the simulation with the 20 mm grid. The distance from top to bottom is 2.1 m with the fire below and the inlet air at the top. The colour shows the water concentration. Note that the water enters at 0.4 m below the top.

The averaged simulated vector fields for the fine and the coarse grid in figure 8 and 9 show a very narrow water mist jet with high velocities in the centre, compared with measurements as shown in figure 7. The same pattern is seen for both grids and in the following the finer grid shown in figure 8 is used for the comparison with the experimental result shown in figure 7.

There is little radial movement in the simulated water mist jet compared to the measurements. The measurements show that zero vertical velocity is reached at approximately the same level below the nozzle (1100 mm), regardless of the radial distance. The simulations with the 10 mm grid show that zero vertical velocity is reached at 600 mm below the nozzle at the radial distance of 100 mm from the centre line as shown in figure 8. At the centre line zero velocity is at 750 mm below the nozzle. The fire plume seems to enclose the spray in the simulation.

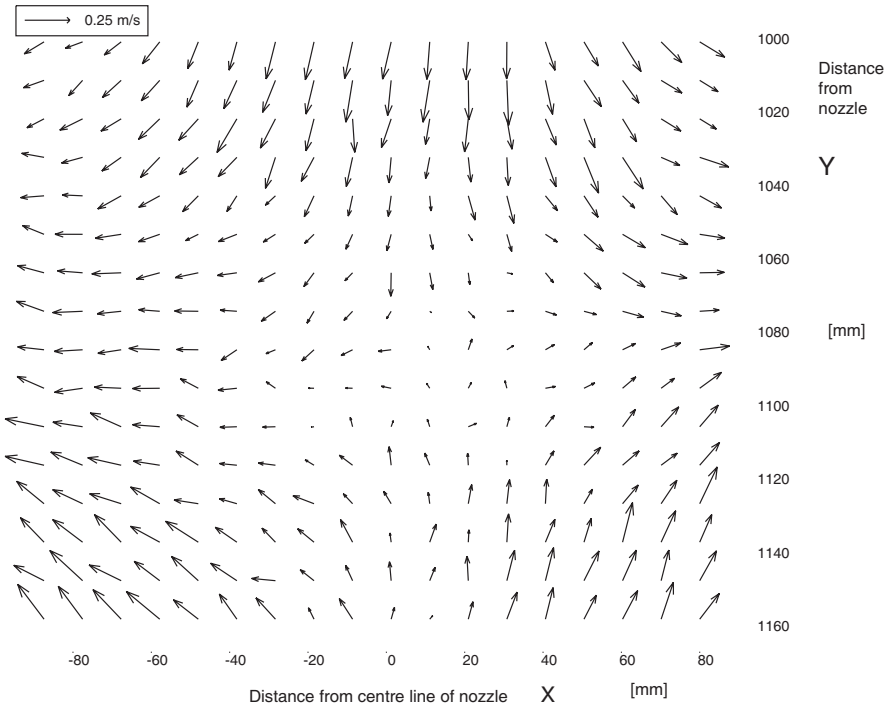

Figure 7. Vector field from measurement with PIV, fire, 1000 mm to 1160 mm below nozzle

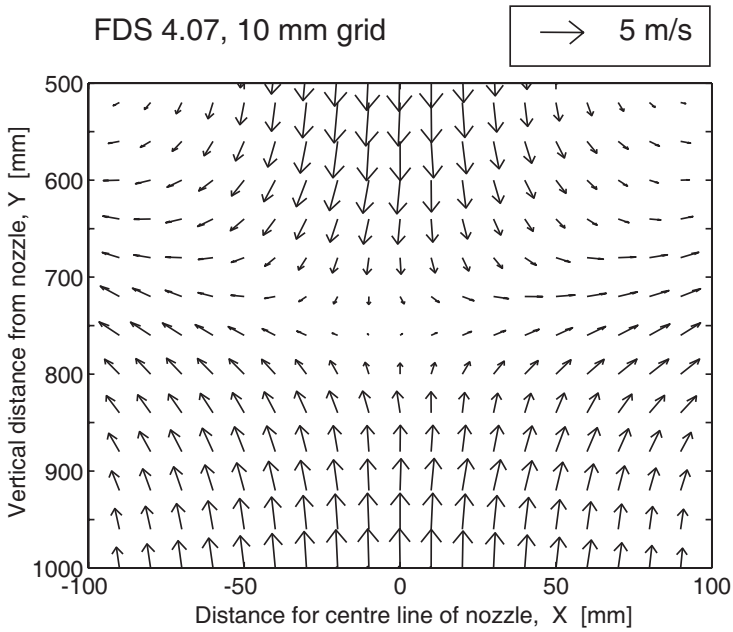

Figure 8. Average vector field from simulation with 10 mm grid and fire, 500 mm to 1000 mm below nozzle

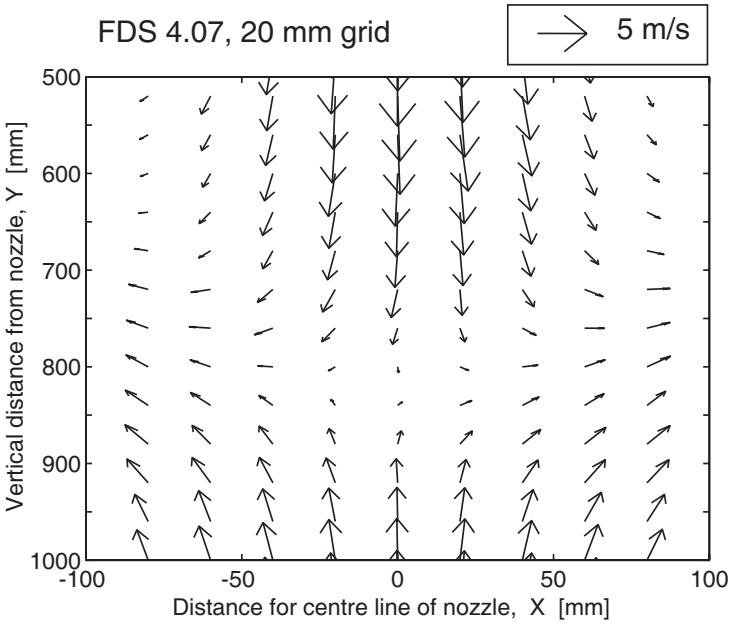

Figure 9 Average vector field from simulation with 20 mm grid and fire, 500 mm to 1000 mm below nozzle

7.3 Problems with simulations of water mist

The reason for the large discrepancies between measurements and simulations is probably the way turbulence is handled in the simulations. The high speed camera pictures of the spray show a highly transient and turbulent spray pattern caused by collapse of the spray around 150 mm below nozzle. This will inevitably lead to a considerable entrainment of air in the spray and spreading of the droplets.

In the simulations there is not enough spreading of the water droplets and this can be caused by insufficient turbulent dispersion and lack of turbulence in the specifications of the boundary conditions for the droplets and air inserted in the calculations. In FDS it is not possible to define injection droplet velocity fluctuations. Thus the droplets are injected using the same velocity for a given location. Furthermore the air is injected above the nozzle without introducing turbulence.

In the LES turbulence model in FDS the largest turbulent eddies are directly modelled in the calculation grid as mentioned in chapter 5. Turbulent velocity fluctuations from these eddies are transferred to the water droplets. The smaller eddies are modelled by the Smagorinsky sub grid model. The turbulent energy contained on the sub grid scale does not influence the velocity of the droplets according to the FDS Technical Reference Guide [58]. If a large proportion of the turbulent energy is modelled by the sub grid model this will therefore result in insufficient impact of the turbulence on the droplets - and thereby insufficient turbulent dissipation.

To achieve a sufficient turbulent momentum transfer it would be necessary with considerably finer grid, or to include a model for turbulent energy transfer for the sub grid turbulence to the droplets.

The poor results when no fire is present can be the consequence of the above-mentioned problems modelling turbulence. FDS is a CFD code specifically made for calculations on fires. The FDS reference manual states that flow in the room should be controlled by the fire [58]. This is not the case when modelling water mist with no fire present.

7.4 Recommendations for future simulations

Convincing simulations in FDS on water mist have not yet been done in this present work. In the following, simulation strategies are described and commented and a possible new strategy is suggested.

1) Modelling of the whole spray
Modelling water mist spray from the nozzle has been attempted previously with RANS models as described in chapter 5. These simulations generally failed to simulate the collapse of the cone and the droplets continued radial outward. Furthermore, momentum transfer from droplets to air was not successfully modelled.

To obtain proper simulation of the very complex zone around the nozzle, a very fine grid is required. Furthermore, a collision model for the droplets should be included. Until now, this has not been a viable approach when doing full-scale fire simulations.

2) The strategy for modelling the water mist spray using the LES model FDS described in this chapter was to avoid simulating the highly complex zone around the nozzle. Water was injected after the turbulent zone, and an air jet with the required momentum was created. However, this strategy failed due to the lack of turbulence influence on the water mist jet.

To get better simulation results, a way of handling the interaction of the droplets and the turbulence has to be found. The inlet boundary conditions for the water droplets and air in FDS should allow the specification of a fluctuating component.

Chapter 7 Simulations in FDS compared with experimental results

Chapter 8 Conclusions

The focus of this project has been to achieve a better understanding of the physics of water mist systems for extinguishment of a fire and to provide measurements results that can be used for simulating water mist.

Measurements have been conducted on the spray from a high-pressure system of 100 bars. Experiments have been conducted on a hollow cone nozzle without fire and with fire as well as a full cone nozzle without fire. Both were single nozzles, to avoid the interaction of water jets from several smaller nozzles and to simplify the task at this initial stage. Several measurement techniques have been used.

It has been found that the standard measurement method Phase Doppler Anemometry (PDA) used in conjunction with Particle Image velocimetry (PIV) gives a good description of the spray. The PDA measurements provide corresponding values of droplet diameters and velocities, but only in points. PIV on the other hand will give a complete velocity profile through the spray. The PIV method that is normally used only for measurement of a single particle size bias the velocity of the larger droplets. However with knowledge about droplet distribution and velocities that can be obtained from PDA measurements the PIV measurements can be judged. In places where the specific droplet size is uniform or where all drops move at the same speed, PIV measurements are very useful.

A high speed camera has been used for visual inspection of the spray with regards to shape and turbulence.

The volumetric water distribution has also been studied. For this purpose PDA, Laser Tomography and water density apparatus has been used. PDA did not perform well for the measurement of water density. Laser Tomography provided useful data, but the method is sensitive to droplet size. The water density apparatus has been improved and show potential, however further improvements are needed.

The physics of water mist has been studied both with respect to measurement and with theoretical considerations.

A methodology has been developed for drawing the spray pattern of a water mist spray. Droplet sizes and velocities are illustrated, and the method allows a visual inspection of the spray.

The measured sprays have been studied closely and they have been characterised by four zones :
- a conical zone with small fast drops in the middle and large fast drops in the cone where the bulk of the water is.
- an inflow zone where air has been sucked to the low pressure centre of the spray transporting larger droplets at low velocity to the centre of the spray. At this stage, centre velocities are considerably larger than velocities at the sides
- a transition zone where the spray collapses and a larger spread in droplets sizes is seen.
- a turbulent zone with a uniform droplet and velocity distribution across the spray.

Measurements have been the basis for simulations of water mist with CFD. Initial simulations of water mist using a RANS code (CFX 10.0) have included the complete spray volume from the outlet of the nozzle. The results have, however not been good, as the droplets continued radially instead of bending downwards and the air velocities were too low. This is probably due to inadequate simulation of the complex physics in the initial zone and too poor time resolution to give the correct momentum transfer from water to air.

A new approach has therefore been used for the simulations with the LES model in FDS 4.07. In this approach the simulations of the water mist spray is not done in the zone close to the nozzle. Instead the boundary conditions are set in the turbulent zone, based on the conducted measurements. This approach resulted in droplets moving downwards and air at relatively high velocities as should be expected.

The simulations did not give sufficient mixing. One reason being that no turbulence was set for the water and air jet boundary condition. Secondly there is in FDS no coupling of the turbulence from the subgrid turbulence model to the water droplets. If the grid is too coarse, which is often the case when doing full scale fire modelling. Too much energy is therefore handled by this subgrid model.

It is therefore suggested that in future calculations using FDS and the above approach, air and droplet turbulence must also be set as a boundary condition and a better way of handling the interaction of the droplets and the turbulence has to be implemented.

Chapter 8 Conclusions

References

1. Sardqvist, S. *Fire brigade use of water*. in *Interflam 1999, Proceedings of the 8th conference*. 1999. Edinburgh, Scotland: Interscience Communications Ltd.
2. Sardqvist, S. and G. Holmstedt, *Water for Manual Fire Suppression.* Journal of Fire Protection Engineering, 2001. **11**(4): p. 209-231.
3. *NFPA 750: Standard on Water Mist Fire Protection Systems*. 1996, National Fire Protection Association: Quincy, Massachusetts.
4. Papavergos, P.G., *Fine Water Sprays for Fire Protection: A Halon Replacement Option*, in *Halon Option Technical Working Conference*. 1991: Albuquerque, NM, USA.
5. Wighus, R. and P. Aune, *Engineering Relations for Water Mist Fire Suppression Systems*, in *Halon Options Technical Working Conference*. 1995: Albuquerque, NM, USA.
6. Dlugogorski, B.Z., et al., *Water vapour as an inerting agent*, in *Halon Options Technical Working Conference*. 1997: Albuquerque, NM, USA.
7. Pepi, J.S. *Advances in the Technology of Intermediate Pressure Water Mist Systems for the protection of Flammable Liquid Hazards*. in *Halon Option Technical Working Conference*. 1998. Albuquerque, NM, USA.
8. Wighus, R., *An Empirical Model for Extinguishment of Enclosed Fires with Water Mist*, in *Halon Options Technical Working Conference*. 1998: Albuquerque, NM, USA.
9. Mawhinney, J.R. and G.G. Back, *Water mist fire suppression systems*, in *SFPE Handbook of fire protection engineering, 3rd ed*, P.J. DiNenno, Editor. 2002, National Fire ProtectionAssociation: Quincy, MA USA.
10. Pedersen, K.S., et al., *Vanntåke anvendt i bygninger, Utredning om forsknings- og utviklingsbehov*. 2003, SINTEF: Trondheim, Norway.
11. *The mist in Madrid.* Fire Safety Engineering, England, 2007(April): p. 51.
12. Turnbull, A., *Water mist demystified.* Industrial Fire Journal, England, 2006(September): p. 41-46.
13. *Water mist for Fitness First.* Fire Safety Engineering, England, 2005(February): p. 38.
14. *Market Development 2006, International Water Mist Association*. News 2007 26.03.2007 [cited; Available from: http://www.iwma.net/.
15. Brinson, A., *Executive Director*. 2007, European Fire Sprinkler Network: London.
16. Husted, B.P. and G. Holmstedt, *Influence of draft curtains on sprinkler activation – comparison of three different models.* Journal of Fire Protection Engineering, Reviewed, not published.
17. *NFPA 750: Standard on Water Mist Fire Protection Systems*. 2006, National Fire Protection Association: Quincy, Massachusetts.

18. Husted, B.P., G. Holmstedt, and T. Hertzberg, *The physics behind water mist systems*, in *IWMA Conference*. 2004: Rome.
19. Andersson, P. and G. Holmstedt, *Limitations of Water Mist as a Total Flooding Agent.* Journal of Fire Protection Engineering, 1998. **9**(4): p. 31-50.
20. Adiga, K.C., et al., *A computational and experimental study of ultra fine water mist as a total flooding agent.* Fire Safety Journal, 2007. **42**(2): p. 150-160.
21. Pietrzak, L.M. and J.A. Ball, *A physical based fire suppresion computer simulation - definition, feasibility assessment, developments plan and applications*. 1983, Mission Research Corporation: Santa Barbara, Ca, USA.
22. Pietrzak, L.M. and J.J. Dale, *Comparison of post-flashover compartment fire suppression tests to fire demand model predictions*. 1991, Mission Research Corporation: Santa Barbara, Ca, USA.
23. Pietrzak, L.M., *Improvements to the water vaporization and surface cooling calculations in the Fire Demand Model*. 1993, Toyon Research Corporation: Goleta, Ca, USA.
24. Vaari, J., *A transient one-zone computer model for total flooding water mist fire suppression in ventilated enclosures.* Fire Safety Journal, 2002. **37**(3): p. 229-257.
25. Gardiner, A.J., *The mathematical modelling of the interaction between sprinkler sprays and the thermally buoyant layers of gases from fires, Ph.D. thesis*, in *The Fire and Explosion Group*. 1988, South Bank University: London.
26. Jackman, L.A., *Sprinkler spray interactions with fire gases, Ph.D. thesis*, in *Explosion and Fire Research Unit*. 1992, South Bank University: London.
27. Carlsson, J., et al., *Anwendung von CFD-Programmen für brandtechnische Berechnungen.* vfdb-Zeitschrift, 2006. **3**: p. 127-131.
28. Hertzberg, T., et al., *Vattendimma: Teori, fysik och simulering. BRANDFORSK projekt 514-021*. 2004, Borås, Sweden: Brandteknik, SP.
29. Husted, B.P., et al., *Comparison of PIV and PDA droplet velocity measurement techniques on two high-pressure water mist nozzles.* Fire Safety Journal, Submitted.
30. van der Graaf, G., *Personal Communication, Question regarding gpiv*. 2006.
31. Moisy, F., *pivmat - a Piv post-processing and data analysis toolbox for Matlab*. 2006, FAST - Univ. Paris Sud & CNRS UMR 7608: Paris.
32. Baur, T. and J. Köngeter, *High-Speed PIV and the Post-Processing of Time-Series Results*, in *EUROMECH 411 - European Mechanics Society. Application of PIV to Turbulence Measurements, Developments of 3 C Stereoscopic and Holographic Techniques*. 2000: University of Rouen, France.
33. Troolin, D.R., E.K. Longmire, and W.T. Lai, *Time resolved PIV analysis of flow over a NACA 0015 airfoil with Gurney flap.* Experiments in Fluids, 2006. **41**(2): p. 241-254.

References

34. Eisenberg, S., W. Reckers, and B. Wieneke. *Visualization and piv measurements of high-speed flows and other phenomena with novel Ultra-high-speed ccd camera*. in *West East High Speed Flow Fields 2002*. 2002. Marseille, France: CIMNE, Barcelona, Spain.
35. Bauckhage, K. and H. Flögel, *Simultaneous measurement of droplet size and velocity in nozzle sprays, paper 18.1*, in *Proc. 2nd Int. Symp. of Laser Anemom. to Fluid Mech.* 1984: Lisbon, Portugal.
36. Saffmann, M., H. Buchhave, and H. Tanger, *Simultaneous measurement of size, concentration and velocity of spherical particles by a laser Doppler method, paper 8.1*, in *Proc 2nd Int. Symp. of Laser Anemom. to Fluid Mech*. 1984: Lisbon, Portugal.
37. Bachalo, W.D. and M.J. Houser, *Phase/Doppler spray analyser for simultaneous measurement of drop size and velocity distributions.* Optical Engineering, 1984. **23**: p. 583-590.
38. Lefebvre, A.H., *Atomization and sprays*. 1989, New York: Hemisphere Publishing Corp.
39. Zhang, Z. and S. Ziada, *PDA measurements of droplet size and mass flux in the three-dimensional atomisation region of water jet in air cross-flow.* Experiments in Fluids, 2000. **28**(1): p. 29-35.
40. Nolan, P.F., *Feasibility study of using laser-high speed cine system for the characterisation of droplets from sprinkler sprays, (Prepared for Brandforsk, Sweden)*. 1989, Explosion and Fire Group, South Bank Polytechnic: London, UK.
41. Triballier, K., C. Dumouchel, and J. Cousin, *A technical study on the Spraytec performances: influence of multiple light scattering and multi-modal drop-size distribution measurements.* Experiments in Fluids, 2003. **35**(4): p. 347-356.
42. Hirleman, E.D. and L.G. Dodge. *Performance comparison of Malvern instruments laser diffraction drop size analyzer*. in *Third International Conference on Liquid Atomisation and Spray Systems, July 8-10*. 1985. London, England: Institute of Energy.
43. Virden, A., *Working range for water droplets (personal communication)*. 2007, Malvern Instruments.
44. Teipel, U., *Problems in Characterizing Transparent Particles by Laser Light Diffraction Spectrometry.* Chemical Engineering & Technology, 2002. **25**(1): p. 13-21.
45. Dodge, L.G., D.J. Rhodes, and R.D. Reitz, *Drop-size measurement techniques for sprays - Comparison of Malvern laser-diffraction and aerometrics phase/Doppler.* Applied Optics 1987. **26**(June): p. 2144-2154.
46. Andersson, P. and G. Holmstedt, *An instrument for determining the total water content in air when extinguishing fires.* Fire and Materials, 1999. **23**(4): p. 187-192.
47. Almén, V. and P. Irwert *Mätning av vattentäthet i vattendimma*, in *Report 5185*. 2007, Department of Fire Safety Engineering, Lund University Sweden.

References

48. Wang, Y., Y. Li, and S. Weng, *Experimental investigation on inner two-phase flow in counter-flow spray saturator for HAT cycle.* Applied Thermal Engineering, 2006. **26**(17-18): p. 2417-2424.
49. Andersson, P., *Evaluation and Mitigation of Industrial Fire Hazards, Ph.D. Thesis, LUTVDG/(TVBB-1055)*, in *Department of Fire Safety Engineering*. 1997, Lund University, Sweden.
50. Laven, P., *MiePlot - Computer program for scattering of light from a sphere using Mie theory & the Debye series* 2005: Geneva, Switzerland
51. Hinds, W.C., *Aerosol Technology. Properties, behavior and measurement of airborne particles*. 1982, New York: John Willey & Sons.
52. Bockasten, K., *Transformation of Observed Radiances into Radial Distribution of the Emission of a Plasma.* J. of the Optical Society of America, 1961. **51**(9): p. 943-947.
53. Born, M. and E. Wolf, *Principles of optics*. 7th ed. 1999, Cambridge: Cambridge University Press.
54. Kak, A.C. and M. Slaney, *Principles of Computerized Tomographic Imaging*. 1988, New York: IEEE Press.
55. Shepp, L.A. and B.F. Logan, *The Fourier Reconstruction of a Head Section.* IEEE Transactions on Nuclear Science, June 1974. **21**(3): p. 21-43.
56. Andersson, P. and G. Holmstedt, *Fullskaliga släckförsök med olika vattendimmasystem i container 50 m^3 i Karlskrona 26/8-29/8 1996, Report 3089*. 1996, Department of Fire Safety Engineering, Lund University: Lund.
57. Dlugogorski, B.Z., et al., *Propagation of laminar flames in wet premixed natural gas-air flames.* Trans IChemE Part B: Proc Saf & Env Prot 1998. **76**: p. 81-89.
58. *Fire Dynamics Simulator (Version 4) Technical Reference Guide*, in *NIST Special Publication 1018*, K. McGrattan, Editor. March 2006, National Institute of Standards and Technology Gaithersburg, MD USA.
59. *ANSYS CFX-Solver, Release 10.0, Theory Manual, Ansys Europe Ltd.* 2005.
60. Rubini, P.A. and J.B. Moss, *Coupled soot and radiation calculations in compartment fires*, in *Second International Conference on Fire Research and Engineering*. 1997: NIST, Maryland, USA.
61. McGrattan, K. and G. Forney, *Fire Dynamics Simulator (Version 4) User's Guide, NIST Special Publication 1019*. March 2006, National Institute of Standards and Technology, : Gaithersburg, MD USA.
62. Crowe, C.T., M.P. Sharma, and D.E. Stock, *The particle-source-in cell (PSI-cell) model for gas-droplet flows.* Journal of Fluids Engineering, 1977. **99**: p. 304-312.
63. Husted, B.P., et al. *Lagrangian prediction of particulate two-phase flows at high particle loadings*. in *Fourteenth International Conference on Numerical methods in Fluid Dynamics*. 1994. Bangalore, India: Springer-Verlag, 1995.
64. Sheppard, D.T. and R.M. Lueptow, *Characterization of fire sprinkler sprays using particle image velocimetry.* Atomization and Sprays, 2005. **15** p. 341-362.

References

65. Gant, S.E., *CFD Modeling of Water Spray Barriers, HSL/2006/79*, F.a. Explosion, Editor. 2006, Health & Saferty Laboratory, UK.
66. Sinai, Y.L., et al., *CFD modelling of fire suppression by water spray: A feasibility study examining a pool fire in a simple enclosure*, in *Third International Water Mist Conference*. 2003: Madrid, Spain.
67. Hua, J., et al., *A numerical study of the interaction of water spray with a fire plume.* Fire Safety Journal, 2002. **37**(7): p. 631-657.
68. Trelles, J., J.R. Mawhinney, and P.J. DiNenno. *Characterization of a High-Pressure Multi-jet Water Mist Nozzle for the Purposes of Computational Fluid Dynamics Modeling*. in *Computational Simulation Models in Fire Engineering and Research*. 2004. Santander, Spain: GIDAI.
69. Salewski, M., *LES of Jets and Sprays Injected into Crossflows, Ph.D thesis*, in *Department of Energy Science*. 2006, Lund University.
70. Nordin, N., *Complex chemistry modelling of diesel spray combustion, Ph.D-thesis*, in *Department of Thermo and Fluid Dynamics*. 2001, Chalmers university of technology: Göteborg, Sweden.
71. Walmsley, S.J. and A.J. Yule, *A study of the Sprays Produced by Fire Suppression Sprinkler Systems*, in *Eighth International Conference on Liquid Atomization and Spray Systems*. 2000: Ca, USA.
72. Tewarson, A., *Generation of Heat and Chemical Compounds in Fires*, in *SFPE Handbook of fire protection engineering, 3rd ed*, P.J. DiNenno, Editor. 2002, National Fire ProtectionAssociation: Quincy, MA USA.
73. Verheijen, P.J.T., *Statistical Distributions in Particle Technology*. 2004, Department of Chemical Engineering, Technical University Delft: Delft, The Netherlands.
74. Chan, T.-S., *Measurements of Water Density and Drop Size Distributions of Selected Esfr Sprinklers.* Journal of Fire Protection Engineering, 1994. **6**(2): p. 79-87.
75. Van Zandt, T., *How to fit a response time distribution.* Psychonomic Bulletin & Review, 2000. **7**(3): p. 424-465.
76. The MathWorks Inc., *Matlab version 7.1*. 2005.
77. Wen, J.X., et al., *Validation of FDS for the prediction of medium-scale pool fires.* Fire Safety Journal, 2007. **42**(2): p. 127-138.